Charmed Baryon Resonances and Mesons in Hot and Dense Matter

Clara Estela Jiménez Tejero

Charmed Baryon Resonances and Mesons in Hot and Dense Matter

Clara Estela Jiménez Tejero

Ph.D. thesis

December 2011

Programa de doctorat de Física Avançada
Bienni 2005-2007
Departament d'Estructura i Constituents de la Matèria
Universitat de Barcelona

Tesi dirida per
Isaac Vidaña i Angels Ramos

Prologue

This thesis is a memory of my doctoral work concerning the theoretical analysis of dynamically generated baryons resonances with charm in free space as well as the study of the properties of the charmed baryon resonances and charmed mesons in hot and dense matter. These studies have given rise to the following scientific contributions:

- C. E. Jiménez-Tejero, I. Vidaña, A. Ramos. Open charm baryon resonances beyond the zero range approximation. Phys. Rev. C 80, 055206 (2009).
- C. E. Jiménez-Tejero, L. Tolós, I. Vidaña, A. Ramos. Charm Hadrons in Dense Matter. Few Body Systems, 50, 351-353 (2011).
- D. Gamermann, C. E. Jiménez-Tejero, A. Ramos. Radiative decays of dynamically generated charmed baryons. Phys. Rev. D, 83, 074018 (2011).
- C. E. Jiménez-Tejero, L. Tolós, I. Vidaña, A. Ramos. Open charm meson in nuclear matter at finite temperature beyond the zero range approximation. Phys. Rev. C, 84, 015208 (2011).

Other parts of my doctoral work, such as the study of hypernuclei with strange and/or charm content, are not included in this thesis. The preprints in preparation concerning these studies are the following:

- C. E. Jiménez-Tejero, I. Vidaña, A. Ramos. Binding energy of Λ hypernuclei from realistic hyperon-nucleon interactions.
- C. E. Jiménez-Tejero, I. Vidaña, A. Ramos. Λ_c properties in finite nuclei within a microscopic many-body approach.

Agradecimientos

En primer lugar quiero dar las gracias a mis directores de tesis, Isaac Vidaña y Angels Ramos, por introducirme en el mundo del "charm". Sin vuestra ayuda no habría sido posible sacar esta tesis adelante. Isaac, lo primero de todo, gracias por haber apostado por mi y por haberme dado la oportunidad de hacer la tesis en la Universidad de Barcelona. Por enseñarme que las cosas se hacen poco a poco y con cuidado. Por tu rigurosidad y honestidad. También "moito obrigada" por tu hospitalidad y por hacer tan interesantes, cultural y culinariamente hablando, mis estancias en Coimbra. Angels, muchas gracias por tu esfuerzo didáctico y por tu paciencia, desde sentarnos a calcular un propagador, buscar un error en un programa o plantear una buena estrategia para una charla. También por tu energía positiva, cercanía y confianza a lo largo de todo el proceso.

A Laura Tolós, con la que he tenido el placer de colaborar. Gracias por tus enseñanzas en el medio nuclear y sobre todo por haberme transmitido la paciencia y minuciosidad necesarias para desempeñar tal tarea. También por haber hecho tan agradable y familiar mi estancia en Groningen, por estar siempre dispuesta a hacer cosas divertidas y ser una gran amiga.

A Daniel Gamerman, gracias por proponer una colaboración de la cual ha salido un bonito trabajo para mi tesis.

Bruno, gracias por tu ayuda y apoyo, como compañero de grupo y amigo. Por enseñarme a valorar el tiempo de los demás y el mío propio. Sobre todo gracias por hacerme las preguntas incómodas que, durante la tesis, han hecho que tantas veces pusiera los pies en la tierra.

Noela, gracias por tu ayuda incondicional en todos los ámbitos, desde lo académico a lo personal. Por haberme aportado tanto en cada fase de la tesis y por haberte leído el manuscrito con tanto esmero.

Aleix, gracias por transmitirme tu pasión por la ciencia y por recordarme que hay que pensar antes de hacer. Sin olvidar tus buenos consejos que han agilizado y materializado gran parte de los resultados recopilados en esta tesis.

A mis compañeros con los que he tenido la suerte de compartir despacho. Porque entre todos hemos sabido crear un buen clima de trabajo con la dosis necesaria de diversión. Esto ha sido para mí un aliciente positivo para acudir a la facultad cada día. En especial a Chumi por su nobleza, complicidad e imitaciones "pajariles" con las que me saludaba cada mañana. A Escartín por estar siempre dispuesto a ayudar y ser un apoyo importante y a las últimas incorporaciones Axel y Marina.

A los miembros del grupo de física hadrónica y nuclear, con los que he pasado momentos memorables. En especial a Volodya, Artur, Assum y Muntsa.

Además de hacer una tesis, he tenido la oportunidad de ejercer la docencia en varias asignaturas de la carrera. He compartido buenos momentos, y también

he aprendido mucha física con los profesores y compañeros de laboratorio. Gracias a Antoni Planes, Lluís Manyosa, Jose María Fernández, Mario Centelles, Toni García, Jose María Sancho, y muy especialmente a Montse García, Aurora Fernández y Alessandro Camboni.

A mis compañeros y amigos de doctorado, en especial a Javi, el hombre de la sonrisa perpetua e historias increíbles, con quien compartir un café se puede convertir en toda una aventura. A Xavi por su risa contagiosa y por ser una pieza clave en sacar adelante nuestro cineclub y a David por su sentido del humor y su carácter abierto al diálogo.

A los estudiantes de doctorado del despacho de al lado, gracias por patrocinar el té de las cinco y por ser tan majetes.

A los componentes del recien formado grupo de "brainstorming", que hacen que este cambio de etapa no me parezca tan brusco.

Al personal administrativo y técnico del departamento, por la ayuda prestada y papeleos variados.

Quería dar las gracias también a las chicas de copistería, en especial a M^{a} Ángeles, por animarme a hacer un diseño para la portada de la tesis.

Gracias también al "desastriño" de David, por seguir de cerca cada uno de mis pasos e interesarse en mi tema de investigación. ¡Quién nos iba a decir que seríamos capaces de escribir una tesis en inglés cuando hace unos años no sabíamos ni pedir las llaves de casa!

Quería agradecer también el apoyo y amistad que he recibido fuera del ámbito universitario. Muchas gracias a todos: Aina, Ábalon, Alicia, Anna, Àlex, Eneko, Erin, Ester, Fernando, Flora, Gwendolyn, Ignasi, Irene, Joana, Joaquín, Karola, Lisa, Manuela, Noelia, Pilar, Richard, Sandra, Tamara y Xevi.

Y finalmente, un gracias infinito a mi familia, por todo su cariño y apoyo.

A mi familia

Contents

List of Figures

List of Tables

Notation

We present the different abbreviations and symbols which will appear in this thesis

B-S	Bethe-Salpeter
L-S	Lippman-Schwinger
KSFR	Kawarabayashi-Suzuki-Fayyazuddin-Riazuddin
W-T	Weinberg-Tomozawa
$s,\ t,\ u$	Mandelstam variables
TVME	t-vector meson exchange
DR	Dimensional regularization
S	Strangeness
C	Charmness
T	Topness
B	Bottomness
I	Isospin
J	Total angular momentum
P	Parity
L	Orbital angular momentum
l	Relative orbital angular momentum

Q	Electric charge
σ_i	Pauli matrices
γ_i	Gamma matrices
q ($\overline{q}$)	quark (antiquark)
u	Up
d	Down
s	Strange
c	Charm
b	Bottom
t	Top
M	Meson
B	Baryon
R	Resonance
m_i	Mass of the meson i
M_i	Mass of the baryon i
λ	Cut-off momentum
f	Meson coupling constant
g	Universal coupling constant
Γ	Resonance width
$g_i,\ g_{RBM}$	Coupling of a resonance to a meson–baryon channel (i)
g_{BBM}	Baryon-baryon-meson coupling
$g_{\gamma MM}$	Photon–meson–meson coupling
T	Temperature
ρ_0	Normal nuclear saturation density

1

Introduction

1.1 The discovery of charm

The Quark Model (QM), proposed independently by Gell-Mann [GM64] and Zweig [Zwe64] in 1964, was already established in the early seventies. In 1968 it was shown in a series of deep inelastic experiments at the Stanford Linear Accelerator Center (SLAC) [B^+69a, B^+69b] that protons were not elementary particles. Nevertheless, the physics community were reluctant to identify those smaller point-like objects as quarks. Particle physicists were aware of the QM but there was a sense that quarks might just be a mathematical framework to understand the complexity of the nature but not necessarily the reflection of physical real objects. On the one hand, there was a zoo of particles with a variety of different properties, and all of them could fit in the QM by the combination of three different quarks in the case of baryons and of a quark and an antiquark in the case of mesons. However, there were no traces of a particle that could be identified

as a quark. At that time, the theory of Quantum Chromodynamics (QCD) was in the process of development. The formalism was beginning to show that there was a reason why a quark cannot be seen by itself[1], but that idea did not really spread so much. The physics community needed a stronger experimental proof of the real existence of quarks. This proof finally arrived in November of 1974, giving name to the so-called, "November revolution".

By that time there were two big experimental facilities in the United States where experiments were going in parallel with one another. Although they worked quite differently, both of them contributed to a big discovery. On the one hand, the SLAC facility was upgraded to channel positrons and make them collide against electrons. It was a matter–antimatter clean collision, converting the initial energy in the creation of new particles. Besides, researchers at the Brookhaven laboratory were running the same kind of experiment but in the other way around, selecting electron-positron pair events from the data of proton-target collisions. In the summer of 1974 the Ting's group at Brookhaven noticed something special in the data, a bump in the cross-section around 3 GeV. It was a very unusual signal because it was very narrow and it had a high statistic in the rate of events, many orders of magnitude higher than anything seen before. That bump was indicating a new sort of particle in nature, a resonance decaying into a muon–antimuon pair around 3 GeV. Meanwhile, the Burton Richter's team at SLAC hit energies around 3 GeV in November of 1974, where particles were appearing at hundred times the regular event rate. This is where both stories converge, the particle discovered at SLAC was exactly the same which was discovered by the Brookhaven's group. Both papers were submitted at the same time to a journal in 11th of November of 1974 [A$^+$74a, A$^+$74b] and two years later they shared the Nobel Prize. Since the finding of the particle was a two discoverers success, it was finally referred as J/ψ[2]. The very special features about the J/ψ particle were its narrowness, which means that it lives for a really long time, combined with its high mass[3]. Almost immediately it was understood that the J/ψ was a

[1] When two quarks are separated in a high-energy collision, the color force creates a quark and an anti-quark pair out of the vacuum.

[2] The first letter J looks like the Chinese character for Ting's name and SLAC group proposed the greek letter ψ in connection to the SPEAR accelerator.

[3] Particles of such high masses were expected to decay more rapidly via strong processes.

meson hiding a new kind of property.

Years before the "November revolution" there were predictions of a fourth type of quark in nature. By that time, the quark picture, composed of two light quarks and one heavy one, was not symmetric. The light up (u) and down (d) quarks make most of the ordinary matter and have $2/3$ and $-1/3$ electrical charge, and the strange (s) quark is a heavier version of the d quark but unstable. The question easily arises and a heavy partner of the u quark was expected to exist.

In 1964, J. Bjorken and S. L. Glashow suggested [BG64] the existence of a new type of quark, which they named "charm" (c), because its incorporation in the QM would make the quark picture very elegant. However, at that time it was still an speculative idea without the support of a firm theoretical prediction. On top of that, there was no experimental evidence yet. As the years went by, stronger arguments were made by S. L. Glashow, J. Iliopoulos, and L. Maiani [GIM70]. Their proposal, now called "GIM mechanism" from the initials of the three authors, was a convincing argument for the existence of the still undiscovered charm quark to solve a number of problems that particle physicists were facing at that time[4]. The fact that the mass of the J/ψ particle was twice the predicted mass for the charm quark, induced to understand that it was a meson made up of a charm and an anti–charm quark pair, a system called "charmonium". Then, a whole industry of charm began in particle accelerators, all the new open (charm content $C \neq 0$) and hidden ($C = 0$) charmed baryons and mesons predicted in QM where found experimentally.

The "November revolution" was not about new ideas, it was about converting the idea of a quark from an abstract proposition to a well established entity in nature. The finding of the J/ψ particle was a critical event that lead physicists to believe in quarks as the building blocks of hadrons.

[4]The flavor-changing decay modes involving the Z-Boson in weak interactions were predicted but not observed to happen. The GIM mechanism naturally suppress Flavor Changing Neutral Currents (FCNC) as well as transitions in weak interactions, by the introduction of the charm quark, whose mass should be at the GeV scale.

Name	Mass [MeV]	J^P	$\frac{Q}{e}$	I	I_3	(S,C,B,T)
"up" u	$1.7 - 3.3$	$\frac{1}{2}^+$	$\frac{2}{3}$	$\frac{1}{2}$	$\frac{1}{2}$	(0,0,0,0)
"down" d	$4.1 - 5.8$	$\frac{1}{2}^+$	$-\frac{1}{3}$	$\frac{1}{2}$	$-\frac{1}{2}$	(0,0,0,0)
"strange" s	101^{+29}_{-21}	$\frac{1}{2}^+$	$-\frac{1}{3}$	0	0	(-1,0,0,0)
"charm" c	1270^{+70}_{-90}	$\frac{1}{2}^+$	$\frac{2}{3}$	0	0	(0,1,0,0)
"bottom" b	$4200 + 70$	$\frac{1}{2}^+$	$-\frac{1}{3}$	0	0	(0,0,1,0)
'top" t	$172000 \pm 900 \pm 1300$	$\frac{1}{2}^+$	$\frac{2}{3}$	0	0	(0,0,0,1)

Table 1.1: The six flavors of quarks with their respective properties, mass and quantum numbers.

1.2 From quarks to hadron molecules

Nowadays, it is generally accepted that QCD is the underlying theory of the strong force. Quarks (see Table 1.1) are the fundamental constituents which interact via the strong force, by the interchange of particles called gluons[5]. We do not observe isolated quarks in nature but bound states of quarks called hadrons. Hadrons are classified in two groups, baryons and mesons which have half-integer and integer spin, respectively. In the most common and simple picture, baryons are described as a compound of three quarks and mesons as a quark–antiquark pair. Before going into more details on the hadron spectrum, we will give a general description of the highly non linear nature of the strong force and of the main theoretical techniques employed to understand it. As QED, QCD depends on a coupling constant which defines the strength of the interaction between constituents. To understand the main features of the strong force we show the energy dependence of the QCD coupling constant in Fig. 1.1 in which we can distinguish two different energy regimes. For high momentum transfer Q (or short distance), the coupling constant α_g reaches small values so that a perturbative expansion

[5]QCD was built in analogy to QED, the theory of the electromagnetic force between charged particles interacting via the emission and absorption of photons.

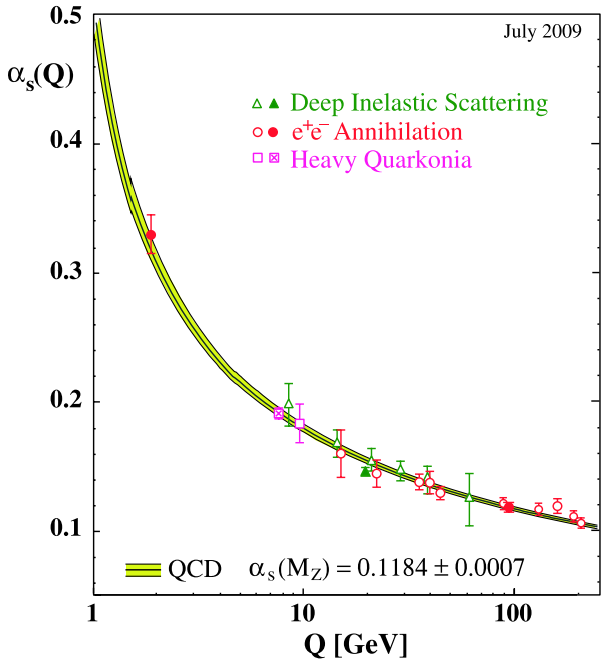

Figure 1.1: Summary of measurements of the strong coupling constant of QCD as function of the energy scale. There are two distinct energy regimes, confinement at low energies and asymptotic freedom at high energies. Plot taken from [Bet09].

is allowed for calculations. This region is referred to as the asymptotic freedom regime and it gives information on the interaction of quarks and gluons at short distances, where they interact weakly and behave as free particles. However, when Q approaches small values, the constant α_g increases dramatically and therefore one cannot longer rely on perturbative methods. In this low-energy regime quarks and gluons interact strongly and therefore are confined into hadrons. In this way, to study hadron spectroscopy, which lay in the $Q \approx 1$ GeV region, one has to build non-perturbative methods that can describe the rich spectrum of hadrons observed.

The only approach to exactly solve QCD at low energy is lattice QCD theory. This method has the power of calculating the hadron spectrum from first princi-

ples (quarks and gluons) without any assumption. It is formulated in a discrete space-time lattice and the only parameters are the bare masses of the quarks and the strong coupling constant. The physical quantities have a well behaved limit when the lattice spacing a tends to zero, and gives the continuum QCD. However, validating QCD through lattice theory needs high time consuming numerical simulations and the size of the uncertainties depend on the computer technology, which needs to be improved.

Alternative and complementary methods to lattice have also been developed to understand QCD at low energies. Typically employed are the phenomenological models such as an effective field theory inspired on QCD. In this kind of approaches, one has to build a theory which describes the specific system with hadronic degrees of freedom, ignoring the substructure at higher energies (quarks and gluons). Specifically in this thesis we will focus on studying one sort of baryon resonances using effective field theory techniques.

Now, let's go back again to the hadron spectrum. In one side, it is accepted that the most common observed baryons are made of three quarks (qqq) or of a quark–antiquark pair ($q\overline{q}$) in the case of mesons. In Table 1.2 we show the different meson and baryon J^P states that one can build in the mentioned traditional configurations, depending on the total spin of the quarks and the orbital angular momentum (L). The QM is mostly interested in describing hadrons with no angular momentum $L = 0$, also called ground state hadrons. As we show in Table 1.2, taking into account the spin and the parity of a quark ($\frac{1}{2}^+$) and of an anti–quark ($\frac{1}{2}^-$), the quantum numbers for the ground state baryons in the qqq configuration correspond to $J^P = \frac{1}{2}^+,\ \frac{3}{2}^+$, while $J^P = 0^-, 1^-$ correspond to the ground state mesons in the $q\overline{q}$ configuration. Apart from the traditional picture of hadrons, there is no fundamental rule which forbids any other kind of bound states between quarks. The complete wave function for a baryon can be expressed (excluding gluon degrees of freedom) as a superposition of many configurations

$$|B> \rightarrow |qqq>,\ |qqqq\overline{q}>,\ |qqqq\overline{q}q\overline{q}>\ \ ... \tag{1.1}$$

and for a meson

$$|M> \rightarrow |q\overline{q}>,\ |q\overline{q}q\overline{q}>,\ |q\overline{q}q\overline{q}q\overline{q}>\ \ ... \tag{1.2}$$

Baryon (qqq)			Meson ($\overline{q}q$)		
spin	$J^P(L=0)$	$J^P(L=1)$	spin	$J^P(L=0)$	$J^P(L=1)$
$\uparrow\downarrow\uparrow$	$\frac{1}{2}^+$	$\frac{1}{2}^-$, $\frac{3}{2}^-$	$\uparrow\downarrow$	0^-	1^+
$\uparrow\uparrow\uparrow$	$\frac{3}{2}^+$	$\frac{1}{2}^-$, $\frac{3}{2}^-$, $\frac{5}{2}^-$	$\uparrow\uparrow$	1^-	0^+, 1^+, 2^+

Table 1.2: Quantum numbers (J^P) for a baryon and a mesons in the traditional QM picture for different values of the orbital angular momentum, $L = 0, 1$.

Those configurations different from the traditional ones are called exotic. The fact that some of the observed baryons (mesons) do not fit with the QM predictions for the qqq ($q\overline{q}$) configuration support the idea of the existence of other exotic types of bound states.

In this thesis we are interested on studying the baryon resonances which can be formed from the interaction of a meson and a baryon. Such baryons and in general all hadron molecules are referred as dynamically generated resonances as their existence depends on the attractive character of the dynamics between the interacting hadrons. As we will see, the $\Lambda(1405)$ resonance from the strange sector and its charm counterpart, the $\Lambda_c(2595)$ resonance, are both good examples of an exotic baryon in the spectrum. We show in Table 1.3 different baryon molecules that can be formed from the interaction of ground state mesons, pseudoscalar 0^- or vector 1^-, and ground state baryons with $\frac{1}{2}^+$ or $\frac{3}{2}^+$.

A series of pioneer works [BF61, Wyl67, DWR67, LW67, Raj72, SW88], based on a t-channel vector meson exchange force, already predicted a wealth of s-wave baryon resonances generated by coupled channel dynamics with effective hadronic degrees of freedom rather than quarks and gluons. The earlier approaches have been readapted in the last decade to the modern language of chiral Lagrangians [KSW95, NRA01a, OR98, MO00, OOR00, OM01, NRA01b, IOVV02, LK02, GRNRAVV03, ORB02, ROB02, JOO$^+$03, OPV05, BNW05, BMN06, HJH08, HJR08]. Also, many resonances in the light SU(3) sector, which cannot be described properly by quark models [CI86] unless substantial meson-baryon components are included [GVV08], have been identified with dynamical states generated

Baryon molecule $(q\bar{q})(qqq)$		
meson⊕baryon	$J^P(L=0)$	$J^P(L=1)$
$0^- \oplus \frac{1}{2}^+$	$\frac{1}{2}^-$	$\frac{1}{2}^+, \frac{3}{2}^+$
$0^- \oplus \frac{3}{2}^+$	$\frac{3}{2}^-$	$\frac{1}{2}^+, \frac{3}{2}^+, \frac{5}{2}^+$
$1^- \oplus \frac{1}{2}^+$	$\frac{1}{2}^-, \frac{3}{2}^-$	$\frac{1}{2}^+, \frac{3}{2}^+, \frac{5}{2}^+$
$1^- \oplus \frac{3}{2}^+$	$\frac{1}{2}^-, \frac{3}{2}^-, \frac{5}{2}^-$	$\frac{1}{2}^+, \frac{3}{2}^+, \frac{5}{2}^+, \frac{7}{2}^+$

Table 1.3: Quantum numbers (J^P) for the different baryonic molecules which can be dynamically generated from the interaction of a meson (0^- or 1^-) and a baryon ($\frac{1}{2}^+$ or $\frac{3}{2}^+$), for two different values of the relative orbital angular momentum, $L = 0, 1$.

from the interactions of mesons of the pseudoscalar 0^- octet with the $\frac{1}{2}^+$ ground state baryons. Some consequences of these studies, such as the two-pole nature of the $\Lambda(1405)$, are confirmed through the analysis [MOR05, JOS09] of different experimental reactions [TEFK73, P$^+$04, B$^+$77]. In recent years it was demonstrated that, besides the s-wave baryon resonances, many more states can be generated dynamically. Baryon resonances with $J^P = \frac{3}{2}^-$ were studied based on the leading order chiral Lagrangian with the decuplet $\frac{3}{2}^+$ fields [KL04a, SOVV05, RSMO06, DOS06b]. D-wave baryon resonances were also generated dynamically with vector meson degrees of freedom [LWF02, GRNS06, TGRN08, GOV09, SSOV10, OR10]. Another promising line of research is the recent interpretation of low lying positive parity states like the $J^P = \frac{1}{2}^-$ resonances as molecular states of two pseudoscalar mesons (0^-) and one baryon ($\frac{1}{2}^+$) [MTKO08b, MTKO08a, KMTO08, JKE08, KEJ08]. All these results support the so-called hadrogenesis conjecture, formulated a few years ago by Lutz and Kolomeitsev, according to which resonances not belonging to the large-N_c ground state of QCD are generated by coupled-channel dynamics [LK02, LK01, Lut02, LWF02, LK04b].

The coupled-channel unitary scheme was extended to include the charm de-

gree of freedom for the first time by Lutz, Kolomeitsev and Hofmann in [KL04a, KL04b, LK04b, HL04, HL05, HL06, LK04a, LK05], and later by other authors [GOSVV07, GO07, TSBM04, MR06], motivated in part by the clear parallelism between the behavior of the $\Lambda(1405)$ in the $C = 0, S = -1$ sector with the $\Lambda_c(2595)$ in the $C = 1$ and $S = 0$ one.

In all the mentioned models, which generate resonances dynamically, an interaction based on the t-channel exchange of vector mesons is used as the driving force for the $s-$wave scattering of pseudo-scalar mesons off ground state baryons. The limit $t \to 0$ is implemented, leading to a vector type Weinberg-Tomozawa (W-T) zero-range interaction. To be consistent with the spin-flavor Heavy Quark Symmetry that develops in this heavy sector [IW89, Neu94, MW00], the vector mesons and $J = \frac{3}{2}^+$ baryons have recently been included in the basis of meson-baryon states, employing a static spin-flavor SU(8) scheme [GR$^+$09] similar to that developed in the light sector [GRNS06, TGRN08].

1.3 Charmed baryon spectrum

Charmed baryons refer to the set of baryons which contain at least one charm quark. The charm flavor can be introduced by extending the SU(3) symmetry group to the SU(4) one, which represents the baryon spectra made of u, d and s light quarks. Therefore, the SU(4) decomposition of a three-quark state reads:

$$q \otimes q \otimes q \equiv 4 \otimes 4 \otimes 4 \to 20_S \oplus 20'_{M_A} \oplus 20'_{M_S} \oplus \overline{4}_S \tag{1.3}$$

where the 20_S-plet is symmetric under the interchange of any two quarks, the $20'_{M_A}$- and $20'_{M_S}$-plets have mixed symmetry and describe the same states, and the $\overline{4}$-plet is symmetric. Here the 20-plet and the $20'$-plets explain all the charmed baryons in the ground state.

Due to Pauli exclusion principle the baryon wave function must be antisymmetric[6] and then the 20-plet and the $20'$-plets are paired with the $J = \frac{3}{2}$ and

[6]The total wave function of a baryon is

$$|\Psi >_A = |\Psi^{color} >_A \times |\Psi^{spin}\Psi^{flavor}\Psi^{space} >_S \ , \tag{1.4}$$

where A and S refers to antisymmetric and symmetric character of the wave function.

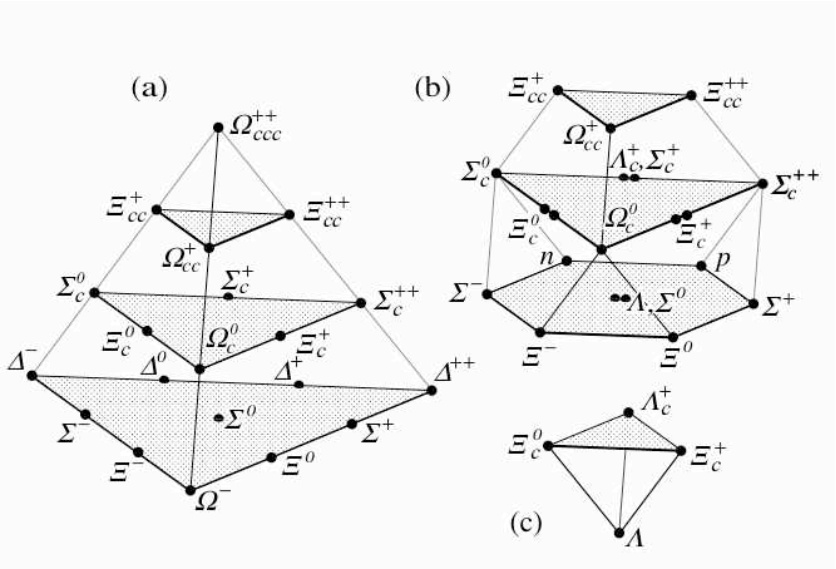

Figure 1.2: The SU(4) multiplets made of u, d, s and c quarks. The 20-plet (a), the $20'$-plets (b) and the $\overline{4}$-plet. Taken from PDG [N$^+$10].

the $J = \frac{1}{2}$ baryons, respectively, as it is illustrated in Fig. 1.2. The SU(3) light baryon multiplets are contained in the SU(4) representation and form the basis of the 20-plet and the $20'$-plets, as it can be seen in the Figure. If the symmetry were exact, all baryons would acquire the same mass. The multiplets containing only u and d quarks exhibit an almost excellent isospin symmetry ($m_u \approx m_d \approx 0$) but due to the finite mass of the strange quark ($m_s \approx 150$ MeV) the SU(3) is an approximated although still well behaved symmetry that describes the spectra of strange baryons. In the case of the SU(4) symmetry group, although it is largely broken by the large mass of the charm quark ($m_c \approx 1.2$ GeV) it works surprisingly well when describing the charmed baryon spectra. All the observed baryons are described in the Particle Data Group (PDG) [N$^+$10] and are classified by its mass[7], name[8], and isospin (I)[9]. Thus, the baryons made of u, d quarks are

[7]The mass of a state is the energy where the maximum of the peak is located.

[8]The name of the different baryons are related to the flavor content.

[9]There are baryons with different isospin number because the u and d quarks have $I = \frac{1}{2}$ (see Table 1.1).

named as N ($I = \frac{1}{2}$) or Δ ($I = \frac{3}{2}$). If they consist on two u, d quarks and one s quark they are referred as Λ ($I = 0$) and Σ ($I = 1$). Those with one u or d quark and two s quarks are called Ξ ($I = \frac{1}{2}$) and in the absence of u and d quarks they are called Ω ($I = 0$) (see Fig. 1.4). If we replace one of the s quarks in the latter configurations by a c quark the suffix c is added to the particle names and then we obtain the Λ_c, Σ_c, Ξ_c and Ω_c charmed baryons. If replacing two s quarks by two c ones we have the doubly charmed baryons, Ξ_{cc} and Ω_{cc}. Finally, the triply charmed baryon is the Ω_{ccc} state[10].

The spectrum for the Λ_c and Σ_c states is expected to be similar to the strange one and in the case of Ξ_c states the number of excited states is supposed to be richer than that of the Ξ spectrum, as it contains both strange and charm flavor.

The study of charmed hadrons is receiving an increased attention thanks to the efforts of a series of collaborations, both at lepton colliders (CLEO, BELLE, BaBar) and hadron facilities (CDF@Fermilab, PHENIX and STAR@RHIC, FAIR@GSI, ALICE@LHC). The new results confirm with better statistics previously seen charmed states and are also giving rise to the discovery of a large amount of new hadrons.

At present, 37 charmed baryons are known and they are grouped in 21 isospin multiplets. All of them have charm content $C = 1$, doubly or triply charmed baryons are still missing in the spectra. In the Table 1.5 we show the different charmed baryons ordered by the first experimental observation of at least one of the isospin multiplets. As it can be seen, the number of charmed baryons detected has increased considerably in the last years since the first measurement of the $\Sigma_c(2455)^{++}$ state [C$^+$75] in 1975. We also represent the different charmed states in Fig. 1.3 (white panels) and compared with the best established isospin multiplets with strange content $S = -1$ (grey panels).

Most of the charmed ground state baryons which belong to the SU(4) multiplets have been observed. In Fig. 1.3 they are represented with a solid circle ($J^P = \frac{1}{2}^+$) or a solid square ($\frac{3}{2}^+$). The still experimentally missing charmed baryons are the iso-doublet states Ξ_{cc} with $J^P = \frac{1}{2}^+$[11] and the triply charmed

[10]The same is applied if we replace the s quark by a b quark, and then the b suffix is added to the particle name. Baryons containing the t quark are not expected to be observed because of the short time decay.

[11]Note that there are evidences of a doubly charmed state at 3520 MeV, which is assigned

Strange		Charm					
C=0		C=1		C=2		C=3	
Baryon	qqq	Baryon	qqq	Baryon	qqq	Baryon	qqq
Λ^0	uds	Λ_c^+	udc	✗		✗	
Σ^+	uus	Σ_c^{++}	uuc	✗		✗	
Σ^0	uds	Σ_c^+	udc				
Σ^-	dds	Σ_c^0	ddc				
Ξ^0	uss	Ξ_c^+	usc	Ξ_{cc}^{++}	ucc	✗	
Ξ^-	dss	Ξ_c^0	dsc	Ξ_{cc}^+	dcc		
Ω^-	sss	Ω_c^0	ssc	Ω_{cc}^+	scc	Ω_{ccc}^{++}	ccc

Table 1.4: Quark components of the strange baryons and the charmed ones, with charm content $C = 1, 2$ or 3.

state, the Ω_{ccc} ($J^P = \frac{3}{2}^+$). Note that the isoscalar Λ_c and Λ ground states with $J^P = \frac{3}{2}^+$ are forbidden states, as well as the $J^P = \frac{1}{2}^+$ quantum number for the strange Ω^- ground state. Moreover, in the Ξ_c spectrum there are two additional ground state baryons with $J^P = \frac{1}{2}^+$, named as $\Xi_c'^+$ and $\Xi_c'^0$, which belong to the mixed symmetry $20'$-plets. In addition to the charmed baryons of the ground state, there exists a whole spectrum of excited resonances. Despite of the well established status of most of the charmed baryons, none of their J^P quantum numbers have been measured with the exception of the excited $\Lambda_c(2595)^+$ ($J^P = \frac{1}{2}^-$) and $\Lambda_c(2880)^+$ ($J^P = \frac{5}{2}^+$) states. The rest of the J^P quantum numbers are deduced from their decay modes or by comparison of the measured masses with the expectation from QM.

In particular, we want to determine whether some of the excited baryon states in the spectrum behave more as a baryon molecule dynamically generated from the s-wave interaction of a meson and a baryon, instead of being a genuine qqq state. The states with negative parity are candidates of being that sort of baryon molecule for s-wave interaction, and, depending on the interacting particles (see

to the production of the Ξ_{cc}^+ state with $J^P = \frac{1}{2}^+$ [M$^+$02].

First observation	Particle
1975	$\Sigma_c(2455)$ [C$^+$75]
1980	Λ_c^+ [C$^+$80]
1983	Ξ_c [B$^+$83]
1985	Ω_c^0 [B$^+$85]
1993	$\Lambda_c^+(2625)$ [A$^+$93a] $\Sigma_c(2520)$ [A$^+$93b]
1995	$\Lambda_c^+(2595)$ [E$^+$95] $\Xi_c(2645)$ [A$^+$95]
1999	$\Xi_c(2815)$ [A$^+$99] Ξ_c' [J$^+$99a]
2001	$\Lambda_c^+(2880)$ [A$^+$01] $\Lambda_c^+(2765)$ [A$^+$01] $\Xi_c(2790)$ [C$^+$01a]
2005	$\Sigma_c(2800)$ [M$^+$05a]
2006	$\Xi_c(2980)$ [C$^+$06a] $\Xi_c(3080)$ [C$^+$06a] $\Omega_c^0(2770)$ [A$^+$06]
2007	$\Lambda_c^+(2940)$ [A$^+$07a]
2008	$\Xi_c(2930)$ [A$^+$08a] $\Xi_c(3055)$ [A$^+$08b] $\Xi_c(3123)$ [A$^+$08b]

Table 1.5: Charmed baryons ordered by the year when the first member of every isomultiplet was observed in the different isospin families, the Λ_c (I=0), Σ_c (I=1), Ξ_c ($\frac{1}{2}$) and Ω_c (I=0).

Tab. 1.3), they can have $J^P = \frac{1}{2}^-$, $\frac{3}{2}^-$ or $\frac{5}{2}^-$. We have already commented in Sec. 1.2 that models based on a coupled-channel aproach and Chiral Lagrangians have succesfully described states from the light sector which did not fit in the QM, like the already mentioned $\Lambda(1405)$ resonance. Historically, it was the first time that a resonance, having a mass difficult to be reproduced in the QM, was proposed to be a meson-baryon ($\overline{K}N$) bound state [DT59b]. This state is predicted to have $J^P = \frac{1}{2}^-$ and can be dynamically generated in coupled channels models from the interaction of pseudoscalar mesons (0^-) with $\frac{1}{2}^+$ baryons. In addition to the $\Lambda(1405)$, the success of coupled-channel models is extended to all the negative parity states in the strange sector. The $\Lambda(1670)$ and the $\Xi(1690)$ resonances can also be dynamically generated from the interaction of pseudoscalar mesons (0^-) and baryons ($\frac{1}{2}^+$) [KL04a]. Besides, the $\frac{1}{2}^-$ resonances can also be generated from the interaction of vector mesons (1^-) with baryons. This is the case of the $\Lambda(1800)$ and the $\Sigma(1750)$ resonances, both with $\frac{1}{2}^-$, which are generated in [OR10] as $1^- \oplus \frac{1}{2}^+$ molecules, as well as the $\Xi(1950)$ with unknown J^P quantum numbers. With respect to the $\frac{3}{2}^-$ states, they are also well described with dynamical models and, like the $\frac{1}{2}^-$ states, they also admit different descriptions. The coupled channel models which employ pseudoscalar mesons (0^-) and baryons with $\frac{3}{2}^+$ as main ingredients can dynamically generate the $\Lambda(1520)$, the $\Sigma(1670)$ and the $\Xi(1820)$ resonances [KL04a, SOVV05]. Moreover, the $\Lambda(1690)$ state can be generated with two different descriptions, a $0^- \oplus \frac{3}{2}^+$ [KL04a, SOVV05] and a $1^- \oplus \frac{1}{2}^+$ molecule [OR10].

There are many more states in the strange sector which are succesfully explained from the dynamical point of view but are not presented in Fig. 1.3 because they are out of the energy range we want to show in order to compare with the charm spectrum or because they are qualified with less than three stars in the PDG. These states are the $\Sigma(2000)$ ($\frac{1}{2}^-$), the $\Lambda(2000)$ and the $\Xi(2120)$ and are generated as a $1^- \oplus \frac{1}{2}^+$ molecule in [OR10]. The $\Sigma(2000)$ resonance is also identified in [SSOV10] as a $1^- \oplus \frac{3}{2}^+$ molecule together with many more states. Particularly interesting is the $\Sigma(1940)$ state with $J^P = \frac{3}{2}^-$ because it admits a dynamical description with all the possible meson-baryon ingredients, pseudoscalar mesons with $\frac{3}{2}^+$ baryons [KL04a, SOVV05] and vector mesons with $\frac{1}{2}^+$ baryons [OR10] or with $\frac{3}{2}^+$ baryons [SSOV10]. From all the well established

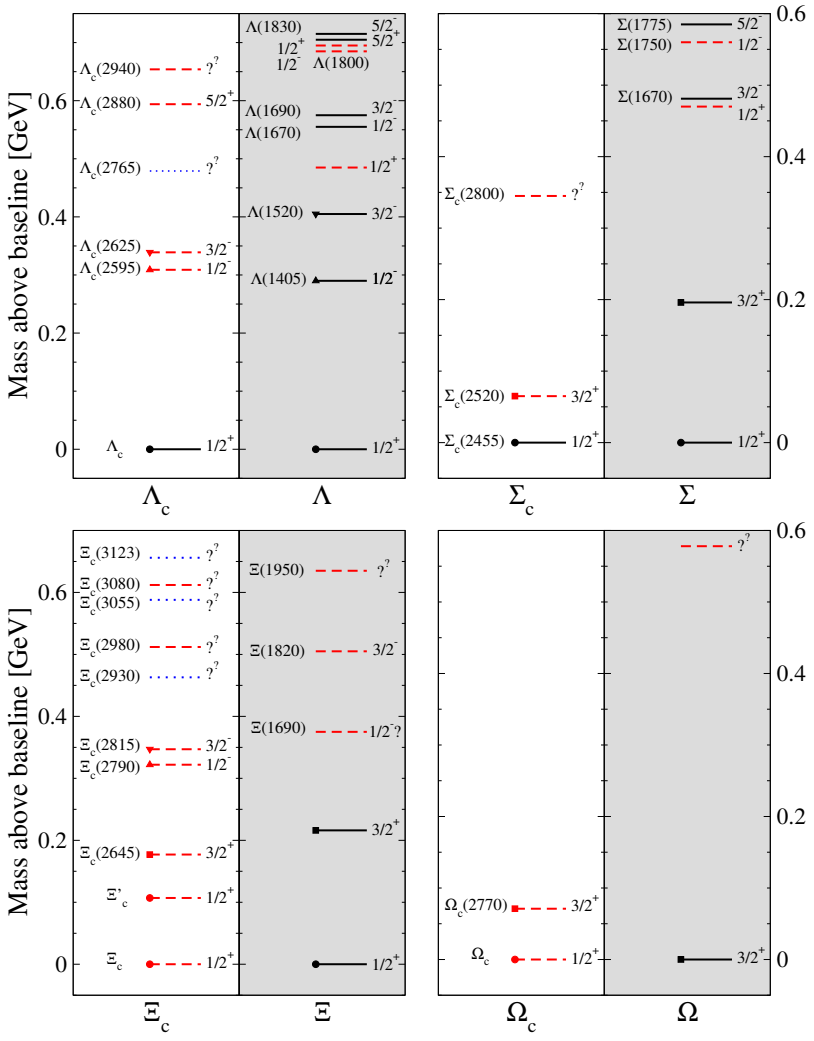

Figure 1.3: The experimental charmed baryons (white panels) and the best established strange baryons (grey panel). Solid lines refers to 4-star baryons, dashed lines to 3-star baryons and dotted lines to baryons with less than 3-stars. The J^P are shown for each state. The mass for all the excited charmed states is shown. In the strange spectrum the name labels are only shown for negative parity states because the are candidates of being s-wave dynamically generated resonances. The lines marked with a circle belong to the same SU(4) $20'$-plet, those with a square belong to the 20-plet and the triangles up and down point to the $\frac{1}{2}^-$ and $\frac{3}{2}^-$ $\overline{4}$-plet.

strange baryon resonances, the only negative parity states which at present cannot be found in the literature as dynamically generated are the $\Sigma(1775)$ and the $\Lambda(1830)$ resonances, both with $J^P = \frac{5}{2}^-$.

In the charmed spectrum there are some negative parity states which are also good candidates of being baryons dynamically generated. There are two states in the Λ_c spectrum which are considered to be the charmed counterparts of the $\Lambda(1405)$ and the $\Lambda(1520)$ resonances, the $\Lambda_c(2595)$ [HL05, MR06, GR$^+$09] and the $\Lambda_c(2625)$ [HL06] states with $J^P = \frac{1}{2}^-$ and $J^P = \frac{3}{2}^-$, respectively. Moreover, there is the $\Lambda_c(2880)$ state which is suggested to have $J^P = \frac{5}{2}^+$ and the $\Lambda_c(2940)$ state, with unknown quantum numbers, which lays very close to the D^*N threshold and it is predicted to be a D^*N molecule with $J^P = \frac{1}{2}^-$ [HLLZ07, GR$^+$09].

In the Σ_c spectrum there is the $\Sigma_c(2800)$ resonance with unknown quantum numbers for which the $J^P = \frac{3}{2}^-$ was suggested [M$^+$05a, A$^+$05]. The fact that it is dynamically generated in [HL06] with such quantum numbers supports this idea. However, the $J^P = \frac{1}{2}^-$ quantum numbers can not be discarded from the data.

In the Ξ_c spectrum there are the $\Xi_c(2790)$ and the $\Xi_c(2815)$ states, interpreted as the $J^P = \frac{1}{2}^-$ and $\frac{3}{2}^-$ charmed analogs to the $\Xi(1690)$ and $\Xi(1820)$ resonances from the strange sector. The $\Xi_c(2980)$ state with unknown quantum numbers is proposed to have $J^P = \frac{5}{2}^+$ as a charmed-strange partner of the $\Lambda_c(2880)$ state, and the $\Xi_c(3080)$ state is suggested to have $J^P = \frac{1}{2}^+,\ \frac{3}{2}^+$ [CC07, EFG08].

We have also included in Tab. 1.5 and Fig. 1.3 for the charm sector those isospin multiplets whose existence is not reliable nowadays and therefore are qualified with less than three stars in the PDG, the $\Lambda_c(2765)^+$, $\Xi_c(2930)$, $\Xi_c(3055)$ and $\Xi_c(3123)$, with unknown quantum numbers and marked with dotted lines in Fig. 1.3.

Particularly in this thesis, we are going to study baryon resonances as molecular bound states of a pseudoscalar meson and a $\frac{1}{2}^+$ baryon, and therefore all the states with $J^P = \frac{1}{2}^-$ or unknown quantum numbers are candidates of being identified with the baryon resonances generated dynamically in our model.

1.4 The t-channel vector meson exchange and the local approach

A common feature of all the mentioned works which generate resonances dynamically (see Secs. 1.2 and 1.3) is the use of a local, zero-range interaction, the origin of which can be traced back to the $t \to 0$ approximation in a t-channel type vector meson exchange diagram. This procedure is justified for on-shell meson-baryon transitions, $MB \to M'B'$, which are diagonal ($M'B' = MB$) and hence the value of t is small as long as one is not too far from threshold. It also holds for non-diagonal amplitudes ($M'B' \neq MB$) that show a moderate difference of masses between the initial and final mesons and baryons involved, as is the case of meson-baryon scattering within the light SU(3) world. However, in the heavy sector one also finds charm-exchange processes for which the difference of masses between the external mesons are comparable with the mass of the charmed vector meson being exchanged. This clearly signals the breakdown of the zero-range approximation which is no longer reliable for these non-diagonal transitions. While one may still argue that many of the dynamically generated states are triggered by a single dominant meson-baryon interaction component and, hence, their energy can be well estimated by the pole position of an uncoupled calculation involving only diagonal amplitudes, the corresponding width will however be determined by non-diagonal amplitudes and will therefore depend on whether the $t \to 0$ approximation is implemented or not. Moreover, it is well known that some resonances owe their origin to a particularly strong coupling between different channels, hence involving non-diagonal transitions, in which case the $t \to 0$ approximation is not at all appropriate for these states. In this thesis we will focus on the study of dynamically generated charmed baryon resonances but defining the interaction between the pseudoscalar meson and the ground state baryon beyond the zero-range approximation.

1.5 Goals of the thesis

The main objective of this thesis is to study baryon resonances generated from the dynamical interaction of two hadrons. We are interested on this study as an alternative approach to explain the increasing number of observed charmed states which apparently do not fit into the traditional three quark picture of a baryon. In particular, we study baryon molecules with $J^P = \frac{1}{2}^-$ which can be formed from the attractive interaction of a pseudoscalar meson (0^-) and a ground state baryon ($\frac{1}{2}^+$) in s-wave ($L = 0$). We focus on this particular sort of baryon molecules because, being the lightest ones within a given set of quantum numbers, they are in general the most stable molecules. Therefore our aim is to contribute to the understanding of the observed charm baryon spectra by checking if the dynamical origin can explain those states which are candidates to be a baryon resonance with $J^P = \frac{1}{2}^-$. The important feature of our model is the description of the meson-baryon interaction in terms of the t-channel vector meson exchange which is fully solved without any approximation.

The first part of the thesis is devoted to study these sort of baryon molecules in free space. In order to learn about the nature of a baryon it is important to study its different types of decays. For this reason, we will calculate the strong decays of dynamically generated resonances into meson–baryon components, as well as the electromagnetic transition of such hadron molecules into the lowest–lying ground states. This first part is organized in four Chapters.

In Chapter 2 we present the two–particle scattering formalism, and the different kernels which describe the interaction of a low lying pseudo-scalar meson with a ground state baryon. Moreover, we will introduce the Bethe-Salpeter equation from which we obtain the coupled channel scattering amplitudes. Every resonant state, extracted from a pole in the scattering matrix, will be characterized by a set of specific parameters. In Chapter 3 we employ a series of simplified toy models, derived from the previous Chapter, to perform a comparative study between the $\Lambda_c(2595)$ and the $\Lambda(1405)$ resonances, which belong to the charm and the strange sector respectively. In Chapter 4 we analyze in detail the effects of going beyond the $t \to 0$ approximation and focus on the study of the $C = 1$ baryon resonances, using the full t-dependence of the t-channel vector exchange kernel,

instead of the $t \to 0$ approximation. In order to extend our understanding on the nature of the excited baryons, we study in Chapter 5 the radiative decay of some of the dynamically generated resonances obtained in the previous Chapter into the respective $J^P = \frac{1}{2}^+$ ground state baryons.

In the second part of the thesis (Chapter 6) we will include medium and temperature effects on the formalism to study the properties of the charmed baryon resonant states in hot and dense matter. This will allow us as well to study the properties of charmed mesons (D, $\overline{D}$, D_s and $\overline{D_s}$) in the nuclear medium which will be simultaneously dressed in the self-consistent calculation for the first time. The behavior of these mesons will influence the charmonium production whose suppression is connected with the possible formation of quark-gluon plasma at a dense matter and high temperature scenario.

Part I

Free space

2

Two body scattering formalism

In this Chapter, we present the free space meson-baryon scattering formalism that we are going to use in the first part of the thesis. In Section 2.1 we will introduce the meson-baryon interaction, from which the t-channel vector meson exchange (TVME) and the Weinberg-Tomozawa (W-T) kernels will be constructed. The Bethe-Salpeter (B-S) equation and the reductions applied to solve it are the subjects of Section 2.2. Finally, in the last Section, we will explain the theoretical characterization of resonances.

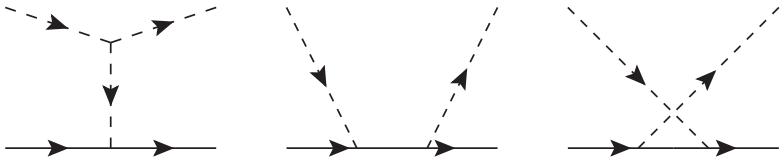

Figure 2.1: Leading order tree level diagrams. Solid lines corresponds to the baryons and dashed lines to mesons. From left to right, t-, s- and u-channel exchange diagrams.

2.1 The meson-baryon interaction

There are three different tree level diagrams that contribute to the low energy meson-baryon interaction up to the order $\mathcal{O}(p)$ in momentum space, as shown in Fig. 2.1. For the s-wave amplitude, the most important piece is the t-channel vector meson exchange diagram. In addition to this term, there are also the s-channel and the u-channel Born terms. The contribution of the s- and u-channel exchange diagrams in the strange sector have been studied in several works. The s-term mainly contributes to the p-wave interaction, and in [KSW95] it is shown that neglecting the u- and s-terms in a first approach to $\overline{K}N$ dynamics in s–wave brings no appreciable differences in the analysis. Also in [OM01] the most appreciable contribution of the s- and u-channel exchanges to the total amplitude strength is found to be about 20% of the t-channel term for energies of about 100 MeV away from the $\overline{K}N$ threshold. In the charm sector, at the energies of our interest, the t-channel exchange diagram is the one that contributes most to the s-wave meson-baryon interaction strength and we will neglect the contribution of the s- and u-channel diagrams. The kernel derived from the t-channel diagram will be shown in the following lines.

2.1.1 The t-channel vector meson exchange kernel

The previous considerations allow us to identify a t-channel exchange of vector mesons as the driving force which describes the s-wave scattering between pseudoscalar mesons in the 16-plet (see matrix in Eq. (2.3)) and ground state baryons in the 20-plet (see expressions in Eq. (2.6)) SU(4) representations, in such a way that it respects chiral symmetry for the light meson sector. For this purpose we

follow the original work of Hofmann and Lutz [HL05], where they exploited the universal vector meson coupling hypothesis. The SU(4) interaction Lagrangian which couples two pseudoscalar mesons and a vector meson field is defined as

$$\mathcal{L}^{SU(4)}_{PPV} = \tfrac{i}{4}\, g \left(\left[\left(\partial_\mu \, \Phi_{[16]} \right), \Phi_{[16]} \right]_- V^\mu_{[16]} \right), \tag{2.1}$$

with the $\Phi_{[16]}$ matrix of pseudoscalar mesons written down as

$$\Phi_{[16]} = \begin{pmatrix} \pi_0 + \frac{\eta}{\sqrt{3}} + \sqrt{\frac{2}{3}}\eta & \sqrt{2}\ \pi_+ & \sqrt{2}\ K_+ & \sqrt{2}\ \bar{D}^0 \\ \sqrt{2}\ \pi_- & -\pi_0 + \frac{\eta}{\sqrt{3}} + \sqrt{\frac{2}{3}}\eta' & \sqrt{2}\ K^0 & -\sqrt{2}\ \bar{D}^- \\ \sqrt{2}\ \bar{K}^- & \sqrt{2}\ \bar{K}^0 & -\frac{2\eta}{\sqrt{3}} + \sqrt{\frac{2}{3}}\eta' & \sqrt{2}\ \bar{D}^-_s \\ \sqrt{2}\ D^0 & -\sqrt{2}\ D^+ & \sqrt{2}\ D^+_s & \sqrt{2}\eta_c \end{pmatrix}, \tag{2.2}$$

and the vector meson matrix, $V^\mu_{[16]}$, as

$$V^\mu_{[16]} = \begin{pmatrix} \rho^\mu_0 + \omega^\mu & \sqrt{2}\ \rho^\mu_+ & \sqrt{2}\ K^\mu_+ & \sqrt{2}\ \bar{D}^\mu_0 \\ \sqrt{2}\ \rho^\mu_- & -\rho^\mu_0 + \omega^\mu & \sqrt{2}\ K^\mu_0 & -\sqrt{2}\ \bar{D}^\mu_- \\ \sqrt{2}\ \bar{K}^\mu_- & \sqrt{2}\ \bar{K}^\mu_{*0} & \sqrt{2}\ \phi^\mu & \sqrt{2}\ \bar{D}^{s,\mu}_- \\ \sqrt{2}\ D^\mu_0 & -\sqrt{2}\ D^\mu_+ & \sqrt{2}\ D^{s,\mu}_+ & \sqrt{2}\ J/\Psi^\mu \end{pmatrix}. \tag{2.3}$$

The factor g is the universal coupling constant which can be related to the meson coupling constant denoted as f, in accordance with the Kawarabayashi-Suzuki-Fayyazuddin-Riazuddin (KSFR) relation [KS66, RF66]. It must hold with the

interaction (Eq. (2.1)) and is defined as

$$g^2 = \frac{(m_{[9]}^{(v)})^2}{2\,f^2}\,, \tag{2.4}$$

with $m_v^{[9]}$ being a representative mass of the light vector mesons from the nonet, that is (ρ^μ, ϕ^μ, ω^μ and K^μ). The value of g is typically taken to be $g \approx 6.6$, which comes from considering the average mass of the light vector mesons and reproduces the width of the ρ meson decaying into two pions, taking $f = f_\pi \approx 93$ MeV in Eq. (2.4). The baryon-baryon-vector meson vertex in SU(4) is described as

$$\mathcal{L}_{BBV}^{SU(4)} = \tfrac{1}{4}\,g \sum_{i,j,k,l=1}^{4} \bar{B}_{ijk}^{[20]}\,\gamma^\mu \left(V_{\mu,\,l}^{[16],k}\,B_{[20]}^{ijl} + 2\,V_{\mu,\,l}^{[16],j}\,B_{[20]}^{ilk} \right)\,, \tag{2.5}$$

where the baryon fields, represented by the tensor B^{ijk}, form a 20-plet in SU(4). The indices i, j, k denote the quark content with the following identification, $1 \to u, 2 \to d, 3 \to s, 4 \to c$:

$$\begin{aligned}
B^{121} &= p,\, B^{122} = n,\, B^{132} = \frac{1}{\sqrt{2}}\Sigma^0 - \frac{1}{\sqrt{6}}\Lambda, \\
B^{124} &= \frac{2}{\sqrt{6}}\Lambda_c,\, B^{141} = -\Sigma_c^{++},\, B^{142} = \frac{1}{\sqrt{2}}\Sigma_c^{+} + \frac{1}{\sqrt{6}}\Lambda_c, \\
B^{143} &= \frac{1}{\sqrt{2}}\Xi_c^{\prime +} - \frac{1}{\sqrt{6}}\Xi_c^{+},\, B^{144} = \Xi_{cc}^{++},\, B^{213} = \frac{2}{sqs}\Lambda, \\
B^{231} &= \frac{1}{\sqrt{2}}\Sigma^0 + \frac{1}{\sqrt{6}}\Lambda,\, B^{232} = \Sigma^-,\, B^{233} = \Xi^-, \\
B^{234} &= \frac{2}{\sqrt{6}}\Xi_c^0,\, B^{241} = \frac{1}{\sqrt{2}}\Sigma_c^{+} - \frac{1}{\sqrt{6}}\Lambda_c,\, B^{242} = \Sigma_c^0, \\
B^{243} &= \frac{1}{\sqrt{2}}\Xi_c^{\prime 0} + \frac{1}{\sqrt{6}}\Xi_c^0,\, B^{244} = -\Xi_{cc}^{+},\, B^{311} = \Sigma^+, \\
B^{313} &= \Xi^0,\, B^{314} = \frac{2}{sqs}\Xi_c^{+},\, B^{341} = \frac{1}{\sqrt{2}}\Xi_c^{\prime +} + \frac{1}{\sqrt{6}}\Xi_c^{+}, \\
B^{342} &= \frac{1}{\sqrt{2}}\Xi_c^{\prime 0} - \frac{1}{\sqrt{6}}\Xi_c^0,\, B^{343} = \Omega_c,\, B^{344} = \Omega_{cc}
\end{aligned} \tag{2.6}$$

The t-channel vector meson exchange contribution, or TVME kernel, can be built from the meson-meson-vector (2.1) and baryon–baryon–vector (2.5) Lagrangians defined above, as

$$\mathcal{V}_{ij}(q_i,q_j) = \frac{1}{2}g^2\sum_v \frac{C_{ij,v}}{t-m_v^2}\left(\frac{\not{q}_j+\not{q}_i}{2} - \frac{q_j^2-q_i^2}{2m_v^2}(\not{q}_j-\not{q}_i)\right) \ , \tag{2.7}$$

being the q_i (q_j) the initial (final) meson momentum and m_v the vector meson mass. The quantities $\not{q}_i$ ($\not{q}_j$) are explicitly written down

$$\not{q}_i = \gamma^\mu q_{i\mu} \ \ ; \ \ \not{q}_j = \gamma^\mu q_{j\mu} \ , \tag{2.8}$$

in terms of the gamma matrices $\gamma^\mu = \{\gamma^0,\gamma^1,\gamma^2,\gamma^3\}$, and the t–Mandelstam variable is defined as

$$\begin{aligned} t &= (q_i - q_j)^2 \\ &= m_i^2 + m_j^2 - 2\left(\omega_i(\vec{q}_i)\omega_j(\vec{q}_j) - \vec{q}_i\vec{q}_j\right) , \end{aligned} \tag{2.9}$$

where $\omega(q_i)$ ($\omega(q_j)$) represents the energy of the initial (final) meson. The SU(4) coefficients, $C_{ij,v}$, denote the strength of the interaction between a pseudoscalar meson and a ground-state baryon mediated by the exchange of a vector meson (v). They are presented in Appendix A for different isospin (I), strangeness (S) and charm (C) sectors and channels (i,j). The kernel interaction is defined in such a way that positive $C_{ij,v}$ coefficients give attraction and negative give repulsion to the transition. To write explicitly the t-channel vector meson exchange diagram one has to project the kernel into the initial and final baryon states, with initial and final momenta p_i and p_j, respectively,

$$\langle \mathcal{V}_{ij} \rangle \ = \overline{u}(p_j)\mathcal{V}_{ij}(q_i,q_j)u(p_i) \, , \tag{2.10}$$

where the function $u(p_i)$ and its adjoint $\overline{u}(p_j)$ ($\overline{u}(p_j) = u^\dagger(p_j)\gamma^0$) are the Dirac four component spinors, normalized as $\overline{u}u = 1$:

$$u_m(p,\sigma) = \sqrt{\frac{E(\vec{p})+M}{2M}}\begin{pmatrix} 1 \\ \frac{\vec{\sigma}\vec{p}}{(E(\vec{p})+M)} \end{pmatrix}\chi_m \ , \tag{2.11}$$

being M and $E(\vec{p})$ the mass and energy of a baryon with momentum $\vec{p}$, $\vec{\sigma}$ the Pauli matrices and χ_m the two–component spinor wave function for spin up ($m = \frac{1}{2}$) or spin down ($m = -\frac{1}{2}$).

The total energy of the system P^0 and the center of mass momentum $\vec{P}$ are given by

$$P^0 = \omega(\vec{q}) + E(\vec{p}) \;\; ; \;\; \vec{P} = \vec{q} + \vec{p}. \tag{2.12}$$

Working in the center-of-mass frame, $\vec{P} = 0$, we have for the initial and final meson and baryon momenta

$$\vec{q}_i = -\vec{p}_i \equiv \vec{k}_i \;\; ; \;\; \vec{q}_j = -\vec{p}_j \equiv \vec{k}_j \, . \tag{2.13}$$

Inserting the quantities $\langle \not{q}_i \rangle$ and $\langle \not{q}_j \rangle$ into Eq. (2.10), where

$$\begin{aligned} \langle \not{q}_i \rangle &= \overline{u} \; \not{q}_i u \\ &= N[\omega_i(\vec{k}_i) + E_i(\vec{k}_i) - M_i \\ &+ \frac{\vec{k}_i \vec{k}_j}{(E_i(\vec{k}_i) + M_i)(E_j(\vec{k}_j) + M_j)} (\omega_i(\vec{k}_i) + E_i(\vec{k}_i) + M_i)] \, , \end{aligned} \tag{2.14}$$

we obtain:

$$\langle \mathcal{V}_{ij} \rangle = \frac{N}{4} \sum_v C_{ij,v} \frac{\alpha + \beta \cos\theta}{a + b \cos\theta} \, , \tag{2.15}$$

where the factor N comes from the normalization of the Dirac spinors:

$$N = \sqrt{\frac{M_i + E_i(\vec{k}_i)}{2M_i}} \sqrt{\frac{M_j + E_j(\vec{k}_j)}{2M_j}} \, , \tag{2.16}$$

and θ is the angle between the initial and the final relative momenta. The functions a, b, α and β, which also depend on the relative momenta, are defined as

$$
\begin{aligned}
a &= m_i^2 + m_j^2 - 2\omega_i(\vec{k}_i)\omega_j(\vec{k}_j) - m_v^2 \\
b &= 2|\vec{k}_i||\vec{k}_j| \\
\alpha &= \omega_i(\vec{k}_i) + E_i(\vec{k}_i) + \omega_j(\vec{k}_j) + E_j(\vec{k}_j) - M_i - M_j \\
&\quad - \frac{m_j^2 - m_i^2}{m_v^2}\left(\omega_j(\vec{k}_j) + E_j(\vec{k}_j) - \omega_i(\vec{k}_i) - E_i(\vec{k}_i) + M_i - M_j\right) \\
\beta &= \frac{|\vec{k}_i||\vec{k}_j|}{(E_i(\vec{k}_i) + M_i)(E_j(\vec{k}_j) + M_j)} \\
&\quad (\omega_i(\vec{k}_i) + E_i(\vec{k}_i) + \omega_j(\vec{k}_j) + E_j(\vec{k}_j) + M_i + M_j \\
&\quad - \frac{m_j^2 - m_i^2}{m_v^2}[\omega_j(\vec{k}_j) + E_j(\vec{k}_j) - \omega_i(\vec{k}_i) - E_i(\vec{k}_i) + M_j - M_i])\,,
\end{aligned}
\tag{2.17}
$$

with

$$
\begin{aligned}
\omega_i(\vec{k}_i) = \sqrt{\vec{k}_i^2 + m_i^2} \;\; ; \;\; \omega_j(\vec{k_j}) = \sqrt{\vec{k}_j^2 + m_j^2} \\
E_i(\vec{k}_i) = \sqrt{\vec{k}_i^2 + M_i^2} \;\; ; \;\; E_j(\vec{k}_j) = \sqrt{\vec{k}_j^2 + M_j^2}\,.
\end{aligned}
\tag{2.18}
$$

Assuming spherical symmetry, one can expand the kernel in partial waves:

$$
V_{i,j;l} = \frac{2l+1}{2}\int_{-1}^{1} d\,(\cos\theta)\,\langle \mathcal{V}_{ij}\rangle\, P_l(\cos\theta)\,, \tag{2.19}
$$

where $P_l(\cos\theta)$ are the Legendre polynomials. Since we want to study resonances with relative angular momentum $l = 0$, we project the kernel in s-wave[1], therefore obtaining the expression of the TVME kernel which describes the interaction between pseudoscalar mesons with ground state baryons in s-wave:

$$
V_{ij;l=0}(\vec{k}_i, \vec{k}_j) = \frac{N}{8} g^2 \sum_v C_{ij,v}\left(\frac{2\beta}{b} + \frac{\alpha b - \beta a}{b^2}\ln\left(\frac{a+b}{a-b}\right)\right)\,. \tag{2.20}
$$

[1]The Legendre polynomial for $l = 0$, $P_0(\cos\theta) = 1$.

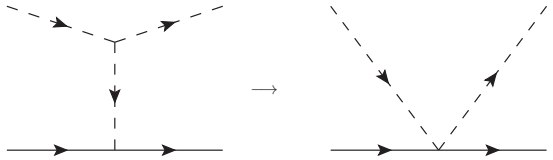

Figure 2.2: The zero–range approximation of the t-channel vector exchange contribution.

2.1.2 The zero-range approximation

For the specific case of $t \ll m_v^2$ we can make the approximation $t \to 0$ in Eq. (2.7), and we get the scattering kernel for contact interactions, $\text{TVME}_{t\to 0}$:

$$V_{ij;l=0}(\vec{k}_i, \vec{k}_j)_{t\to 0} = -\frac{N}{4} g^2 \sum_v \frac{C_{ij,v}}{m_v^2} \alpha \,. \tag{2.21}$$

One can also arrive to the same expression by expanding the logarithm of Eq. (2.20) in the limit $\frac{b}{a} \to 0$ up to the linear term in $\frac{b}{a}$ and setting $a = -m_v^2$.

2.1.3 The Weinberg-Tomozawa kernel

The lowest order chiral Lagrangian of SU(3) that couples the octet of light pseudoscalar mesons to the octet of ground state baryons is given by

$$\begin{aligned} \mathcal{L}^{MB} = & < \overline{B} i\gamma^\mu \nabla_\mu B > - M < \overline{B} B > \\ & + \frac{D}{2} < \overline{B}\gamma^\mu\gamma_5 \{u_\mu, B\} > + \frac{F}{2} < \overline{B}\gamma^\mu\gamma_5 [u_\mu, B]) > , \end{aligned} \tag{2.22}$$

where u is the SU(3) matrix of mesons ϕ and B is the SU(3) matrix for baryons, both of which can be found for example in [OR98], M is the baryon mass and D and F are the low energy constants which are related to the axial charge of the nucleon fixed to $D = 0.8$ and $F = 0.46$, respectively [JOO$^+$03]. The Weinberg-Tomozawa (W-T) term of the Lagrangian is obtained by expanding the covariant derivative in Eq. (2.22) at the level of two meson fields

$$\mathcal{L}^{W-T} = \frac{1}{4f^2} < \overline{B} i\gamma^\mu [\phi(\partial_\mu \phi) - (\partial_\mu \phi)\phi, B] > \,. \tag{2.23}$$

We obtain the W-T interaction kernel by projecting the tree-level amplitude in s-wave,

$$V_{ij;l=0}^{W-T}(\sqrt{s}) = -\frac{N}{8f^2} C_{ij}^{W-T} \alpha_{W-T}\,, \tag{2.24}$$

being C_{ij}^{W-T} the W-T coefficients, and the factor α_{W-T} defined as

$$\alpha_{W-T} = \omega_i(\vec{k}_i) + E_i(\vec{k}_i) + \omega_j(\vec{k}_j) + E_j(\vec{k}_j) - M_i - M_j\,. \tag{2.25}$$

We can also derive the W-T kernel from the expression of the zero–range approximation to the TVME kernel, $\text{TVME}_{t=0}$, given in Eq. (2.21). The first approximation is to consider that the mass of the vector mesons, m_v, is very big compared to the mass of the pseudoscalar mesons in the initial and final state. Next, we re-write the kernel as a function of f instead of using the universal coupling constant g through the KSFR relation (Eq. (2.4)). Finally, considering that the masses of the vector mesons are all equal, we arrive to the expression for the W-T kernel (Eq. (2.24)), where the W-T coefficients are given, for a certain initial and final channel, as the sum over the SU(4) coefficients presented in Appendix A for all possible vector–mesons interchanged:

$$C_{ij}^{W-T} = \kappa \sum_v C_{ij,v}\,. \tag{2.26}$$

The factor κ has been introduced to account for the fact that, in the charm sector, the mass of the exchanged meson in charm exchange transitions is almost twice that of the transitions mediated by non-charmed mesons. Therefore, the factor κ is unity except for the charm exchange transitions where $\kappa = (\frac{m_v}{m_v^c})^2 \approx \frac{1}{4}$.

2.1.4 On-shell kernels

In the center-of-mass frame $\vec{P} = 0$, we calculate the initial and final on-shell momentum, $|\vec{k}_i^{on}|$, $|\vec{k}_j^{on}|$, from the expression

$$\sqrt{s} = \omega(\vec{k}^{on}) + E(\vec{k}^{on})\,, \tag{2.27}$$

obtaining

$$|\vec{k}_{i,j}^{on}| = \frac{1}{2\sqrt{s}}\sqrt{(s-(M_{i,j}+m_{i,j})^2)(s-(M_{i,j}-m_{i,j})^2)}\,. \tag{2.28}$$

In this way, we get the on-shell expressions for the TVME kernel and its zero range approximation $\text{TVME}_{t\to 0}$ changing, in Eqs. (2.20) and (2.21), the functions a, b, α and β of Eq. (2.17) by a^{on}, b^{on}, α^{on} and β^{on}:

$$\begin{aligned}
a^{on} &= m_i^2 + m_j^2 - 2\omega_i(\vec{k}_i^{on})\omega_j(\vec{k}_j^{on}) - m_v^2 \\
b^{on} &= 2|\vec{k}_i^{on}||\vec{k}_j^{on}| \\
\alpha^{on} &= 2\sqrt{s} - M_i - M_j - \frac{m_j^2 - m_i^2}{m_v^2}(M_i - M_j) \\
\beta^{on} &= \frac{|\vec{k}_i^{on}||\vec{k}_j^{on}|}{\left(E_i(\vec{k}_i^{on}) + M_i\right)\left(E_j(\vec{k}_j^{on}) + M_j\right)} \\
&\quad \left(2\sqrt{s} + M_i + M_j - \frac{m_j^2 - m_i^2}{m_v^2}(M_j - M_i)\right)\,.
\end{aligned} \tag{2.29}$$

and, for the on-shell W-T term, changing in Eq. (2.24) the factor α_{W-T} to α_{W-T}^{on}:

$$\alpha_{W-T}^{on} = 2\sqrt{s} - M_i - M_j\,. \tag{2.30}$$

2.2 The Bethe-Salpeter equation

The scattering of two–particles is a relevant dynamical problem of elementary particle physics. Before the Bethe-Salpeter equation was published in 1951 [SB51], the scattering matrix was typically calculated using perturbation theory. However, perturbation theory can never generate a bound state. The reason is that the generation of a bound state is accompanied by the appearance of a pole in the scattering matrix, and any finite sum of perturbative Feynman diagrams can never create such a pole. On the contrary, it is possible to generate the required pole if one sums over an infinite number of diagrams. The work of E. E. Salpeter and H. A. Bethe [SB51], introduced the possibility to reach this as an alternative method to a perturbative expansion. An approximation to the two–body

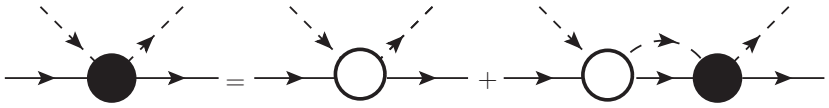

Figure 2.3: Diagrammatic representation of the Bethe-Salpeter equation.The black area corresponds to the T_{ij} matrix and the open circles correspond to the kernel V_{ij}.

scattering amplitude is obtained by solving the relativistic Bethe-Salpeter (B-S) equation [SB51]. Within the B-S formalism, the scattering matrix, $\mathcal{T}_{ij}$, is given by an integral equation in momentum space. Suppressing the spin (J), isospin (I), strangeness (S) and charm (C) quantum numbers for simplicity, the meson–baryon B-S equation takes the form:

$$\begin{aligned}\mathcal{T}_{ij}(k_i,k_j;P) &= \mathcal{V}_{ij}(k_i,k_j;P) \\ &+ i\sum_l \int \frac{d^4k}{(2\pi)^4}\mathcal{V}_{il}(k_i,k_n;P)\mathcal{D}_l(k,P)\tilde{\mathcal{D}}_l(k;P)\mathcal{T}_{lj}(k,k_j;P)\,,\end{aligned} \tag{2.31}$$

where $k_i,\ k_j$ are the relative four momenta of the initial and the final states and k is the momentum of the meson propagating in the intermediate loop, whereas P is the total four momentum of the system. The sum over the index l refers to the different coupled-channels involved in the particular sector studied. $\mathcal{V}_{ij}$ is the kernel which describes the interaction between the meson and the baryon, and the $\mathcal{D}_l$ and $\tilde{\mathcal{D}}_l$ functions are the baryon and meson propagators, respectively

$$\mathcal{D}_l(k;P) = \frac{1}{\not{P} - \not{k}_n - M_l + i\eta} \quad ; \quad \tilde{\mathcal{D}}_l(k;P) = \frac{1}{k_n^2 - m_l^2 + i\eta}\,. \tag{2.32}$$

The B-S amplitude is obtained by summing the contribution to all powers of the interactions contained in the kernel and the meson–baryon propagator. It is the oldest and simplest two-body relativistically covariant scattering equation whose theory and applications have been extensively developed in many branches of physics [B-S]. The off-shell nature of the B-S equation and the inelastic effects which are built into it constitute the main difficulties of the equation. Since it is an off-shell equation it depends explicitly on four variables. Furthermore, to get the solution of the exact B-S equation is an even more difficult task due to

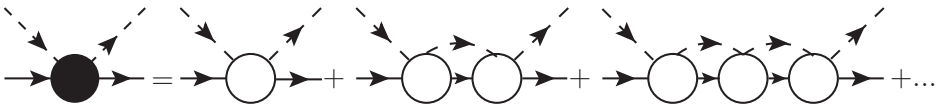

Figure 2.4: Diagrams representing the expansion of the Bethe-Salpeter equation. The black area corresponds to the T_{ij} matrix and the open circles correspond to the kernel V_{ij}.

the presence of poles along the integration contours, contained at the meson and baryon propagators. In order to deal with this complication, a lot of approximated solutions have been considered. One of the alternatives which handles the difficulty with poles along integration contours is to replace the four dimensional B-S equation by a three dimensional reduction, integrating out the time component, k^0, a procedure which yields to the Lippmann-Schwinger (L-S) type equation of non-relativistic quantum mechanics [LS50][2].

Another approximation typically employed is the on-shell reduction of the B-S equation. In this approximation the kernel is split into an on- and an off-shell part [OOR00]. In a one loop diagram, it can be explicitly shown that the contribution from the off-shell part goes into renormalization of couplings and masses and can be omitted in the calculation. These arguments can be extended to higher order loops and then V_{il} and T_{lj} can be factorized outside the integral of Eq. (2.31). This simplifies the coupled integral equations to a set of algebraic equations:

$$T_{ij}^{on} = V_{ij}^{on} + V_{il}^{on} G_l^{on} T_{lj}^{on} \quad \longrightarrow \quad T_{ij}^{on} = (1 - V_{il}^{on} G_l^{on})^{-1} V_{lj}^{on} \,, \tag{2.33}$$

where

$$G_l^{on} = \sum_l \int \frac{d^4k}{(2\pi)^4} \mathcal{D}_l(k,P) \tilde{\mathcal{D}}_l(k;P) \,. \tag{2.34}$$

Both approximations to the B-S equation will be described in the following lines.

[2]The Lippmann-Schwinger equation is the Schrodinger equation for two-particle scattering, with causal boundary conditions, written as an integral equation.

2.2.1 The Lippmann-Schwinger equation

We start describing the Lippmann-Schwinger (L-S) equation or three-dimensional reduction of the B-S equation. First of all we will make a simplification over the baryon propagator as we are only concerned with the positive energy contribution, which, in the center of mass frame $\vec{P}=0$, $P=(\sqrt{s},0)$, reads

$$\mathcal{D}_l(k;P)=\frac{1}{\not{P}-\not{k}_n-M_l+i\eta}\quad\longrightarrow\quad\frac{M_l}{E_l(\vec{k})}\frac{\overline{u_l}u_l}{\sqrt{s}-k^0-E_l(\vec{k})+i\eta}\,, \tag{2.35}$$

where M_l and $E_l(\vec{k})$ stand for the mass and the energy of the intermediate baryon, and k is the relative four-momentum. With respect to the meson propagator it is useful to split it into the positive and negative energy parts

$$\tilde{\mathcal{D}}_l(k;P)=\frac{1}{k_n^2-m_l^2+i\eta}\quad\longrightarrow\quad\frac{1}{2k^0}\left(\frac{1}{k^0+\omega_l(\vec{k})-i\eta}+\frac{1}{k^0-\omega_l(\vec{k})+i\eta}\right), \tag{2.36}$$

where m_l and $\omega_l(\vec{k})=\sqrt{\vec{k}^2+m_l^2}$ are the mass and the energy of the intermediate meson. The next step is to perform a k^0 integration that we separate in two parts, taking into account the expressions (2.35) and (2.36):

$$\begin{aligned}I_1&=\int_0^\infty\frac{dk^0}{k^0}\frac{1}{\sqrt{s}-k^0-E_l(\vec{k})+i\eta}\frac{1}{k^0+\omega_l(\vec{k})-i\eta}\,,\\ I_2&=\int_0^\infty\frac{dk^0}{k^0}\frac{1}{\sqrt{s}-k^0-E_l(\vec{k})+i\eta}\frac{1}{k^0-\omega_l(\vec{k})+i\eta}\,.\end{aligned} \tag{2.37}$$

We calculate the k^0 integration by contour integration, continuing the contour along the real line into the upper or lower half plane. The contours in the respective half planes are completed by describing a semicircle and returning to the real line avoiding the respective poles of the propagator. By taking the limit of infinitely large radius of the semicircle (no contribution in this limit is obtained from the integrals along the arcs of the semicircles), the k^0 integral along the real line can be evaluated as a sum of the contribution of the residues of the poles

inside the contour:

$$\oint_\gamma f(z)\,dz = 2\pi i \sum_{k=1}^{n} \mathrm{Res}(f, z_k^0)\,. \tag{2.38}$$

Specifically in the case of simple poles we apply the following equation to calculate the residues

$$\mathrm{Res}(f, z^0) = \lim_{z\to z^0}(z - z^0)f(z)\,, \tag{2.39}$$

which in turn implies the following results

$$I_1 = 0 \;\;;\;\; I_2 = 2\pi i \frac{1}{\omega_l(\vec{k})} \frac{1}{\sqrt{s} - E_l(\vec{k}) - \omega_l(\vec{k}) + i\eta}\;\; . \tag{2.40}$$

Defining

$$T_{ij} = \overline{u}_i \mathcal{T}_{ij} u_j\,, \tag{2.41}$$

we obtain the L-S equation after the k^0 integration

$$\begin{aligned} &T_{ij}(\vec{k}_i, \vec{k}_j; \sqrt{s}) = V_{ij}(\vec{k}_i, \vec{k}_j) \\ &+ \sum_l \int_0^\infty \frac{dk_n^3}{(2\pi)^3} F(\vec{k}) V_{il}(\vec{k}_i, \vec{k}_n) G_l(\vec{k}_n; \sqrt{s}) T_{lj}(\vec{k}_n, \vec{k}_j; \sqrt{s})\;\; , \end{aligned} \tag{2.42}$$

where the propagator reads

$$G_l(\vec{k}_n; \sqrt{s}) = \frac{M_l}{E_l(\vec{k}_n) 2\omega_l(\vec{k}_n)} \frac{1}{\sqrt{s} - E_l(\vec{k}_n) - \omega_l(\vec{k}_n) + i\eta}\,. \tag{2.43}$$

Since the L-S integral equation diverges at large values of the relative momenta $|\vec{k}|$, one needs to regularize it. Taking into account that the L-S equation must be solved numerically we have inserted in Eq. (2.42) a form factor regulator, $F(\vec{k})$, which depends on a cut-off momentum. Apart from regularizing the integral, the form factor introduces and encodes the complex structure of hadrons in the model. Along the thesis, we will check the dependence of the results with two types of form factors, the dipolar $F_D(\vec{k})$ and the gaussian $F_G(\vec{k})$ one, which contain the

correspondent cut-off parameters, λ_D and λ_G, respectively:

$$F_D(\vec{k}) = \frac{{\lambda_D}^2}{({\lambda_D}^2 + \vec{k}^2)^2} \quad ; \quad F_G(\vec{k}) = \exp\left[\frac{-\vec{k}^2}{2{\lambda_G}^2}\right] . \tag{2.44}$$

We note that the L-S equation employs, for a given value of the total scattering energy $\sqrt{s}$, the transition potential between any arbitrary pair of the relative momenta within the cut-off value. In the case of the TVME kernel, the full dependence on the momentum transfer is kept. This procedure follows the same spirit of the usual meson-exchange models of the nucleon-nucleon interaction [MHE87], also applied to meson-baryon scattering models [BHMG$^+$90, MGHS90, HDH$^+$95, HKMS07].

In order to solve the L-S equation, we can use any of the kernels with off-shell momenta that we have already presented in Section 2.1, the TVME (Eq. (2.20)), the TVME$_{t\to 0}$ (Eq. (2.21)) and the W-T (Eq. (2.24)) kernel. For instance, we will devote the next Chapter to compare the various models that we can build taking into account the particular approximation to the B-S equation and the different kernels we have presented. For a detailed description of the numerical integration of the L-S equation, see Appendix A, where we have also shown the numerical stability of the L-S equation with respect to the type of mesh applied in the integration, as well as the dependence of results to the form factor employed.

2.2.2 The on-shell reduction of the B-S equation

The problem of solving the B-S equation in on-shell approximation is reduced to solving the meson-baryon propagator integral of Eq. (2.34) which also diverges. Thus, it is necessary to apply regularization techniques, as in the L-S integral equation. We present two regularization methods typically adopted in literature for the B-S equation in on-shell approximation, the dimensional regularization and the the cut-off momentum regularization. After that, we will show the dynamical generation of a resonance with both approximations, taking the case of the $\Lambda_c(2595)$ resonance as an example.

• **Dimensional regularization**

The advantage of using dimensional regularization (DR) techniques in order to solve divergent integrals is that translational invariance and gauge invariance is preserved [Lei75]. Contrary to the cut-off method, the DR regularization is less intuitive and is based on the replacement of a four dimensional integral (Eq. (2.34)) by an n–dimensional one:

$$\int_0^\infty d^4k\ f(k)\ \longrightarrow\ \int_0^\infty d^nk\ f(k)\,. \tag{2.45}$$

We integrate in n dimensions and replace $n \to 4-\eta$, obtaining the finite part of the loop function for the physical limit $\eta \to 0$

$$\begin{aligned} G_i^{DR}(\sqrt{s}) = \frac{2M_i}{16\pi^2}\Big\{ a_i(\mu) + \ln\frac{M_i^2}{\mu^2} + \frac{m_i^2 - M_i^2 + s}{2s}\ln\frac{m_i^2}{M_i^2} + \\ \frac{|\vec{k}_i^{on}|}{\sqrt{s}}\ln\frac{M_i^2 + m_i^2 - s - 2|\vec{k}_i^{on}|\sqrt{s}}{M_i^2 + m_i^2 - s + 2|\vec{k}_i^{on}|\sqrt{s}}\Big\}\,, \end{aligned} \tag{2.46}$$

with $|\vec{k}_i^{on}|$ the modulus of the on-shell momentum of channel i (see Eq. (2.28)). The subtraction constants $a_i(\mu)$ for each channel, which determine the finite part of the loop at the renormalization scale $\mu \approx 1$ GeV [MR06], are calculated following the work [HL05] as $G_i^{DR}(\sqrt{s} = \sqrt{m_i^2 + M_i^2}) = 0$, where the channel i is the lightest one for an specific sector. On top of that, some of them can be re-adjusted, remaining close to its natural size $a_i(\mu) \approx -2$ [OOP99, OM01], in order to reproduce experimental data.

• **Cut-off regularization**

As we already mentioned in our discussion of the L-S equation, an obvious choice to regularize a divergent integral is to integrate it for a very large momentum instead of integrating it to infinity. The analytical expression obtained regularizing the integral (Eq. (2.34)) with a cut-off momentum, λ, through a dipolar form factor type is [OOP99]:

$$
\begin{aligned}
G_i^{cut}(\sqrt{s}) = \frac{2M_i}{16\pi^2}\Bigg\{ & \ln\left(\frac{m_i^2 M_i^2}{\lambda^4}\right) - \frac{M_i^2 - m_i^2}{s}\ln\left(\frac{m_i^2}{M_i^2}\right) \\
& + 2\frac{M_i^2 - m_i^2}{s}\ln\frac{1+\sqrt{1+\frac{m_i^2}{\lambda^2}}}{1+\sqrt{1+\frac{M_i^2}{\lambda^2}}} \\
& - 2\ln\left(1+\sqrt{1+\frac{m_i^2}{\lambda^2}}\right)\left(1+\sqrt{1+\frac{M_i^2}{\lambda^2}}\right) \\
& + \frac{4k_i^2}{s}\left(\ln\frac{s - M_i^2 - m_i^2 + 4|\vec{k}_i^{on}|^2\sqrt{1+\frac{m_i^2}{\lambda^2}}}{-s + M_i^2 - m_i^2 + 4|\vec{k}_i^{on}|^2\sqrt{1+\frac{m_i^2}{\lambda^2}}}\right. \\
& \left.\left. + \ln\frac{s + M_i^2 - m_i^2 + 4|\vec{k}_i^{on}|^2\sqrt{1+\frac{m_i^2}{\lambda^2}}}{-s - M_i^2 - m_i^2 + 4|\vec{k}_i^{on}|^2\sqrt{1+\frac{m_i^2}{\lambda^2}}}\right)\right\}.
\end{aligned}
\tag{2.47}
$$

Although the cut-off momentum regularization does not preserve the symmetries that DR does, we introduce it here to simplify the comparison between the off-shell models (using the L-S equation) and the on-shell ones (using the on-shell reduction to the B-S equation) presented in Chapter 3. All models will be regularized with the cut-off method using a common single parameter, the cut-off λ.

• Cut-off versus dimensional regularization

In the following, we want to show that different regularizations schemes applied to the loop function (see Eq. (2.34)) can reproduce the same results by varying in a reasonable way the specific parameters in each model. In Fig. 2.5 we show the modulus of the total T matrix for the coupled-channel system in the $(I = 0,\ S = 0,\ C = 1)$ sector. We want to reproduce the $\Lambda_c(2595)$ resonance, which will be explained in detail in the next Chapter, at 2595 MeV and width $\Gamma = 3$ MeV. We calculate the T matrix with the on-shell approximation and describe the meson-baryon interaction with the W-T kernel (Eq. (2.24)), but using different regularizations of the loop. The parameters to be fitted are the f meson coupling constant coming from the kernel, and from the loop propagator,

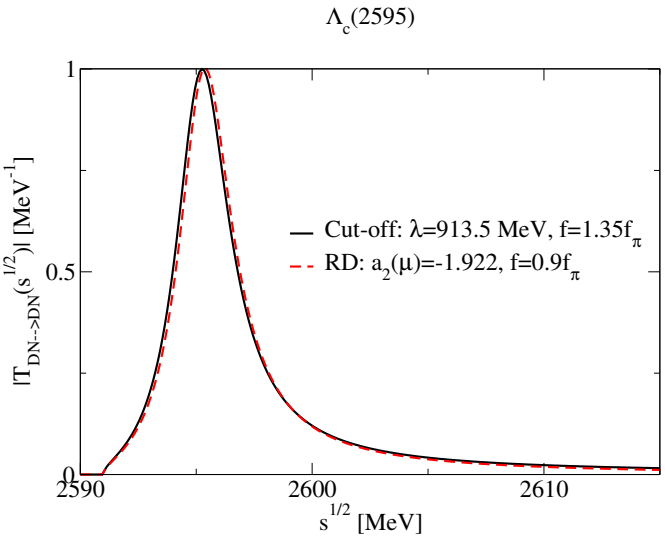

Figure 2.5: The $\Lambda_c(2595)$ resonance generated with the on-shell $T(\sqrt{s})$ matrix for two regularization schemes of the meson–baryon propagator. The solid line corresponds to the cut-off regularization, and the dashed line is the result applying dimensional regularization. Parameters have been fitted to reproduce in both models the position and width to 2595 MeV and having a width of 3 MeV, respectively. For simplicity, the T matrix has been normalized to unity in both models.

the subtraction constants in the DR scheme or the parameter λ in the cut-off regularization scheme. As it is shown in Figure 2.5, tuning the parameters we are able to reproduce the same results for the $\Lambda_c(2595)$ resonance. For the cut-off regularization, the parameters are fixed to $f = 1.35 f_\pi$ and $\lambda = 913.5$ MeV/c, and for the DR scheme at a regularization scale $\mu = 1$ GeV, $f = 0.9 f_\pi$ and the subtraction constant for the second channel (which mostly dominates the resonance), $a_2(\mu) = -1.922$. This relation between the parameters from the cut-off λ and the dimensional regularization parameters, μ, $a_i(\mu)$, are in accordance with the "natural" values discussed in the studies done in [OOP99, OM01], where the following relations are given

$$\mu \approx 1.2\lambda \quad ; \quad a_i(\mu) \approx -2\,. \tag{2.48}$$

• Singularities of the on-shell TVME kernel

Unlike the case of the L-S equation, we will not solve the B-S equation with the full TVME kernel in on-shell approximation. As we will see in the next Section, a bound state is described by the presence of a pole in the T matrix in a certain meson-baryon channel. However this discontinuity must not arise from the interaction kernel V_{ij} itself [LK02]. As we can see in the TVME equation of the kernel (Eq. (2.20)) for on-shell momenta, one finds an infinite which comes from a logarithmic divergence in the kernel when the limit $a^{on} \to b^{on}$ is fulfilled (see Eqs. (2.29)). These singularities, which occur at subthreshold energies, naturally arise from the non-local character of the t, s or u-channel exchange diagrams [LK02]. For the TVME kernel, working with a certain diagonal channel for simplicity, the logarithmic divergences appear at

$$|\vec{k}^{on}|^2 \to -\frac{m_v^2}{2}\,. \tag{2.49}$$

Using Eq. (2.28) relating the total energy of the system $\sqrt{s}$ with the on-shell momentum $|\vec{k}^{on}|$, we see that the logarithmic divergences appear at subthreshold energies. In Fig. 2.6 we show the on-shell TVME kernel for the diagonal DN channel depending on $\sqrt{s}$. One can see two peaks where the kernel goes to minus infinite, each one coming from the different vector meson interchanged, the ρ and the ω meson. These artifacts are located at important energies for the treatment of the meson-baryon dynamics and then we cannot obtain the T matrix using the on-shell reduction of the B-S equation with the TVME kernel. On the other hand, the L-S equation is suitable to be employed in order to calculate the T matrix with the TVME kernel. In this case, the $a \to b$ limit for off-shell energies (see Eqs. (2.17)) is never fulfilled because the off-shell momenta used in the intermediate states of the integral equation are independent of the total energy, and they always fulfill $|\vec{k}|^2 \geq 0$, which will not produce any singularity in the kernel.

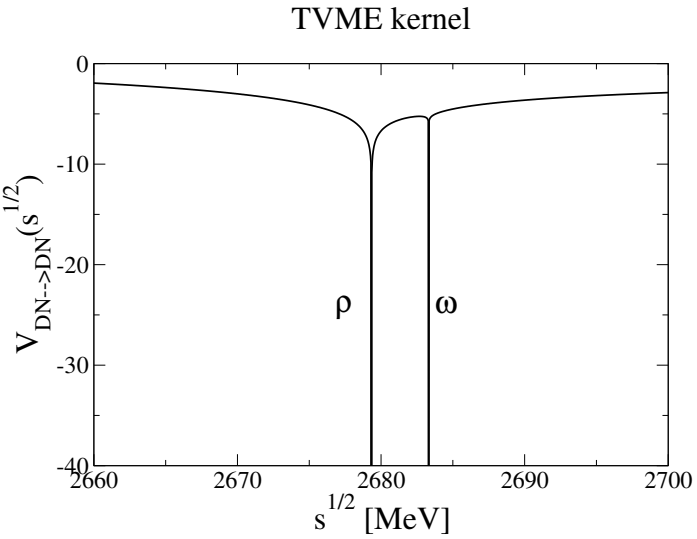

Figure 2.6: On-shell TVME kernel for diagonal DN channel depending on $\sqrt{s}$.

2.3 Characterization of bound states

2.3.1 Pure bound states and resonances

Experimental cross sections present pronounced peaks in the neighborhood of a resonance when the incident energy is varied. Those bumps can be parametrized with a Breit-Wigner function. We extract two parameters from the fit, the position of the maximum M, called the mass of the resonance, and the full width Γ that the peak presents at half its maximum (FWHM), inversely proportional to its time-decay. Theoretically, both parameters are extracted from the T matrix whenever it presents a pole. The loop propagator contained in the T matrix has branch points at every channel of two particles, and therefore we need to search for poles of the T matrix in the complex energy plane. For that purpose we need to consider Riemann sheets. We can expand the T matrix in a Laurent series around the pole position z_0,

$$T^{ij} = \frac{a^{ij}_{-1}}{z - z_0} + a^{ij}_0 + \mathcal{O}(z - z_0)\,. \tag{2.50}$$

The first contribution is called Breit-Wigner term and contains the pole, whose real and imaginary parts correspond to the mass and halfwidth of the resonance, $z_0 = M - i\frac{\Gamma}{2}$.

The physical meaning of a pole in the T matrix depends on the Riemann sheet it is located. Those poles that we can find in the real energy axis, or physical (first) Riemann sheet, are called pure bound states and they are located below the lightest threshold. In this case, the bound-states are stable states that cannot decay via the strong force in any meson–baryon channel of the sector to which it belongs, and thus the bound-state presents a zero width. However, the so called resonance–poles, which are poles of the T matrix located over threshold, can only be found for complex energies, in unphysical Riemann sheets. A resonance–pole represents an unstable system which decays into a more stable one.

The T matrix can be defined on the complex energy plane by analytical continuation, see e.g. [SSL09, NRA01b]. Since the energy is a function of the momentum squared p^2, the T matrix is a single-valued function of the momentum p, but a double–valued function for the energy E. Therefore, there are two possible Riemann-sheets of complex energy, which are specified by the sign of the imaginary part of the momentum p, the physical one with $Im(p) > 0$ and the unphysical one with $Im(p) < 0$. For a multichannel case, the analytic structure of the T matrix becomes more complicated as there are two sheets for each channel. Therefore, an n-channel system gives rise to 2^n Riemann sheets, which will also be specified by all the set of signs of $Im(p_i)$.

From all the possible unphysical sheets, we will just consider the sheet which has the biggest influence into the real energy axis. We will refer to this unphysical sheet as the "second Riemann sheet", and the T–matrix poles in this sheet are the ones which reflect as resonance-poles for real energies.

Since the kernel is real, the second Riemann sheet is defined by changing the sign of the imaginary part of the momentum for open channels, $m_i + M_i < E$, in the propagator function. In that case, the discontinuity of the propagator at the threshold in the real axis is known to be two times its imaginary part [IOVV02]. Therefore, knowing the propagator in the first Riemann sheet, G_i, one determines the propagator in the second Riemann sheet, G_i^{2nd}, as

$$G_i^{2nd}(\sqrt{s}) = \begin{cases} G_i(\sqrt{s}) & at \quad Re(\sqrt{s}) \leqslant m_i + M_i \,, \\ G_i(\sqrt{s}) - 2iIm\left[G_i(\sqrt{s})\right] & at \quad Re(\sqrt{s}) > m_i + M_i \,. \end{cases} \tag{2.51}$$

Since we cannot explore the entire half-complex plane numerically, we choose a finite region for the search of poles in the second Riemann sheet. Those poles with $Im(\sqrt{s}) \geq 300$ MeV are dismissed. It means that we are neglecting poles with $\Gamma > 600$ MeV, whose influence in the real axis is negligible.

2.3.2 Couplings to the different channels

The position of a pole in the second Riemann sheet of the T matrix, T^{2nd}, does not depend on the meson-baryon channel. However, the value of the residues around the pole depends on the specific transition, from a channel i to j, explored. The residue a_{-1}^{ij} from Eq. (2.50), is related to the couplings of the resonance to the different channels as

$$a_{-1}^{ij} = g_i g_j \,. \tag{2.52}$$

We can extract the couplings from the pole in the complex energy plane of the T matrix in several ways. We can calculate it numerically as

$$g_i g_j = \lim_{z \to z_0} (z - z_0) T_{ij}^{2nd}(z) \,, \tag{2.53}$$

with the pole position $z_0 = M - i\frac{\Gamma}{2}$. It can also be extracted by contour integration along a certain path around the pole position z_0

$$a_n^{ij} = \frac{1}{2\pi i} \oint \frac{T_{ij}^{2nd}(z)}{(z - z_0)^{n+1}} dz \,, \tag{2.54}$$

and numerically calculated through an iterative procedure [D$^+$11]:

$$\frac{\partial}{\partial z} \left(\frac{1}{T_{ij}^{2nd}(z)} \right) \Big|_{z_0} = \frac{1}{g_i g_j} \,. \tag{2.55}$$

2.3.3 Cusps or threshold effects

A pole of the T matrix located in other Riemann sheets can reflect in real energies as a cusp located at a certain threshold, therefore it may also leave a distinct signal in the experimental cross section. In scattering matrix theory, a cusp can be properly called a particle because it arises from a pole in the T matrix. However, they are not considered resonances but threshold effects from the experimental point of view.

As an example, let's take the simplest case of a two channel system. The surface of the two channel T matrix has four sheets. As discussed before, the Riemann sheets are classified by the sign of the imaginary part of the momentum:

- Sheet I, $Im(p_1) > 0$ and $Im(p_2) > 0$.
- Sheet II, $Im(p_1) < 0$ and $Im(p_2) > 0$.
- Sheet III, $Im(p_1) < 0$ and $Im(p_2) < 0$.
- Sheet IV, $Im(p_1) > 0$ and $Im(p_2) < 0$.

On the one hand, a pole located on the sheet I (physical sheet) will appear as a pure–bound state for a real energy under the first threshold, as explained above. Moreover, poles in the sheet II would leave a characteristic resonance–pole structure at the energy range between both thresholds (second Riemann sheet). Besides, a pole located at the sheet III will not have any influence in the real axis [FH64]. However, it can be shown that a pole on the sheet IV will be reflected itself as a cusp in the scattering matrix at the energy of the second threshold [FH64]. The height or strength of this cusp increases as the pole position gets closer to the real axis in sheet IV. If we manage to vary the position of the pole, it can jump into the sheet II, and then it may become a visible resonance peak in the real axis located in between the two thresholds.

An example of this case is shown in Fig. 2.7 for a reduced two channel system, $\pi\Sigma_c$ and DN, of the isospin $I = 0$, strangeness $S = 0$, and charm $C = 1$ sector. The two thresholds are located at 2591 MeV for $\pi\Sigma_c$ states and 2806 MeV for DN ones. To see this effect, we force the DN bound state (which experimentally is located at 2595 MeV) to move from one sheet to another through the

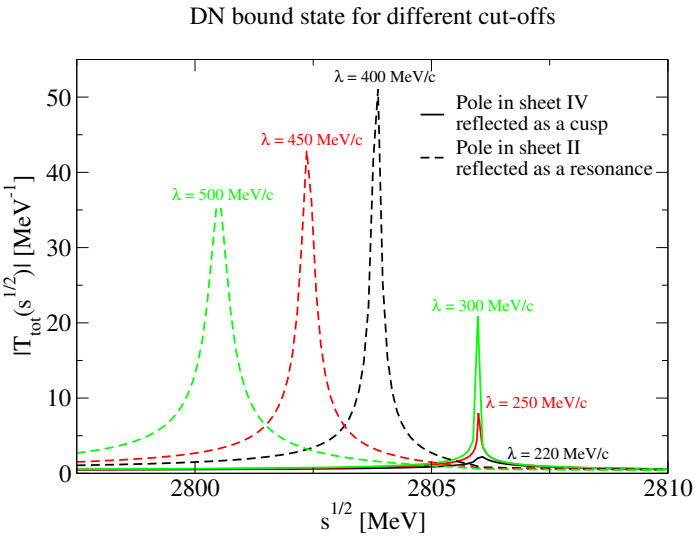

Figure 2.7: We represent the modulus of the total T matrix for two channel system in the ($I = 0$, $S = 0$, $C = 1$) sector with respect to $\sqrt{s}$. We have solved the T matrix with the on-shell reduction of the B-S equation, using the W-T kernel and regularizing the loop with a cut-off λ. We force the DN bound state to move from the DN threshold, where it appears as a cusp structure (solid lines), to energies below threshold, where it becomes a visible resonance (dashed lines) by varying the cut-off parameter from 220 MeV/c to 500 MeV/c. The f meson coupling constant parameter has been fixed to $f = 1.15 f_\pi$.

DN threshold, by varying the cut-off parameter applied to regularize the meson-baryon propagator. As the cut-off value is increased from 220 MeV to 500 MeV, the DN state evolves from a cusp at the DN threshold (pole in the sheet IV) to a clear resonance in between the $\pi\Sigma_c$ and DN thresholds (pole in the sheet II). The solid lines represent situations in which the pole is found in sheet IV, while the dashed lines correspond cases in which the pole is located in sheet II and the aspect is typically the one of a resonance.

2.3.4 Last remarks

There are some advantages in looking for poles in the complex energy plane instead of, for example, parametrizing the different bumps of the T matrix to a

Breit-Wigner function. As an example, one may consider the case when there are two resonances which are so close to each other in the real axis that one cannot disentangle them by analyzing the T matrix in the physical sheet. Looking for poles in the complex energy plane may definitely decide whether the bump in the T matrix is due to a single resonance or the structure is the result of various resonances that overlap each other. This is the case of the double-pole nature of the $\Lambda(1405)$ resonance in the strange sector which will be studied in detail in the next chapter. The $\Lambda(1405)$ was measured in the sixties [ASZ65], and even before its discovery, it was dynamically generated theoretically as an unstable $\overline{K}N$ bound state [DT59b]. However, it was few decades later when the existence of two poles contributing to the invariant $\pi\Sigma$ mass distribution of the nominal $\Lambda(1405)$ was pointed out in [OM01], and was thoroughly analyzed [JOO$^+$03] in the context of chiral models. The wide width of the second pole discovered, together with its close location to the energy position of the $\overline{K}N$ bound state, made it difficult to be distinguishable by just analyzing the T matrix for real energies.

In summary, we will analyze those resonances over threshold which can be related to poles located on the second Riemann sheet, and the pure bound-states below the energy threshold as singularities of the T matrix in the real energy axis, and they will be characterized by the mass M, width Γ and couplings to the different channels g_i.

3

Charm versus strangeness

This Chapter is an attempt to study and compare the $\Lambda(1405)$ and the $\Lambda_c(2595)$ resonances which belong to the strange ($S = -1$) and charm ($C = 1$) sectors, respectively. The $\Lambda(1405)$ is a baryon resonance and its discovery in the sixties [ASZ65] implied for the first time in hadronic physics the need to find alternative ideas to the formation of baryon resonances, different from the 3-quark excited state established in the quark model. The existence of the $\Lambda_c(2595)$ resonance was predicted many years ago but discovered only three decades after the $\Lambda(1405)$ [E$^+$95]. The $\Lambda_c(2595)$ can be considered the charmed homologous of the $\Lambda(1405)$, sharing with it a common physical origin. We will analyze, in a simplified manner, the similarities and differences of these resonances with the representative effective models described in the previous Chapter.

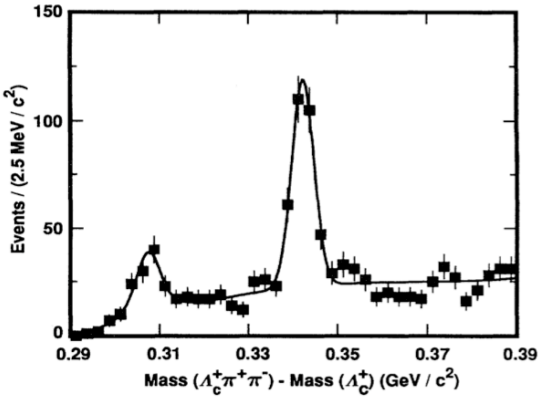

Figure 3.1: Fit to the mass difference $M(\Lambda_c^+\pi^+\pi^-) - M(\Lambda_c^+)$ plot, taken from the published article of the first observation of $\Lambda_c(2595)$, from CLEO experiment [E$^+$95]. The largest peak at a mass difference of 342 MeV/c^2 is related to the $\Lambda_c(2625)^+ \longrightarrow \Lambda_c^+\pi^+\pi^-$ and the smaller but significant one at a mass difference of 308 MeV/c^2 corresponds to the first observation of the $\Lambda_c(2595)^+$ decaying into the $\Lambda_c^+\pi^+\pi^-$ channel.

3.1 The $\Lambda_c(2595)$ and the $\Lambda(1405)$ resonances

The $\Lambda_c(2595)$ charmed baryon was first observed by the CLEO collaboration in 1995 [E$^+$95], and it was the fourth charmed baryon detected since the $\Sigma_c(2455)$ was discovered in 1975 [C$^+$75]. The $\Lambda_c(2595)$ was observed as a peak in the $M(\Lambda_c^+\pi^+\pi^-) - M(\Lambda_c^+)$ mass difference spectrum, together with the already known at that time $\Lambda_c(2625)$ resonance (see Fig. 3.1). After the first observation of the $\Lambda_c(2595)$ resonance three more laboratories, Fermi National Accelerator Laboratory (FNAL) [BFPY03], ARGUS [A$^+$97] and Johns Hopkins University (JHU) [F$^+$96], also confirmed its existence. Nowadays, the $\Lambda_c(2595)$ resonance is one of the best established resonances over the 17 charmed baryons detected. It has $C = 1$, isospin $I = 0$, spin $\frac{1}{2}$ and charge $+1$. The mass of the resonance is 2595.4 ± 0.6 MeV and its total width is $3.6^{+2.0}_{-1.3}$ MeV. It is experimentally seen in the $\Lambda_c\pi\pi$ decay mode but never in the $\Lambda_c\pi$ one, so it seems that the $\Lambda_c(2595)$ is the first excited resonance of the isoscalar Λ_c rather than of the isovector Σ_c state. The branching ratios, or likelihood of the $\Lambda_c(2595)$ to decay to a particular

$\Lambda_c(2595)^+$ decay mode	Branching ratio Γ_i/Γ
Pure 2-body	
$\Sigma_c^{++}\pi-$	0.24
$\Sigma_c^{+}\pi^0$	0.24
$\Sigma_c^{0}\pi^+$	0.24
Pure 3-body	
$\Lambda_c^+\pi^+\pi^0$	0.19
$\Lambda_c^+\pi^0\pi^0$	0.09

Table 3.1: Branching ratio for the $\Lambda_c(2595)$ decay modes, taken from PDG [N$^+$10].

mode [N$^+$10], are given in Table 3.1. It can be appreciated that 3-body $\Lambda_c\pi\pi$ decays represent only 1/3 of the total, whereas most of them come from the 2-body $\Sigma_c\pi$ decay modes. The $\Lambda_c(2595)$ resonance decays almost certainly in s-wave, and expecting that total angular momentum and parity of Σ_c are $J^P = 1/2^+$ (not proven yet), the values for the $\Lambda_c(2595)$ are $J^P = \frac{1}{2}^-$.

It can be useful to compare the results of the charm sector with the hierarchy of the known baryons which are present in the strange sector. The idea is to explore how similar is the spectrum of charmed baryons to that of the strange ones. The $\Lambda_c(2595)$ is well known to be the charmed counterpart of the $\Lambda(1405)$ resonance in the strange sector, by replacing a s quark with a c quark. The reason why it is important for us to understand the characteristics of the $\Lambda(1405)$ is that similar physics should be involved in the $\Lambda_c(2595)$ resonance and, in general, in several resonances of the charm spectrum.

The $\Lambda(1405)$, discovered in 1965 [ASZ65], has strangeness $S = -1$, isospin $I = 0$, spin $\frac{1}{2}$ and charge 0. Its mass and width are, $M = 1405.1^{+1.3}_{-1.0}$ MeV and $\Gamma = 50 \pm 2$ MeV, respectively. It has a special relevance in hadron physics because it opened a crucial debate regarding its nature, whether the $\Lambda(1405)$ is a 3-quark excited state, or it has a dynamical origin, i.e. qualifies better as a molecular state generated by the interaction of a meson and a baryon. This new dynamical origin considered for the first time for the $\Lambda(1405)$ was motivated by the failure of the constituent quark model in the prediction of the mass of the resonance. The quark model has been a very powerful guide in order to classify hadrons found experimentally, however the $\Lambda(1405)$ is an exception. The quark model prediction for the mass of the $\Lambda(1405)$ is approximately 80 MeV higher than the

	$\Lambda_c(2595)$	$\Lambda(1405)$
J^P	$\frac{1}{2}^-$	$\frac{1}{2}^-$
(I,S,C)	$(0,0,1)$	$(0,-1,0)$
Q	$+1$	0
M [MeV]	2595.4 ± 0.6	$1405.1^{+1.3}_{-1.0}$
Γ [MeV]	$3.6^{+2.0}_{-1.3}$	50 ± 2
Decay modes	$\pi\Sigma_c$,$\Lambda_c\pi\pi$	$\pi\Sigma$

Table 3.2: Comparison, for the $\Lambda_c(2595)$ and for the $\Lambda(1405)$, of the main characteristics: quantum numbers, mass, width and main decay modes [N$^+$10].

experimental value. This discrepancy was explained in terms of threshold effects (the $\overline{K}N$ threshold is just above the $\Lambda(1405)$ resonance), and also by the fact that the quark model calculations are restricted to 3-quark states. Therefore, this inconsistency strongly suggests the importance of the dynamical origin for the nature of resonances like the $\Lambda(1405)$.

The first theoretical studies of the dynamical character of resonances were carried out by Richard Dalitz [DT59b, DT59a, DT60], in particular applied to the analysis of the $\Lambda(1405)$ resonance. These studies led to the idea that the $\Lambda(1405)$ was not a regular resonance and that it could be explained as the result of an unstable bound state of the $\overline{K}N$ meson baryon system. The work of Dalitz and others [BF61, Wyl67, DWR67, LW67, Raj72, SW88] was adapted in recent years to the language of chiral Lagrangians. This has allowed the theoretical prediction of the dynamical character of many of the light resonances in the SU(3) sector. In the particular case of the $J^P = 1/2^-$ resonances, they can be generated dynamically from the interaction in s-wave of mesons of the pseudoscalar 0^- octet with the $1/2^+$ ground-state baryons. The two-pole nature of the $\Lambda(1405)$, firstly announced in the theoretical work of [OM01] and deeply analyzed in [JOO$^+$03], is an important consequence of these studies that have been confirmed through analyses [MOR05, JOS09] of different experimental reactions [TEFK73, P$^+$04, B$^+$77]. This implies that the observed $\Lambda(1405)$

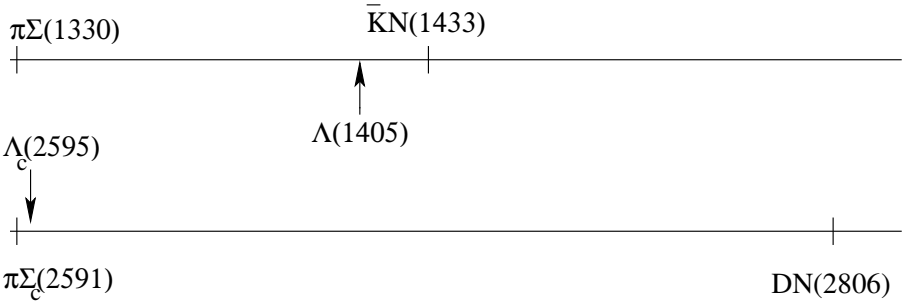

Figure 3.2: The $\Lambda(1405)$ resonance is placed between the $\pi\Sigma$ and $\overline{K}N$ thresholds and the $\Lambda_c(2595)$ between the $\pi\Sigma_c$ and DN ones. The difference is that the $\Lambda(1405)$ is close and below the second threshold, $\overline{K}N$, while the $\Lambda_c(2595)$ is just a few MeV above the first threshold, $\pi\Sigma_c$.

resonance is not the effect of one single pole, but a superposition of the effect of two resonances located around 1405 MeV, which couple to different meson-baryon channels. The low mass resonance is predicted to have a large width and couples mostly to $\pi\Sigma$ channels while the higher mass resonance has a narrower width and couples mainly to the $\overline{K}N$ one. It has already been confirmed that this $\overline{K}N$ molecular state is located around 1420 MeV [JOS09] from experimental data in [B$^+$77] where particles were detected by the bubble chamber, although some more phenomenological models predict it at lower energies [EAY10].

The experimentally tested dynamical origin of the $\Lambda(1405)$ is the main motivation of this thesis which aims at extending the study to the baryons in the charm sector. There are some similarities between the $\Lambda(1405)$ and the $\Lambda_c(2595)$ states, but the dynamics involved in each resonance look different. Despite of the experimentally accepted two double pole structure of the $\Lambda(1405)$, the $\Lambda_c(2595)$ resonance seems to have a single pole structure. Both resonances are placed in between the lightest and the second meson-baryon thresholds (see Fig. 3.2) but the location of each resonance in between the respective thresholds makes them to have different properties. These differences are going to be analyzed through the implementation of different effective models which will be explained below.

B-S equation \ kernel	WT	$\text{TVME}_{t\to 0}$	TVME
On shell	Model 1: WT^{on}	Model 2: $\text{TVME}^{on}_{t\to 0}$	✗
Off shell	Model 3: WT^{off}	Model 4: $\text{TVME}^{off}_{t\to 0}$	Model 5: TVME^{off}

Table 3.3: Summary of the different models we get by combining two different approaches of solving the B-S equation and three types of kernels. Models 1 and 2 solve the on-shell scattering equation and models 3, 4 and 5 solve the off-shell scattering equation. The WT kernel is implemented in models 1 and 3, the $\text{TVME}_{t\to 0}$ is applied in models 2 and 4, and only model 5 uses the complete TVME kernel. The TVME cannot be applied to solve the on-shell scattering equation due to the appearance of a non-physical infinite each time that the interchange of the vector meson between the pseudo-scalar meson and the ground state baryon takes place, as it was already explained in previous Chapter, when the $|\vec{k}^{on}|^2 \to -\frac{m_v^2}{2}$ limit is fulfilled.

3.2 Toy models

We will consider five different effective models to analyze each sector, which result from the combination of two different approaches of solving the B-S equation and three different kernels (see Table 3.3). Both ways of solving the B-S equation were already shown in the previous Chapter, as well as the different kernels considered. We will respectively call "off-shell" to the three-dimensional reduction of the B-S equation or L-S equation (see Eq. (2.42)), and "on-shell" to the on-shell approximation (see Eq. (2.33)). Note that we get five models and not six because, as it was already said in the previous Chapter (see Section 2.2.2 in Chapter 2), the full TVME kernel (see Eq. (2.20)) can not be applied to solve the on-shell B-S equation due to the appearance of non-physical infinities in the kernel when the $|\vec{k}^{on}|^2 \to -\frac{m_v^2}{2}$ limit is fulfilled.

With respect to the three different kernels considered, WT, $\text{TVME}_{t\to 0}$ and TVME type (see Eqs. (2.24), (2.21) and (2.20)), they will be built using on-shell

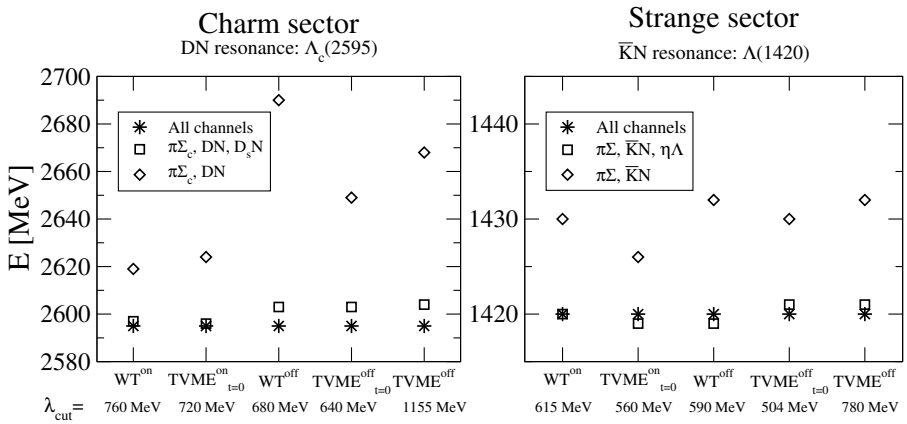

Figure 3.3: Both panels show the position of the resonances for the different coupled-channel systems considered, in the case of charm (left panel) and strange (right panel) sectors. The cut-off is fixed in each sector for the whole system of coupled-channels (marked with star symbols) to reproduce the position of the $\Lambda_c(2595)$ and of the $\Lambda(1420)$ resonance. The square symbols indicate the position of the resonances when the three most important channels are coupled and the diamond symbols are the results when just the first and second channels are considered. There are no important differences between coupling all channels and the case of coupling three channels. Therefore, each sector will be reduced to a three coupled-channel problem.

or off-shell energies depending if they are applied to solve the on-shell or off-shell scattering equation, respectively.

To obtain the T matrix from the off-shell solution of the L-S equation one necessarily has to regularize the integral with a form factor which depends on a cut-off λ (see Eq. (2.44)). To compare more easily between the off-shell and on-shell approaches we will also solve the on-shell T matrix regularizing the loop integral with a cut-off, instead of solving it with the dimensional regularization method as it is usually employed in the on-shell models. This cut-off will be our free parameter to fix the different models to the experimental information available in each sector: the $\Lambda_c(2595)$ resonance in the charm sector, and the $\Lambda(1420)$ resonance in the strange one.

Another parameter we need to fix is the meson coupling constant (f) in the WT kernel or the universal coupling constant (g) in the $\text{TVME}_{t\to 0}$ and TVME

	$\pi\Sigma_c$	DN	$D_s\Lambda$
$\pi\Sigma_c$	$8(\rho)$	$\sqrt{6}(D^*)$	0
DN	$\sqrt{6}(D^*)$	$3(\rho), 3(\omega)$	$2\sqrt{3}(K^*)$
$D_s\Lambda$	0	$2\sqrt{3}(K^*)$	$2(\phi)$

	$\pi\Sigma_c$	DN	$D_s\Lambda$
$\pi\Sigma_c$	8	$\kappa\sqrt{6}$	0
DN	$\kappa\sqrt{6}$	6	$2\sqrt{3}$
$D_s\Lambda$	0	$2\sqrt{3}$	2

Table 3.4: The SU(4) coefficients for the ($I = 0$, $S = 0$, $C = 1$) sector. On the left: the $C_{ij,v}$ which are included at the $\text{TVME}_{t\to 0}$ and TVME kernels. The particle inside the parenthesis is the vector meson interchanged between the meson and the baryon in a specific transition. On the right: the $C_{ij}^{WT} = \sum_V C_{ij,v}$ coefficients corresponding to the W-T kernel. The reduction factor $\kappa = (m_v/m_v^C)^2 \approx 1/4$ is introduced in transitions driven by charmed vector meson exchanges (D^*,D_s and J/ψ).

ones, already introduced in the previous Chapter. Using the KSFR relation in Eq. (2.4) that relates f with g, we will choose f as the common parameter for all the different kernels and it will be fixed to the value $f = 1.15 f_\pi$, where $f_\pi \approx 93$ MeV is the pion decay constant. This value of f has been commonly used for the strange sector in this kind of studies [GRNRAVV03, JOO$^+$03, OR98] and we will also employ it for simplicity in the charm sector.

In order to simplify the analysis to the most important aspects the minimum number of channels will be considered. Reducing each sector to the first two channels would imply to have the most simple coupled channel problem, as both experimentally tested resonances, $\Lambda_c(2595)$ and $\Lambda(1420)$, decay into the first channel and couple strongly to the second one. However, we have found necessary to include one more channel in each sector ($\eta\Lambda$ in the strange sector and $D_s\Lambda$ in the charm one) to keep the most relevant aspects of the full coupled-channel model, while still keeping the simplicity, as it is shown in Fig. 3.3.

In Tables 3.4 and 3.5 we show the SU(4) and SU(3) coefficients for the reduced system of three channels, which have been employed for the different kernels (the complete Tables are given in Appendix A). When the sign of the coefficients for the diagonal transitions is positive it means attraction between channels (in our sign convention), and one expects to find a bound state for an energy close to that meson-baryon threshold. In the case of the charm sector the three diagonal

	$\pi\Sigma$	$\overline{K}N$	$\eta\Lambda$
$\pi\Sigma$	$8(\rho)$	$\sqrt{6}(K^*)$	0
$\overline{K}N$	$\sqrt{6}(K^*)$	$3(\rho), 3(\omega)$	$3\sqrt{2}(K^*)$
$\eta\Lambda$	0	$3\sqrt{2}(K^*)$	0

	$\pi\Sigma$	$\overline{K}N$	$\eta\Lambda$
$\pi\Sigma$	8	$\sqrt{6}$	0
$\overline{K}N$	$\sqrt{6}$	6	$3\sqrt{2}$
$\eta\Lambda$	0	$3\sqrt{2}$	0

Table 3.5: The SU(3) coefficients for the ($I = 0,\ S = -1,\ C = 0$) sector. On the left: the $C_{ij,v}$ coefficients which are included at the $\text{TVME}_{t\to 0}$ and TVME kernels. The particle inside the parenthesis is the vector meson interchanged between the meson and the baryon in a specific transition. On the right: the $C_{ij}^{WT} = \sum_v C_{ij,v}^v$ coefficients corresponding to the W-T kernel.

transitions are attractive but we will only look at the bound states generated by the first two channels, the $\pi\Sigma_c$ and the DN, because we wish to analyze the $\Lambda_c(2595)$ resonance, which appears as a DN bound state. Apart from that, a bound state generated by the $D_s\Lambda \leftrightarrow D_s\Lambda$ transition is expected to be located in the vicinity of the $D_s\Lambda$ threshold at 3084 MeV, being too far from the energy range we are interested in. However in the strange sector the third channel does not introduce any additional bound state because the coefficient of the diagonal transition $\eta\Lambda \leftrightarrow \eta\Lambda$ is zero. The coefficients of the first two channels are identical to the charm sector ones, with the only difference of the non-diagonal transitions in which the vector meson interchanged in the charm sector is the D^* while in the strange sector is the K^*.

In summary, we have five different models to analyze each sector, the charm case is presented in Section 3.3 and the strange sector in Section 3.4. Both of them are simplified to a three coupled channel problem, and the models just depend on one free parameter, the cut-off momentum λ. We will vary this cut-off so as to study how the position of the resonances behaves in each model (see Figs. 3.4, 3.5 and 3.6, 3.7) and finally, we will fix it to the value that reproduces more accurately the experimental information in each sector, showing the numerical results (mass of the resonances, width and couplings) in Tables 3.6 and 3.7.

3.3 Results for the charm sector

We find two resonances in the charm sector, each of them coupled differently to the first two channels, $\pi\Sigma_c$ and DN. They appear as bound states of the $\pi\Sigma_c \leftrightarrow \pi\Sigma_c$ and $DN \leftrightarrow DN$ transitions when solving the uncoupled-channel case. Therefore we will refer to them as $\pi\Sigma_c$ and DN resonances, respectively. We can see in Fig. 3.4 (on-shell models) and Fig. 3.5 (off-shell models) the dependence of both resonances with the cut-off.

At first glance, we observe that the on-shell models gives rise to a milder dependence on the position of the resonances with the cut-off than the corresponding off-shell models (first two panels in Fig. 3.5). This behavior is more pronounced in the case of the $\pi\Sigma_c$ resonance. In on-shell models the $\pi\Sigma_c$ resonance acquires a wide width and its position, which barely changes with the cut-off, is always located above the $\pi\Sigma_c$ threshold while in the off-shell models it always appears below it. The fact that the $\pi\Sigma_c$ resonance is so stable with the cut-off in on-shell models gives rise to a crossing with the DN resonance for a particular value of the cut-off.

Particularly interesting is the case of the non-local TVME^{off} model shown in the third panel of Fig. 3.5. Although the dependence of the DN resonance with the cut-off is qualitatively similar in the on- and off-shell models, it is the TVME^{off} model the one that produces the most stable DN resonance against changes in the cut-off, which must be increased by 600 MeV/c in order to move the DN resonance from the upper DN threshold to the lower $\pi\Sigma_c$ one.

In Table 3.6 we present for the different models, the mass, width and couplings of the DN and $\pi\Sigma_c$ resonances for the cut-off parameter that reproduces the position of the $\Lambda_c(2595)$ resonance as a DN molecule located at the energy of 2595 MeV. In general, the predicted widths for the $\Lambda_c(2595)$ resonance in the different models are slightly smaller than the experimental value of $3.6^{+2.0}_{-1.3}$ MeV, but this is justified from the fact that 1/3 of the width comes from 3-body meson-meson-baryon decay modes while our models just account for 2-body meson-baryon interactions.

We will continue the analysis of Table 3.6 commenting on the difference between on- and off-shell models, excluding for the TVME^{off} model which has no

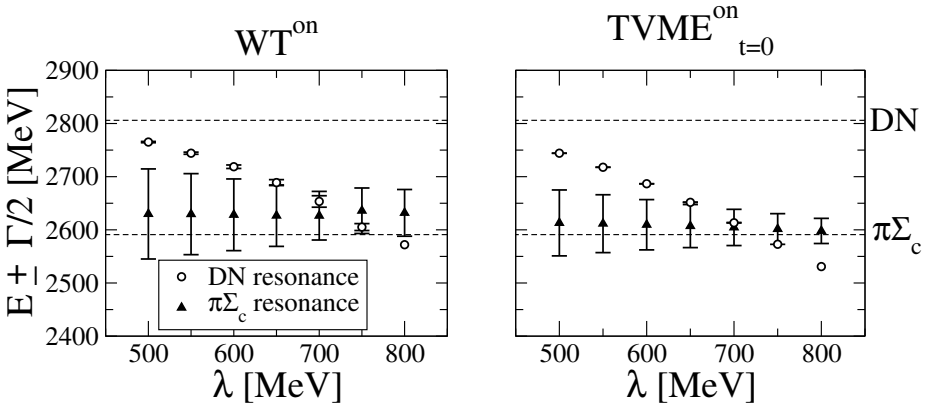

Figure 3.4: Energy and width dependence of the DN and $\pi\Sigma_c$ resonances with the cut-off parameter for the on-shell models: WT^{on} and $\mathrm{TVME}^{on}_{t\to 0}$. The horizontal dashed lines correspond to the $\pi\Sigma_c$ and DN thresholds, at 2591 MeV and 2806 MeV, respectively.

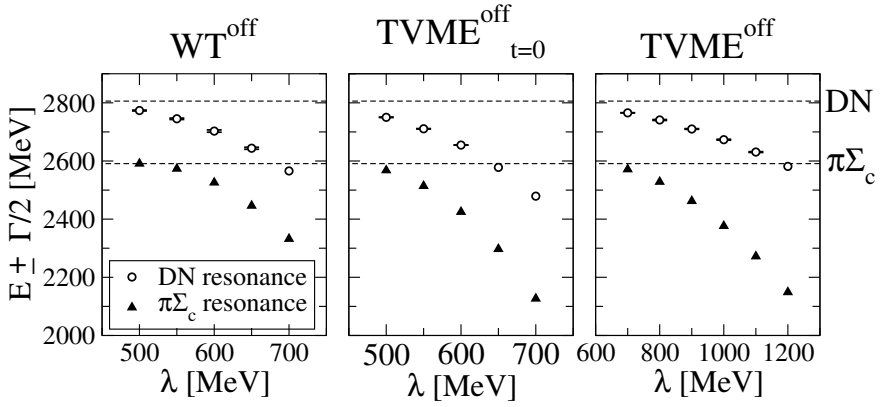

Figure 3.5: Energy and width dependence of the DN and $\pi\Sigma_c$ resonances with the cut-off parameter for the off-shell models: WT^{off}, $\mathrm{TVME}^{off}_{t\to 0}$ and TVME^{off}. The horizontal dashed lines correspond to the $\pi\Sigma_c$ and DN thresholds, at 2591 MeV and 2806 MeV, respectively.

B-S	On-Shell		Off-Shell		
Kernel	WT^{on}	$TVME^{on}_{t\to 0}$	WT^{off}	$TVME^{off}_{t\to 0}$	$TVME^{off}$
λ [MeV/c]	763	722	682	640	1174
M [MeV]	2595	2595	2595	2595	2595
Γ [MeV]	6	0.5	1	0.2	0.7
$g_{\pi\Sigma_c}$	1.2	0.31	0.46	0.19	0.4
g_{DN}	8.0	8.6	11	12	10
$g_{D_s\Lambda}$	4.1	3.5	6.9	5.8	5.3
M [MeV]	2635	2603	2377	2326	2182
Γ [MeV]	87	63	0	0	0
$g_{\pi\Sigma_c}$	2.1	2.2	6.1	7.0	10.0
g_{DN}	3.7	1.3	4.6	1.7	3.2
$g_{D_s\Lambda}$	2.2	0.54	2.0	0.52	1.0

Table 3.6: Masses (M), widths (Γ) and couplings (g_i) of the DN and $\pi\Sigma_c$ resonances once the cut-off has been fitted to reproduce the $\Lambda_c(2595)$ resonance or DN molecule.

equivalent on-shell model to compare with. The on-shell approaches using the WT and $TVME_{t\to 0}$ kernels require larger values of the cut-off than the corresponding off-shell ones. This difference comes essentially from the numerator which is basically proportional to the sum of the incoming and outgoing meson energies, $\omega(\vec{k}_{in}) + \omega(\vec{k}_{out})$ with $\omega(\vec{k}) = \sqrt{k^2 + m^2}$. Considering the $\Lambda_c(2595)$ resonance, it is easy to see that for the on-shell cases the $DN \leftrightarrow DN$ interaction is less intense than for the off-shell ones because the resonance lies below the DN threshold and the on-shell meson energies, built from negative k^2_{on} values, are smaller than the off-shell ones, obtained from positive k^2_{off} values.

The essential difference between the WT and the TVME$_{t\to 0}$ kernels (either on- or off-shell) lies in the second term of the TVME$_{t\to 0}$ interaction. Since this piece of the kernel makes the interaction to be smaller for the non-diagonal transitions like $\pi\Sigma_c \leftrightarrow DN$, the couplings of the $\Lambda_c(2595)$ to $\pi\Sigma_c$ states are smaller and therefore the width of the resonance as well. This effect can be appreciated in both on-shell and off-shell approaches where the widths of the $\Lambda_c(2595)$ and its coupling to $\pi\Sigma_c$ states are considerably smaller for the TVME$_{t\to 0}$ kernel than for the WT one.

Finally, we will briefly advance some remarks as far as the difference between the off-shell TVME$_{t\to 0}$ and TVME models is concerned, as they will be treated with more details in the next Chapter. We observe that the $t \to 0$ kernel needs a much smaller cut-off to generate the $\Lambda_c(2595)$ resonance at its position than the finite range interaction. As we will show in Chapter 4, this difference comes from the smaller strength of the diagonal matrix elements in the non-local kernel compared to those of the local one. Another difference is that the local model presents a much narrower width for the $\Lambda_c(2595)$ than the non-local one, and this is due to the different magnitude of the non-diagonal matrix elements, which are larger in the finite range approach. As we will see in Fig. 4.1 of Chapter 4, the positive character of the variable t for non diagonal transitions explains this difference.

3.4 Results for the strange sector

In the strange sector we also find two poles coupled to $\pi\Sigma$ and $\overline{K}N$ channels. Similarly to the charm sector we will refer to them as $\pi\Sigma$ and $\overline{K}N$ resonances, respectively. Many of the already analyzed aspects of Fig. 3.4 and 3.5 in the charm sector are also valid for the strange one (see Figs. 3.6 and 3.7). One of them is the behavior of the resonance that couples mostly to the first channel, the $\pi\Sigma$ resonance, which acquires a width for certain values of the cut-off in on-shell models, while in the off-shell models it always appears under the lightest threshold. We find that, in general, the position of the resonances for on-shell models shows a milder dependence on the cut-off value, as we found for the charm case. In contrast with the charm case, there is no crossing between the

resonances because the $\pi\Sigma$ resonance always appears under the $\overline{K}N$ one for both on- and off-shell models.

In Table 3.7 we present, for the different models, the mass, width and couplings of both resonances for the cut-off parameter that reproduces the position of the $\Lambda(1420)$ resonance as a $\overline{K}N$ molecule located at the energy of 1420 MeV. Depending on the model, the $\Lambda(1420)$ resonance shows a variety of widths which go from 17 MeV to 42 MeV. We can apply for Table 3.7 the same discussion between the different models that we have made for Table 3.6 in the previous Section. One difference worth to mention is the smaller couplings of both resonances to the $\overline{K}N$ channel, compared to the coupling of the charmed resonances to the DN one. However, for those models in which the strange resonances are located above the $\pi\Sigma$ threshold, their coupling to the first channel is bigger than for the charmed resonances. Therefore, their width is much wider than for the charmed resonances. Also the cut-offs in the strange sector are smaller than the ones in the charm sector since the systems are placed in different energy domains, separated about 1000 MeV/c from each other.

As we obtained for the charm sector, the resonances are further apart in off-shell models than in on-shell ones. We can compare our results on the strange sector with other works in literature. The $\pi\Sigma$ and $\overline{K}N$ resonances are $40-60$ MeV far apart in on-shell models (see Table 3.7), in agreement with [BMN06, GRNRAVV03, JOO$^+$03, OR98], where the separation between both resonances is less than 70 MeV. However, in the off-shell models the separation between both resonances is bigger. The off-shell approaches of Table 3.7 show that both resonances are 130-180 MeV far and, in the off-shell model developed in [HKMT10], the distance between them is around 100 MeV. The discrepancy between our off-shell approaches and that of the [HKMT10] can be a consequence of the simplicity of our one-meson exchange model, in contrast with the one in [HKMT10], where box-diagrams and σ-exchange terms, among other things, are also included.

An important consequence of the closeness of the resonances in on-shell models is the overlap between the two bound states. In the strange sector this is the origin of the so-called "two-pole nature" of the $\Lambda(1405)$, meaning that the experimental resonance observed around 1405 MeV is actually the superposition of the two poles, the narrower one at higher energy couples more strongly to $\overline{K}N$ states

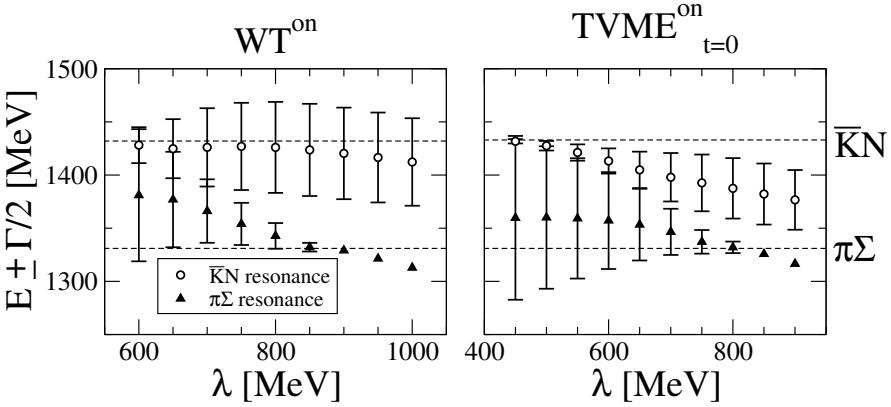

Figure 3.6: Energy and width dependence of the $\overline{K}N$ and $\pi\Sigma$ resonances with the cut-off parameter for the on-shell models: WT^{on} and $\mathrm{TVME}^{on}_{t\to 0}$. The horizontal dashed lines correspond to the $\pi\Sigma$ and $\overline{K}N$ thresholds, at 1330 MeV and 1433 MeV, respectively.

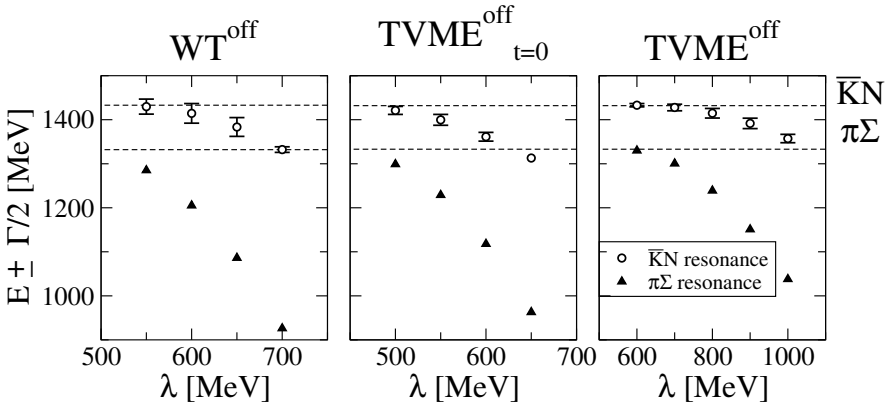

Figure 3.7: Energy and width dependence of the $\overline{K}N$ and $\pi\Sigma$ resonances with the cut-off parameter for the off-shell models: WT^{off}, $\mathrm{TVME}^{off}_{t\to 0}$ and TVME^{off}. The horizontal dashed lines correspond to the $\pi\Sigma$ and $\overline{K}N$ thresholds, at 1330 MeV and 1433 MeV, respectively.

B-S	On-Shell		Off-Shell		
Kernel	WT^{on}	$TVME^{on}_{t\to 0}$	WT^{off}	$TVME^{off}_{t\to 0}$	$TVME^{off}$
λ [MeV/c]	615	560	580	506	770
M [MeV]	1420	1420	1420	1420	1420
Γ [MeV]	40	17	42	19	20
$g_{\pi\Sigma}$	1.7	0.94	1.25	0.89	0.95
$g_{\overline{K}N}$	2.9	2.6	3.0	3.0	2.9
$g_{\eta\Lambda}$	1.5	1.1	2.1	1.6	1.6
M[MeV]	1380	1358	1241	1293	1260
Γ [MeV]	115	109	0	0	0
$g_{\pi\Sigma}$	2.8	2.5	4.3	3.6	4.3
$g_{\overline{K}N}$	2.6	1.6	4.6	3.0	3.2
$g_{\eta\Lambda}$	0.8	0.4	1.9	0.95	1.1

Table 3.7: Masses (M), widths (Γ) and couplings (g_i) of the $\overline{K}N$ and $\pi\Sigma$ resonances once the cut-off has been fitted to reproduce the $\Lambda(1420)$ resonance or $\overline{K}N$ molecule.

and the wider one at lower energy couples more strongly to $\pi\Sigma$ states, as seen in the first two columns of Table 3.7. However, in spite of the overlap of the two states also present in the charm sector with on-shell models (see Fig. 3.4), this "two-pole nature" has not been experimentally identified. The reason lies in the very different relative couplings of the two states found by the models to the $\pi\Sigma_c$ and DN channels. The DN state at 2595 MeV couples relatively very weakly to $\pi\Sigma_c$, becoming very narrow and, therefore, standing out very distinguishably from the $\pi\Sigma_c$ state that, in the on-shell models, appears only few MeV higher in energy but is much wider and will essentially contribute as a background.

4

Dynamical generation of charmed baryon resonances

One of the main interests of this thesis is to study the effects of going beyond the zero range approximation in the $t-$channel vector-exchange driving force. For this purpose, we will explore the different open-charm meson-baryon sectors by solving the Lippman-Schwinger (L-S) equation with the TVME kernel. This is an extension of the work of Hofmann and Lutz [HL05] in which the $t \to 0$ approximation was applied to the kernel. We will justify the need of dealing with the t-dependence and discuss its effects on the dynamical generation of baryon resonances obtained in the model, some of which can be clearly identified with recently observed states.

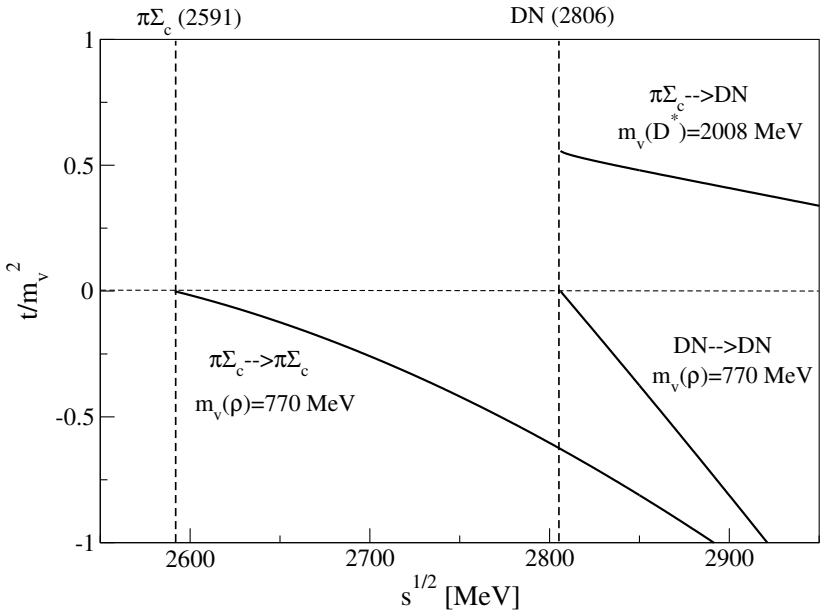

Figure 4.1: Dependence of the four momentum transfer t/m_v^2 on the center–of–mass energy $\sqrt{s}$ for different transition amplitudes.

4.1 Going beyond the zero range approximation

In Chapter 3 we already introduced the differences that the resonances present depending on the model we use. In this Section we are particularly interested in understanding the importance of the non-local terms in the meson-baryon interaction by comparing the off-shell TVME (Eq. (2.20)) and TVME$_{t\to 0}$ (Eq. (2.21)) kernels. Both models will account in this Chapter for the complete set of coupled channels and we will fix the universal coupling constant to $g = 6.6$, as in the work of Hofmann and Lutz [HL05], instead of considering the meson coupling constant $f = 1.15f$ MeV used as a common parameter in the toy models of the previous Chapter.

In order to illustrate the validity of the $t \to 0$ approach we show in Fig. 4.1 the value of t/m_v^2 as a function of $\sqrt{s}$, where m_v is the mass of a representative meson exchanged, which we take to be the ρ meson mass for diagonal transitions

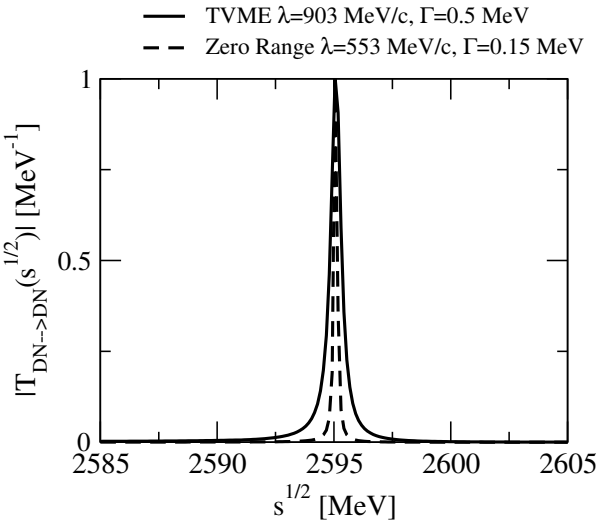

Figure 4.2: Imaginary part of the scattering amplitude of the elastic process $DN \to DN$ in the $(I, S, C) = (0, 0, 1)$ sector as a function of $\sqrt{s}$ for the finite range interaction of Eq. (2.20) (solid line) and the zero range approximation defined in Eq. (2.21) (dashed line). The incoming and outgoing relative momenta $\vec{k}_i$ and $\vec{k}_j$ have been taken equal to 0.

and the D^* meson mass for charm exchange ones. To accomplish this, we use Eq. (2.9) which is given in terms of on-shell energies and momenta (Eq. (2.28)). The range of energies goes roughly between the $\pi\Sigma_c$ and DN thresholds, thereby covering the region of the $J^P = \frac{1}{2}^-$ resonance $\Lambda_c(2595)$, which is a prime example of a dynamically generated open charmed baryon state in various approaches [LK05, TSBM04, LK04a, HL05, HL06, MR06]. It also expands beyond the DN threshold for about 300 MeV in order to explore the energy region that will be relevant in future studies of the D-meson self-energy in the nuclear medium. As one can see, the value of t/m_v^2 is only close to zero for diagonal transitions around their corresponding energy threshold, and its size is comparable to one at energies of interest in the present study. For the non-diagonal $\pi\Sigma_c \to DN$ transition, t/m_v^2 never goes to zero and acquires values of the order of 0.5.

We compare in Fig. 4.2 the results obtained using the non-local off-shell kernel (Eq. 2.20) with those taking the limit $t \to 0$ (Eq. (2.21)). We represent the

$(I,\ S)$	States
$(\frac{1}{2}, -3)$	$\bar{K}\Omega_c$
$(0, -2)$	$\bar{K}\Xi_c$, $\bar{K}\Xi_c'$, $D\Xi$, $\eta\Omega_c$, $\eta'\Omega_c$, $\bar{D}_s\Omega_{cc}$, $\eta_c\Omega_c$
$(1, -2)$	$\pi\Omega_c$, $K\Xi_c$, $K\Xi_c'$, $D\Xi_c$
$(\frac{1}{2}, -1)$	$\pi\Xi_c$, $\pi\Xi_c'$, $\bar{K}\Lambda_c$, $\bar{K}\Sigma_c$, $D\Lambda$, $\eta\Xi_c$, $D\Sigma$, $\eta\Xi_c'$ $K\Omega_c$, $D_s\Xi$, $\eta'\Xi_c$, $\eta'\Xi_c'$, $\eta_c\Xi_c$, $\bar{D}_s\Xi_{cc}$, $\bar{D}\Omega_{cc}$, $\eta_c\Xi_c'$
$(\frac{3}{2}, -1)$	$\pi\Xi_c$, $\pi\Xi_c'$, $\bar{K}\Sigma_c$, $D\Sigma$
$(0, 0)$	$\pi\Sigma_c$, DN, $\eta\Lambda_c$, $K\Xi_c$, $K\Xi_c'$, $D_s\Lambda$, $\eta'\Lambda_c$, $\eta_c\Lambda_c$, $\bar{D}\Xi_{cc}$
$(1, 0)$	$\pi\Lambda_c$, $\pi\Sigma_c$, DN, $K\Xi_c$, $\eta\Sigma_c$, $K\Xi_c'$, $D_s\Sigma$, $\eta'\Sigma_c$, $\bar{D}\Xi_{cc}$, $\eta_c\Sigma_c$
$(2, 0)$	$\pi\Sigma_c$
$(\frac{1}{2}, 1)$	$K\Lambda_c$, D_sN, $K\Sigma_c$
$(\frac{3}{2}, 1)$	$K\Sigma_c$

Table 4.1: Coupled-channel meson-baryon states with charm $C = 1$ and all possible combinations of isospin, strangeness $(I,\ S)$.

imaginary part of the scattering amplitude of the elastic process $DN \to DN$, as a function of $\sqrt{s}$ for zero incoming and outgoing relative momenta. We can see that, by adjusting the cut-off value conveniently, both models of the kernel can generate this state dynamically. However, the zero range approximation needs a cut-off value of $\lambda = 553$ MeV/c while the finite range interaction requires a substantially larger value of $\lambda = 903$ MeV/c[1].

This is easily understood from the fact that the $DN \to DN$ diagonal matrix elements of the non-local kernel, largely responsible for generating the resonance, are smaller in magnitude than those of the local one. The large difference between the cut-off momenta is just a reflection of the importance of the non-local terms

[1]Note that the cut-offs generating the DN bound state at the position of the $\Lambda_c(2595)$, are slightly smaller than the ones shown in Table 3.6 for the toy models of previous Chapter. There are two reasons that can explain this. The first one is that the DN bound state feels more attraction when coupling all the channels. The second one has to do with the value set for $g = 6.6$, which is equivalent to consider $f = f_\pi$. This value is lower than the one chosen in the previous Chapter $f \approx 1.15\ f_\pi$ and therefore the strength of the kernel gets increased.

in this problem. Once the $\Lambda_c(2595)$ resonance is conveniently located to its experimental position by both prescriptions, there remain substantial differences in its width. The local kernel produces a very narrow resonance, of width 0.15 MeV, while the resonance generated by the finite range kernel has a width of 0.5 MeV, closer to the empirical value of $3.6^{+2.0}_{-1.3}$ MeV. Again, this is due to the different magnitude of the non-diagonal matrix elements $DN \to \pi\Sigma_c$, which are larger in the finite range approach. We also observe that the results obtained with the low cut-off in the approximation $t \to 0$ for the $\Lambda_c(2595)$ agree (mass, width and couplings) with former studies of meson-baryon resonances of Hofmann and Lutz in [HL05] and Garcia-Recio *et al.,* in [GR$^+$09].

The results of Figs. 4.1 and 4.2 clearly point to the need of exploring the effects beyond the $t \to 0$ approximation, an attempt that is taken in the present work by considering the full t-dependence of the scattering kernel given by Eq. (2.20). The amplitudes describing the scattering of the pseudoscalar mesons off the ground-state baryons are obtained by solving the L-S equation (see (2.42)), already introduced in Chapter 2. Our results for the properties of the baryon resonances with charm in various strangeness and isospin sectors are shown in the next Section.

4.2 Results for the $C = 1$ sectors

All the possible isospin (I) and strangeness (S) sectors with charm $C = 1$ that can be built from the s-wave scattering of pseudoscalar mesons with $J^P = \frac{1}{2}^+$ baryons are shown in Table 4.1, together with the corresponding meson-baryon coupled channels. In this work, we will first study the cases in which some resonance with either $J^P = \frac{1}{2}^-$ or unknown spin-parity has already been observed. This includes the sectors with isospin, strangeness quantum numbers $(I, S) = (0, 0)$, $(1, 0)$ and $(\frac{1}{2}, -1)$, corresponding respectively to Λ_c, Σ_c and Ξ_c states, the experimental information of which is gathered in Table 4.2. We will next explore the sector $(I, S) = (0, -2)$ of the Ω_c states which so far has no experimental evidences for $J^P = \frac{1}{2}^-$ states. Finally, we will comment on the $(I, S) = (\frac{1}{2}, 1)$ sector that can only be realized with the presence of 5 quarks. The rest of the $C = 1$ sectors of Table 4.1 will not be commented in this Section because they do not present bound states in the model, nor there is experimental evidence of resonances with

Resonance	J^P	I, S	Γ[MeV]	Decay modes	Status
$\Lambda_c(2595)^+$	$\frac{1}{2}^-$	$0, 0$	$3.6^{+2.0}_{-1.3}$	$\Lambda_c\pi\pi$, $\Sigma_c\pi$	***
$\Lambda_c(2765)^+$	$?^?$	$?, 0$	~ 50	$\Lambda_c\pi\pi$	*
$\Lambda_c(2940)^+$	$?^?$	$0, 0$	17^{+8}_{-6}	DN, $\Sigma_c\pi$	***
$\Sigma_c(2800)$	$?^?$	$1, 0$	$75^{+22}_{-17}(\Sigma_c^{++})$,$62^{+60}_{-40}(\Sigma_c^+)$ $61^{+28}_{-18}(\Sigma_c^0)$	$\Lambda_c\pi$	***
$\Xi_c(2790)$	$\frac{1}{2}^-$	$\frac{1}{2}, -1$	$< 15(\Xi_c^+)$, $< 12(\Xi_c^0)$	$\Xi_c'\pi$	***
$\Xi_c(2930)$	$?^?$	$?, -1$	36 ± 13	$\Lambda_c K$	*
$\Xi_c(2980)$	$?^?$	$\frac{1}{2}, -1$	$26 \pm 7(\Xi_c^+)$, $20 \pm 7(\Xi_c^0)$	$\Lambda_c\bar{K}\pi, \Sigma_c\bar{K}$	***
$\Xi_c(3055)$	$?^?$	$?, -1$	17 ± 13	$\Lambda_c\bar{K}\pi, \Sigma_c\bar{K}$	**
$\Xi_c(3080)$	$?^?$	$\frac{1}{2}, -1$	$5.8 \pm 1.0(\Xi_c^+)$ $5.6 \pm 2.2(\Xi_c^0)$	$\Lambda_c\bar{K}\pi, \Sigma_c\bar{K}$ $\Sigma_c^*\bar{K}$	***
$\Xi_c(3123)$	$?^?$	$?, -1$	4 ± 4	$\Sigma_c^*\bar{K}$	*

Table 4.2: Masses, widths, decay modes and status of experimental $C = 1$ baryon resonances with $J^P = \frac{1}{2}^-$ or unknown. The expected isospin I and strangeness content S are also shown.

such quantum numbers.

Since the value of the cut-off λ is the free parameter of our model, and given the limited amount of data for charmed baryon resonances, it will be adjusted to the position of the well-known $\Lambda_c(2595)$ resonance, and the same value will be used for the other sectors explored in this work. We also investigate the effect of a gaussian-type form factor, as well as the dependence of our results on the value of the cut-off employed.

In the following we will present the results for each sector. Firstly, we will present the map of the bound states generated for the decoupled channel system, in order to visualize which are the diagonal channels responsible for the appearance of resonances and how they move when all the channels are coupled. Note that diagonal channels with positive $C_{ii,v}$ coefficients (see Eq. 2.7) will be in general those generating a bound state. After that, we will present the couplings

Λ_c resonances ($I = 0,\ S = 0$)				
Diagonal channels	Threshold E [MeV]	Diagonal $C_{ii,v}$	Decoupled M, Γ [MeV]	Coupled M, Γ [MeV]
$\pi\Sigma_c \leftrightarrow \pi\Sigma_c$	2591	$8(\rho)$	2270, 0	2168, 0
$DN \leftrightarrow DN$	2806	$3(\rho),\ 3(\omega)$	2652,0	2595, 0.5
$\eta\Lambda_c \leftrightarrow \eta\Lambda_c$	2832	0	✗	✗
$K\Xi_c \leftrightarrow K\Xi_c$	2963	$3(\rho), -1(\omega), 2(\phi)$	2942, 0	2805, 0.01
$K\Xi_c' \leftrightarrow K\Xi_c'$	3070	$3(\rho), -1(\omega), 2(\phi)$	3052, 0	3070(cusp)
$D_s\Lambda \leftrightarrow D_s\Lambda$	3085	$2(\phi)$	3085(cusp)	3085(cusp)
$\eta'\Lambda_c \leftrightarrow \eta'\Lambda_c$	3243	0	✗	✗
$\eta_c\Lambda_c \leftrightarrow \eta_c\Lambda_c$	5265	0	✗	✗
$\bar{D}\Xi_{cc} \leftrightarrow \bar{D}\Xi_{cc}$	5307	$3(\rho), -1(\omega), 4(J/\psi)$	5265, 0	5248, 7

Table 4.3: We show, for the ($I = 0,\ S = 0,\ C = 1$) sector, the different diagonal transitions with the threshold of the channels in the first and second column. The coefficients of the diagonal channels are given in the third column with the specific vector meson interchanged. The positive diagonal coefficients give attraction to the transition, generating a bound state (fourth column) in the uncoupled system. When we couple the channels, each bound state changes its position and acquires a width if it can decay in at least one channel.

of each resonance to the different channels. As the cusp-like structures do not appear as infinities in the second Riemann sheet of the complex energy plane, they will be omitted from the table of couplings.

4.2.1 Λ_c resonances ($I = 0,\ S = 0$)

In this sector there exists the experimental $\Lambda_c(2595)$ resonance, already introduced in the previous Chapter, which has been extensively studied in various works in recent years [TSBM04, LK04a, HL05, HL06, MR06].

Our search of resonances in this sector produces five pure bound states and a cusp structure in the decoupled-channel system shown in the fourth column of Table 4.3. When the channels are coupled, the pure bound-state at 3052 MeV

Λ_c resonances ($I=0,\ S=0$)				
M [MeV]	2168	2595	2805	5248
Γ [MeV]	0	0.5	0.01	7
Couplings $\lvert g_i \rvert$				
$\pi\Sigma_c(2591)$	10.5	0.32	0.004	0.44
$DN(2806)$	3.02	11.	0.21	0.33
$\eta\Lambda_c(2832)$	0.08	0.42	2.16	0.24
$K\Xi_c(2963)$	0.12	0.52	4.26	0.39
$K\Xi_c'(3070)$	4.79	0.23	0.004	0.21
$D_s\Lambda(3085)$	1.30	6.	0.19	0.19
$\eta'\Lambda_c(3243)$	0.14	0.69	0.006	0.50
$\eta_c\Lambda_c(5265)$	0.41	2.	0.02	1.4
$\bar{D}\Xi_{cc}(5307)$	0.57	0.05	1.1	4.17

Table 4.4: Masses, widths and couplings of the resonances in the ($I=0,\ S=0,\ C=1$) sector.

moves towards the $K\Xi_c'$ threshold, which is the meson-baryon channel which generates the resonance, and then it becomes a cusp-like structure. However, in [HL05, GR$^+$09] the $K\Xi_c'$ state appears as a resonance located at 3036 and 3053 MeV, respectively. Also, the cusp structure at the $D_s\Lambda$ threshold (see fourth and fifth columns in Table 4.3) appears as a resonance in [HL05, GR$^+$09] located at 3038 and 3153 MeV, respectively. In Table 4.4 we show the widths and couplings of the bound states to the various meson baryon states, omitting the cusp-like structures. The first and second resonances at 2168 and 2595 MeV where already studied in the last Chapter for a simplified model, and couple mostly to the first and second channel, respectively.

The $\Lambda_c(2595)$, which is basically a DN state, couples very weakly to its only possible decaying channel $\pi\Sigma_c$, thereby explaining its narrowness. We obtain an even narrower resonance at 2805 MeV, which is a $K\Xi_c$ bound system, a state also

Σ_c resonances ($I = 1,\ S = 0$)				
Diagonal channels	Threshold E [MeV]	Diagonal $C_{ii,v}$	Decoupled M, Γ [MeV]	Coupled M, Γ [MeV]
$\pi\Lambda_c \leftrightarrow \pi\Lambda_c$	2424	0	✗	✗
$\pi\Sigma_c \leftrightarrow \pi\Sigma_c$	2591	$-1(\rho),\ 3(\omega)$	2581, 0	2551, 0.15
$DN \leftrightarrow DN$	2806	$-1(\rho), 3(\omega)$	2805, 0	2804, 5
$K\Xi_c \leftrightarrow K\Xi_c$	2963	$-1(\rho), -1(\omega), 2(\phi)$	2963(cusp)	2963(cusp)
$\eta\Sigma_c \leftrightarrow \eta\Sigma_c$	2999	0	✗	✗
$K\Xi_c' \leftrightarrow K\Xi_c'$	3070	$-1(\rho), -1(\omega), 2(\phi)$	3070(cusp)	3070(cusp)
$D_s\Sigma \leftrightarrow D_s\Sigma$	3162	$2(\phi)$	3162(cusp)	3162(cusp)
$\eta'\Sigma_c \leftrightarrow \eta'\Sigma_c$	3410	0	✗	✗
$\bar{D}\Xi_{cc} \leftrightarrow \bar{D}\Xi_{cc}$	5307	$-1(\rho), -1(\omega), 4(J/\psi)$	5307(cusp)	5307(cusp)
$\eta_c\Sigma_c \leftrightarrow \eta_c\Sigma_c$	5432	0	✗	✗

Table 4.5: The same as Table. 4.3 but for the ($I = 1,\ S = 0,\ C = 1$) sector.

found around the same energy in [HL05] and [GR$^+$09]. Note that this resonance couples non-negligibly to DN and it could explain part of the structures seen below 2.85 GeV in the D^0p invariant mass spectrum measured by the BaBar collaboration [A$^+$07b]. The fourth bound state, which appears at 5248 MeV, couples mostly to the last channel $\bar{D}\Xi_{cc}$, and, although it can decay in to the first eight channels, it is quite narrow because couples weakly to all of them. There is no evidence for Λ_c states over 3000 MeV yet, but, as far as we know there are no experimental studies analyzing resonances at such high energies.

4.2.2 Σ_c resonances ($I = 1,\ S = 0$)

Using the same cut-off that generates dynamically the $\Lambda_c(2595)$ resonance in the $(I, S, C) = (0, 0, 1)$ sector, we predict four cusps and two narrow resonances at 2581 and 2805 MeV (see Table 4.5) that appear right below the thresholds of the channels to which they couple mostly, namely $\pi\Sigma_c$ and DN, respectively. The

Σ_c resonances ($I=1,\ S=0$)		
M [MeV]	2551	2804
Γ [MeV]	0.15	5
Couplings $\lvert g_i \rvert$		
$\pi\Lambda_c(2424)$	0.05	0.27
$\pi\Sigma_c(2591)$	3.7	0.16
$DN(2806)$	1.17	2.12
$K\Xi_c(2963)$	0.04	0.20
$\eta\Sigma_c(2999)$	0.74	0.11
$K\Xi_c'(3070)$	2.15	0.14
$D_s\Sigma(3162)$	0.58	1.80
$\eta'\Sigma_c(3410)$	0.04	0.19
$\bar{D}\Xi_{cc}(5307)$	0.85	0.15
$\eta_c\Sigma_c(5432)$	0.12	0.56

Table 4.6: Masses, widths and couplings of the resonances in the ($I=1,\ S=0,\ C=1$) sector

position of the $\pi\Sigma_c$ state moves 30 MeV backward in energy when the channels are coupled while the DN state remain almost at the same energy position, as it can be seen from Table 4.5. The couplings of both states with respect to the different channels are shown in Table 4.6. Since the $\Sigma_c(2551)$ resonance couples negligibly to its only allowed strong decaying channel, $\pi\Lambda_c$, it appears as a narrow peak which makes it easy to miss given the energy resolution of the meson-baryon invariant masses built up in the present experiments. The couplings to the different meson-baryon states of the second Σ_c resonance at 2804 MeV allow one to identify it with the state found in [HL05] at a substantially lower energy, 2680 MeV, using a subtraction method to regularize the loops, as well as that found in [MR06] around 2750 MeV, using a cut-off method which preserves isospin symmetry in the regularization scheme. Our result is obviously closer

to that of the latter work. The Belle Collaboration reported recently [M$^+$05b] an isotriplet of excited charmed baryons, $\Sigma_c(2800)$, decaying into $\Lambda_c^+\pi^-$, $\Lambda_c^+\pi^0$ and $\Lambda_c^+\pi^+$ pairs and having a width of around 60 MeV with more than 50% error. Although this resonance has been tentatively assumed to decay to $\Lambda_c\pi$ pairs in d-wave and its spin parity estimated to be $J^P = 3/2^-$, actual angular distributions have not been measured and the fits to $\Lambda_c\pi$ spectra cannot rule out s-wave type decays. Hence, our state at 2805 MeV could be easily identified with the $\Sigma_c(2800)$ resonance, provided three-body decay mechanisms not accounted for in our model, could explain the large width observed experimentally.

4.2.3 Ξ_c resonances $(I = 1/2,\ S = -1)$

The results in this sector are presented in Tables 4.7 and 4.8. We will start directly by the analysis of the results obtained for coupled-channels in Table 4.8, where, apart from the four cusp structures placed at $\overline{K}\Lambda_c$, $K\Omega_c$, $D_s\Xi$ and $\overline{D}_s\Xi_{cc}$ thresholds, we predict several bound states which we explain in detail in the following lines.

The two pure bound states at 2515 and 2549 MeV are placed less than one pion mass above the Ξ_c member of the $J^P = \frac{1}{2}^+$ ground state antitriplet, $(\Lambda_c^+, \Xi_c^+, \Xi_c^0)$, and below the mass of the Ξ_c' member of the $J^P = \frac{1}{2}^+$ sextet, $(\Sigma_c^0, \Sigma_c^+, \Sigma_c^{++}, \Xi_c'^0, \Xi_c'^+, \Omega_c^0)$. This implies that these bound states would decay electromagnetically through the emission of $\Xi_c\gamma$ pairs and may have been detected at photon energies of about 50 and 80 MeV in the experiment where the Ξ_c' was observed [J$^+$99b]. Although no apparent signals are reported, we note that the limited statistical significance of the spectra measured in [J$^+$99b] prevents one from ruling out the existence of these bound states. Moreover, their production rate would also be somewhat inhibited by the fact that they are predominantly 5 quark-component states. Note also that, lowering gradually the value of the cut-off to somewhat below 700 MeV, the first state at 2515 MeV eventually becomes a resonance, but quite narrow due to its weak coupling to the first channel, whereas the second state at 2549 MeV, which is $\pi\Xi_c$ molecule, rapidly becomes so wide that it would be difficult to be distinguished from the background.

In addition, our model gives three more resonances above the $\pi\Xi_c$ threshold and below 3 GeV, placed at 2733, 2840 and 2977 MeV. The local model of [HL05]

Ξ_c resonances ($I = 1/2,\ S = -1$)				
Diagonal channels	Threshold E [MeV]	Diagonal $C_{ii,v}$	Decoupled M, Γ [MeV]	Coupled M, Γ [MeV]
$\pi\Xi_c \leftrightarrow \pi\Xi_c$	2609	$4(\rho)$	2601, 0	2549, 0
$\pi\Xi_c' \leftrightarrow \pi\Xi_c'$	2715	$4(\rho)$	2715, 0	2515, 0
$\bar{K}\Lambda_c \leftrightarrow \bar{K}\Lambda_c$	2779	$2(\omega)$	2779 (cusp)	2779 (cusp)
$\bar{K}\Sigma_c \leftrightarrow \bar{K}\Sigma_c$	2946	$4(\rho),\ 2(\omega)$	2786, 0	2733, 34
$D\Lambda \leftrightarrow D\Lambda$	2985	$2(\omega)$	2983, 0	2977, 4
$\eta\Xi_c \leftrightarrow \eta\Xi_c$	3018	0	✗	✗
$D\Sigma \leftrightarrow D\Sigma$	3062	$4(\rho),\ 2(\omega)$	2887	2840, 0.58
$\eta\Xi_c' \leftrightarrow \eta\Xi_c'$	3124	0	✗	✗
$K\Omega_c \leftrightarrow K\Omega_c$	3192	$4(\rho)$	3185, 0	3192 (cusp)
$D_s\Xi \leftrightarrow D_s\Xi$	3288	$4(\rho)$	3268, 0	3288 (cusp)
$\eta'\Xi_c \leftrightarrow \eta'\Xi_c$	3428	0	✗	✗
$\eta'\Xi_c' \leftrightarrow \eta'\Xi_c'$	3534	0	✗	✗
$\bar{D}_s\Xi_{cc} \leftrightarrow \bar{D}_s\Xi_{cc}$	5408	$4(\rho)$	5408 (cusp)	5408 (cusp)
$\bar{D}\Omega_{cc} \leftrightarrow \bar{D}\Omega_{cc}$	5429	$4(\rho)$	5429 (cusp)	5382, 7
$\eta_c\Xi_c \leftrightarrow \eta_c\Xi_c$	5450	0	✗	✗
$\eta_c\Xi_c' \leftrightarrow \eta_c\Xi_c'$	5556	0	✗	✗

Table 4.7: The same as Table. 4.3 but for the ($I = \frac{1}{2},\ S = -1,\ C = -1$) sector.

also obtains three resonances in this energy region, located in general at somewhat lower masses and showing a different order of appearance, as can be inferred from the values of their couplings to the different meson-baryon components. More specifically, the lowest resonance in the local model appearing at 2691 MeV and coupling strongly to $D\Sigma$ should be identified with our middle resonance at 2840 MeV. The next two resonances appear quite close in the scheme of [HL05], at 2793 MeV and 2806 MeV, coupling mostly to $\bar{K}\Sigma_c$ and $D\Lambda$, respectively, while

Ξ_c resonances ($I = 1/2,\ S = -1$)						
M [MeV]	2515	2549	2733	2840	2977	5382
Γ [MeV]	0.	0.	34	0.58	4	7
Couplings $\lvert g_i \rvert$						
$\pi\Xi_c(2609)$	0.65	4.47	0.05	0.06	0.31	0.33
$\pi\Xi_c'(2715)$	4.84	0.76	1.77	0.01	0.22	0.22
$\bar{K}\Lambda_c(2779)$	0.48	3.21	0.19	0.10	0.19	0.32
$\bar{K}\Sigma_c(2946)$	6.90	1.01	7.37	0.93	0.16	0.31
$D\Lambda(2985)$	1.03	0.30	0.96	1.54	2.95	0.48
$\eta\Xi_c(3018)$	0.13	1.04	0.13	0.18	0.10	0.11
$D\Sigma(3062)$	2.91	0.89	3.64	8.82	1.74	0.41
$\eta\Xi_c'(3124)$	4.04	0.59	3.47	0.46	0.07	0.14
$K\Omega_c(3192)$	4.40	0.68	1.47	0.07	0.21	0.22
$D_s\Xi(3288)$	1.74	0.15	0.92	4.71	2.51	0.27
$\eta'\Xi_c(3428)$	0.16	0.05	0.15	0.53	0.06	0.49
$\eta'\Xi_c'(3534)$	0.01	0.03	0.09	0.11	0.28	0.01
$\bar{D}_s\Xi_{cc}(5408)$	0.02	0.01	0.25	0.35	0.71	2.34
$\bar{D}\Omega_{cc}(5429)$	1.10	0.53	1.18	0.24	0.03	2.48
$\eta_c\Xi_c(5450)$	1.17	1.10	0.55	0.04	0.03	1.34
$\eta_c\Xi_c'(5556)$	0.04	0.08	0.26	0.33	0.82	0.04

Table 4.8: Masses, widths and couplings of the resonances in the ($I = \frac{1}{2},\ S = -1,\ C = -1$) sector.

in our case they are further apart from each other, at 2733 and 2977 MeV. The crossing in the ordering of states is another consequence of the non-local scheme employed in the present work, which gives rise to somewhat different transition amplitudes than those obtained with local models.

Ω_c resonances ($I=0,\ S=-2$)				
Diagonal channels	Threshold E [MeV]	Diagonal $C_{ii,v}$	Decoupled M, Γ [MeV]	Coupled M, Γ [MeV]
$\bar{K}\Xi_c \leftrightarrow \bar{K}\Xi_c$	2963	$3(\rho),\ 1(\omega), -2(\phi)$	2962, 0	2959, 0
$\bar{K}\Xi_c' \leftrightarrow \bar{K}\Xi_c'$	3070	$3(\rho),\ 1(\omega), -2(\phi)$	3068, 0	2966, 1.1
$D\Xi \leftrightarrow D\Xi$	3189	$3(\rho),\ 1(\omega)$	3114, 0	3117, 16
$\eta\Omega_c \leftrightarrow \eta\Omega_c$	3246	0	✗	✗
$\eta'\Omega_c \leftrightarrow \eta'\Omega_c$	3656	0	✗	✗
$D_s\Omega_{cc} \leftrightarrow D_s\Omega_{cc}$	5528	$-2(\phi),\ 4(J/\psi)$	5528 (cusp)	5528 (cusp)
$\eta_c\Omega_c \leftrightarrow \eta_c\Omega_c$	5678	0	✗	✗

Table 4.9: The same as Table. 4.3 but for the ($I=0,\ S=-2,\ C=1$) sector.

The resonances we obtain over 3 GeV can be compared with the results in [HL05], where a $K\Omega_c$ molecule at 3114 MeV is related with a cusp structure that in our model appears at 3192 MeV (see fifth column in Table 4.7), and a very wide resonance, coupling mostly to $\overline{D}\Omega_{cc}$ channel at 4274 MeV [HL05], in our model is placed at 5382 MeV with a much narrow width (see Table 4.8). This big difference in the width of the $\overline{D}\Omega_{cc}$ state is due to the much bigger coupling of the resonance to the $\eta'\Xi_c$ channel in [HL05] than in our model.

Recently, several Ξ_c states have been observed by the CLEO [C$^+$01b], Belle [C$^+$06b] and BaBar [A$^+$08b] collaborations, out of which the three star possible candidates to be identified with one of our states are at 2790, 2980 and 3080 MeV (see Table 4.2). A change of the cut-off value within a reasonable range could bring any of our two lower mass resonances (excluding our bound states) to agree in position with the $\Xi_c(2790)$ but the width would turn out to be twice wider than the observed one in the case of the lower mass state. The $\Xi_c(2980)$ could be easily associated to either one of the two higher mass states found here below 3 GeV. However, the experimental analysis of [A$^+$08b] concludes that the $\Xi_c(2980)^+$ state decays in about 50% of the cases into $\Sigma_c^{++}K^-$ pairs, which makes our state at 2840 MeV, showing a stronger coupling to $\bar{K}\Sigma_c$, the most likely candidate to

Ω_c resonances ($I = 0,\ S = -2$)			
M [MeV]	2959	2966	3117
Γ [MeV]	0.	1.1	16
Couplings $\lvert g_i \rvert$			
$\bar{K}\Xi_c(2964)$	1.36	0.43	0.51
$\bar{K}\Xi_c'(3070)$	2.04	4.49	0.27
$D\Xi(3189)$	2.03	1.68	5.34
$\eta\Omega_c(3246)$	1.67	3.69	0.24
$\eta'\Omega_c(3656)$	0.10	0.07	0.35
$D_s\Omega_{cc}(5528)$	0.17	1.17	0.19
$\eta_c\Omega_c(5678)$	0.28	0.21	1.03

Table 4.10: Masses, widths and couplings of the resonances in the ($I = 0,\ S = -2,\ C = 1$) sector.

be associated to the $\Xi_c(2980)$.

4.2.4 Ω_c resonances ($I = 0,\ S = -2$)

In this sector we predict the existence of a bound state at 2959 MeV, near the lowest threshold, two resonances placed at 2966 and 3117 MeV as can be seen in Tables 4.9 and 4.10, and a cusp structure at the $D_s\Omega_{cc}$ threshold . The possible bound state could be detected through the decay into $\Omega_c\gamma$ states with photons of $E_\gamma = 260$ MeV in the center-of-mass frame. The resonance placed at 2966 MeV is very narrow ($\Gamma = 1.1$ MeV) according to the low coupling of the resonance to the only channel in which it can decay ($\bar{K}\Xi_c'$) and the little available phase space. The resonance at 3117 MeV with a width of $\Gamma = 16$ MeV is a $D\Xi$ molecule that can decay to $\bar{K}\Xi_c$ and $\bar{K}\Xi_c'$ states.

The work of [HL05] also finds three states but placed at lower energies, 2839, 2928 and 2953 MeV, which follows the trend observed for other sectors. The pattern of couplings to the various meson-baryon states also differs a little owing

$(I = 1/2,\ S = 1)$				
Diagonal channels	Threshold E [MeV]	Diagonal $C_{ii,v}$	Decoupled M, Γ [MeV]	Coupled M, Γ [MeV]
$K\Lambda_c \leftrightarrow K\Lambda_c$	2779	$-2(\omega)$	✗	✗
$D_sN \leftrightarrow D_sN$	2908	0	✗	✗
$K\Sigma_c \leftrightarrow K\Sigma_c$	2946	$4(\rho),\ -2(\omega)$	2946 (cusp)	2946 (cusp)

Table 4.11: The same as Table. 4.3 but for the $(I = \frac{1}{2},\ S = 1,\ C = 1)$ sector.

to the different interaction model used. The highest energy resonance in [HL05], coupling strongly to $\bar{K}\Xi_c'$ and $\eta\Omega_c$, would correspond to our middle one, while the lowest one in [HL05], coupling strongly to $D\Xi$, would be the equivalent to our resonance at higher energy.

4.2.5 Resonances of five quarks

We have also analyzed the sectors corresponding to resonances that cannot be realized with only three quarks and, therefore, their existence would be signalling the presence of pure five quark states. Out of the three possible sectors, namely $(I,\ S,\ C) = (2,\ 0,\ 1)$, $(\frac{1}{2},\ 1,\ 1)$ and $(\frac{3}{2},\ 1,\ 1)$, we only find hints of a possible resonance in the case $(I = \frac{1}{2},\ S = 1,\ C = 1)$, where we see a cusp-like structure placed at the threshold of the $K\Sigma_c$ channel to which the state couples more strongly. This behavior is shown in Table 4.11 and in the first column of coupling constants displayed in Table 4.12, which have been obtained using our nominal cut-off value of 903 MeV/c. According to the mechanism discussed in [TGRN08], the coupling constants should vanish if the resonance was placed right at the $K\Sigma_c$ threshold, which explains the smallness of their values. In order to see whether the cusp structure would eventually become a clear resonance with a slight change of parameters, we also display in Table 4.12 our results for two other values of the cut-off, 1200 and 1400 MeV. One can clearly see that the cusp structure becomes a more bound and wider resonance as the cut-off value increases, while the coupling constants become larger.

$(I = 1/2,\ S = 1)$					
λ [MeV/c]	903	$\rightarrow$	1200	$\rightarrow$	1400
M [MeV]	2946 (cusp)	$\rightarrow$	2941	$\rightarrow$	2924
Γ [MeV]	narrow	$\rightarrow$	5	$\rightarrow$	12
Couplings $\lvert g_i \rvert$					
$K\Lambda_c(2779)$	$< 10^{-3}$	$\rightarrow$	0.04	$\rightarrow$	0.10
$D_sN(2908)$	$< 10^{-3}$	$\rightarrow$	0.84	$\rightarrow$	1.68
$K\Sigma_c(2946)$	$< 10^{-3}$	$\rightarrow$	1.79	$\rightarrow$	3.59

Table 4.12: Masses, widths and couplings of the resonances in the $(I = \frac{1}{2},\ S = 1,\ C = 1)$ sector for different cut-off values: 903, 1200 and 1400 MeV/c.

4.3 Dependence on model parameters

We finalize this Chapter by exploring the dependence of our results on the shape and size of the form factor employed, which are ingredients of the model that are not constrained by symmetry arguments.

First, by replacing the dipole-type form factor by a Gaussian one (see Eq. (2.44)), we are able to adjust the position of $\Lambda_c(2595)$ with a Gaussian cut-off value of $\lambda = 543$ MeV/c. The corresponding width is exactly the same as that found for the dipole-type form factor as it is shown in panel *b*) of Fig. B.2 on Appendix B.

When exploring the other sectors, the Gaussian form factor gives rise to the same resonances, some of them slightly displaced by at most 50 MeV from the position found with the dipole-type form factor but having essentially the same width. Retaining the dipolar form factor, we next explore the effects of varying the value of the cut-off λ between 600 and 1200 MeV/c, that is, up to 300 MeV/c below and above the nominal value of 903 MeV/c used in this work. This variation produces changes in the positions and widths of the resonances within certain ranges, the general trend of which are summarized in the following points:

(I,S)	λ [MeV/c]	Theory M [MeV]	main channel	Γ [MeV]	Experiment M [MeV]	Γ [MeV]
$(0,0)$ Λ_c	903	2595	DN	0.5	2595.4 ± 0.6	$3.6^{+2.0}_{1.3}$
$(1,0)$ Σ_c	1100	2792	DN	16	2801^{+4}_{-6}	75^{+22}_{-17} (Σ_c^{++})
					2792^{+14}_{-5}	62^{+60}_{-40} (Σ_c^{+})
					2802^{+4}_{-7}	61^{+28}_{-18} (Σ_c^{0})
$(\frac{1}{2},-1)$ Ξ_c	814	2790	$\bar{K}\Sigma_c$	55	2789.1 ± 3.2	< 15 (Ξ_c^{+})
	980	2790	$D\Sigma$	0.5	2791.8 ± 3.3	< 12 (Ξ_c^{0})
	655	2970	$D\Sigma$	1.2	2971.4 ± 3.3	26 ± 7 (Ξ_c^{+})
	960	2970	$D\Lambda$	5.1	2968.0 ± 2.6	20 ± 7 (Ξ_c^{0})

Table 4.13: Masses, widths and main coupled channel of states that can be identified with well established resonances in various sectors.

- A resonance that lies far below –by 50 to 200 MeV– the meson-baryon threshold to which it couples more strongly may change its position by an amount comparable with the variation of the cut-off value. The larger the cut-off the more bound the resonance becomes.

- The width of the resonance only changes appreciably for cut-off values that move the resonance above the threshold of a meson-baryon channel to which the resonance couples significantly.

- Weakly bound resonances change their positions more moderately, at most by 10 MeV for changes of cut-off values within 100 MeV/c. In this case, the width tends to increase as the resonance becomes more bound because of the disappearance of the distortions induced by the closeness of the threshold, a phenomenon also known as Flatté effect [Fla76].

4.4 The $\Lambda_c(2595)$, $\Sigma_c(2800)$, $\Xi_c(2790)$ and $\Xi_c(2980)$ resonances

Having explored the systematics to the cut-off changes, we finally summarize in Table 4.13 the states which, taking an appropriate cut-off value within the range explored, could be identified with a well established resonance of $J^P = \frac{1}{2}^-$ or unknown spin-parity. These states are the $\Lambda_c(2595)$, $\Sigma_c(2800)$, $\Xi_c(2790)$ and the $\Xi_c(2980)$, and they will be represented in Figs. 4.3, 4.4, 4.5 and 4.6, respectively, as the modulus square of the coherent sum of all transition amplitudes going to a final meson-baryon state to which the resonances can decay, namely:

$$\sum_{M'B'} \mid C^R_{M'B'} T_{M'B'\to MB}(\sqrt{s}) \mid^2 , \tag{4.1}$$

where the values of the coefficients $C^R_{M'B'}$ would depend on the specific reaction used to excite the resonance and, in this graphical example, have all been taken to one.

The amplitudes have been calculated for zero incoming and outgoing relative momenta. To compare to actual experiments, one should use the appropriate excitation coefficients and transition matrix elements going to the on-shell final momentum. Therefore, the results in the Figures should be considered merely illustrative. In general, a resonance couples dominantly to a given channel and the value of the maximum of Eq. (4.1) is basically proportional to the modulus squared of the product of the resonance couplings to the dominant and decaying channels, $g_{M'B'}$ and g_{MB}, and inversely proportional to the resonance width Γ.

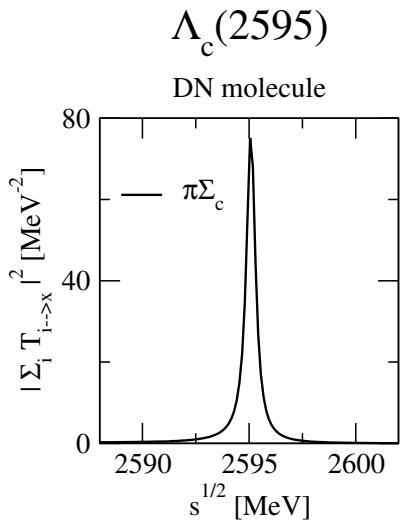

Figure 4.3: Modulus square of the coherent sum of all transition amplitudes going to any of the possible final meson-baryon decaying channels, as a function of $\sqrt{s}$, for the ($I = 0$, $S = 0$, $C = 1$) sector. The incoming and outgoing relative momenta $\vec{k}_i$ and $\vec{k}_j$ have been taken equal to 0.

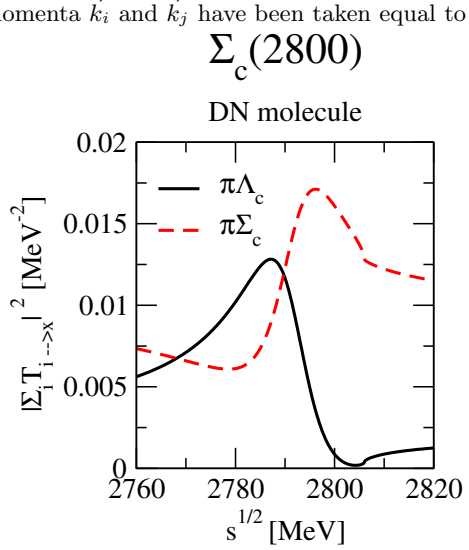

Figure 4.4: The same as Fig. 4.3 but for the $\Sigma_c(2800)$ resonance in the ($I = 1$, $S = 0$, $C = 1$) sector.

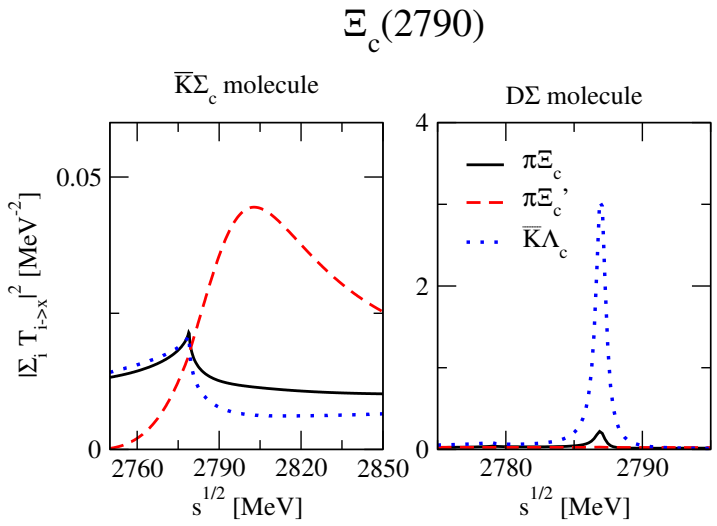

Figure 4.5: The same as Fig. 4.3 but for the $\Xi_c(2790)$ resonance in the ($I = \frac{1}{2}$, $S = -1$, $C = 1$) sector.

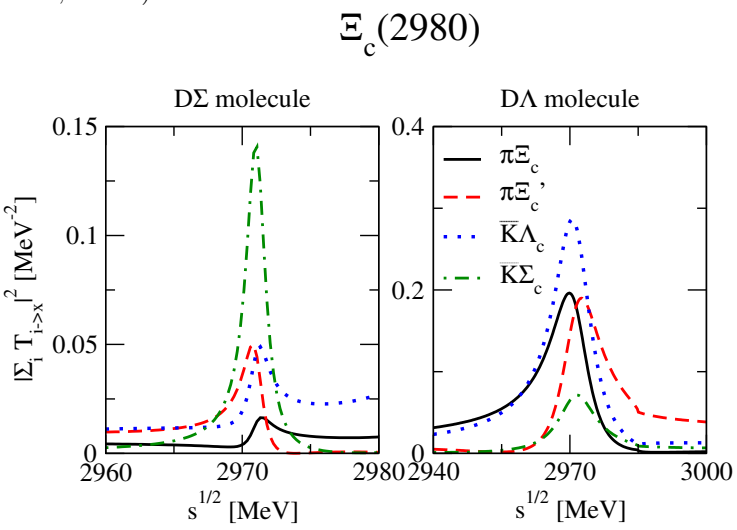

Figure 4.6: The same as Fig. 4.3 but for the $\Xi_c(2980)$ resonance in the ($I = \frac{1}{2}$, $S = -1$, $C = 1$) sector.

5

Radiative decays of charmed baryons

In this Chapter we study the radiative decay of dynamically generated $J^P = \frac{1}{2}^-$ charmed baryons into the ground state of $J^P = \frac{1}{2}^+$ baryons. Since different theoretical interpretations of these baryonic resonances, and in particular of the $\Lambda_c(2595)$, give different predictions, a precise experimental measurement of these decays would be an important step for understanding their nature. After a general introduction we will review the baryon resonances that are taken into account in this study and present the radiative decay formalism in Section 5.2. Results are presented in Section 5.3.

5.1 Introduction

The decay modes of a resonance may provide a way of learning about the nature of the state: whether it fits in the conventional qqq-baryon or $q\bar{q}$-meson picture or it has a more exotic interpretation. In particular, the radiative decays into lower lying states may represent a significant part of the decay width when the hadronic modes are suppressed by phase-space restrictions or/and small values of the coupling constants. Note that electromagnetic transitions are also useful in the determination of the quantum numbers of states decaying into a final hadron with well established quantum numbers.

Radiative decays of ground state heavy flavored baryons have been studied within many different approaches, like Heavy Hadron Chiral Perturbation Theory (HHCPT) [C$^+$93, Che97, Sav95, BPS00] –an approach which combines Heavy Quark (HQ) symmetry with the chiral symmetry in the light sector–, employing light-cone QCD sum-rules [ZD99], supplementing HQ symmetry with a SU($2N_f$)×O(3) symmetry in the light diquark system [TKO01], or implementing also dynamical effects for the internal quark structure of the hadrons within the relativistic three-quark model (RTQM) [IKLR99, IKL99] or other non-relativistic quark models [DSVD94, FR97, MPV09].

Many of the former approaches have also been applied to obtain the radiative decays of excited heavy flavored baryons, such as the $\Lambda_c(2595)$. A first qualitative estimation was given in [Cho94], where the HHCPT formalism was extended to include the lowest lying excited baryon doublet, $\Lambda_c(2595)$ ($J^P = \frac{1}{2}^-$) and $\Lambda_c(2625)$ ($J^P = \frac{3}{2}^-$). The results of [TKO01] were obtained by exploiting the alternative light diquark SU($2N_f$)×O(3) symmetry. Radiative decays of excited charmed baryons were also calculated within the relativistic quark model of [IKLR99, IKL99], as well as using light-cone QCD sum-rules in [Zhu00]. All these works consider the excited heavy baryon as being an orbital excitation of the three-quark Qqq system with a unit of angular momentum inserted between the heavy quark Q and the light diquark qq. A different perspective is provided by the model of [Cho96], for example. This model considers the excited $\Lambda_c(2595)$ and $\Lambda_c(2625)$ as being D^*N bound systems in the first excited state of a harmonic potential adjusted phenomenologically to reproduce the spin-averaged excitation

energy. Another example is the model of [DFG$^+$10] which considers the radiative decay of the $\Lambda_c(2940)$ in a hadronic D^*N molecular picture.

In the present Chapter we study the radiative decays of excited baryons in the $C = 1$ sector. We focus on the resonances $\Lambda_c(2595)$, $\Sigma_c(2800)$, $\Xi_c(2790)$ and $\Xi_c(2980)$, all having $J^P = \frac{1}{2}^-$, which have been generated as meson-baryon molecular states on several models based on coupled-channel dynamics [TSBM04, LK04a, LK05, HL05, HL06, MR06, GR$^+$09, JTRV09]. The radiative transitions to baryons of the $J^P = \frac{1}{2}^+$ ground state multiplet proceeds, as we will see, through the coupling of the photon to the various meson-baryon components of the resonance, as determined by the coupled-channel dynamical model of this thesis. This is essentially different from the quark models for which, in the heavy quark limit, the photon only couples to the light diquark system. Therefore, a precise measurement of the radiative decays of excited heavy flavored baryons could help in understanding their internal structure.

The radiative decays of dynamically generated charmed mesons have already been addressed recently. In [GDO07, FGLM07, LS08], the radiative decay of the $D^*_{s0}(2317)$ meson has been studied from the point of view that it is generated dynamically mainly from the interaction of the D meson with a kaon. Also radiative decays of the puzzling $X(3872)$ have been calculated from the point of view that this state is a $D^*\bar{D} + c.c.$ molecule [DFG$^+$10]. More recently, many different radiative decays of the controversial X, Y and Z states have been analyzed assuming that their structure is determined by the interactions of two vector mesons [LMO10, MNHO11, BMO11].

This chapter is organized as follows: in the next Section we review the dynamically generated $J^P = \frac{1}{2}^-$ baryon resonances from the interaction of ground state baryons with pseudo-scalar mesons and present the framework for evaluating the diagrams needed in the calculation of the radiative decays of the resonances. The results of the calculation are discussed in Section 5.3.

MB	g_{RBM} $2595 + i0.25$ [MeV]
$\pi\Sigma_c$	$0.06 - i0.31$
DN	$-0.13 + i11$
$\eta\Lambda_c$	$-0.005 + i0.42$
$K\Xi_c$	$-0.006 + i0.52$
$K\Xi_c'$	$0.03 - i0.23$
$D_s\Lambda$	$-0.06 + i6$
$\eta'\Lambda_c$	$-0.01 + i0.69$
$\eta_c\Lambda_c$	$0.02 - i2$
$\bar{D}\Xi_{cc}$	$0.007 + i0.05$

Table 5.1: Coupling coefficients g_{RBM} of the $\Lambda_c(2595)$ pole to the different channels

5.2 Radiative decay calculation

We start this Section by reviewing the meson-baryon states presented in Table 4.13 from previous Chapter for which we are going to study its radiative decay. The complex values of the coupling of the resonances to the various charged meson-baryon states are listed in Tables 5.1 to 5.3. The radiative reaction we study is given by:

$$B^*(P,\chi_i) \quad \rightarrow \quad \gamma(K,\epsilon)B(Q,\chi_f)\,, \tag{5.1}$$

where P, K and Q are four-momenta which are related by $P = K + Q$, ϵ is the photon polarization and χ_i and χ_f are the polarization of the initial and final spin $\frac{1}{2}$ baryons B^* and B, respectively.

For the evaluation of these radiative decays, we follow a gauge invariant scheme already used for non-charmed resonances [BBMN05, DOS06a, Dor07, GOD07]. As shown there, the mechanisms for the decay of the resonance B^* into γB are

MB	g_{RBM} $2792 + i8.16$ [MeV]
$\pi\Lambda_c$	$0.19 + i0.53$
$\pi\Sigma_c$	$-0.28 + i0.12$
DN	$-0.60 - i3.6$
$K\Xi_c$	$0.31 + i0.28$
$\eta\Sigma_c$	$0.06 - i0.21$
$K\Xi_c'$	$-0.13 + i0.24$
$D_s\Sigma$	$0.42 + i3.1$
$\eta'\Sigma_c$	$-0.05 - i0.35$
$\bar{D}\Xi_{cc}$	$0.22 + i0.28$
$\eta_c\Sigma_c$	$0.13 + i1$

Table 5.2: Coupling coefficients g_{RBM} of the $\Sigma_c(2800)$ pole to the different channels

given by the diagrams of Fig. 5.1, where the photon couples to the constituent mesons and baryons. The amplitude for the radiative decay has the structure:

$$-i\mathcal{M} \quad = \quad T_{\mu\nu}\epsilon^{\nu}\bar{\chi_f}\sigma^{\mu}\chi_i\,, \tag{5.2}$$

with $\sigma_\mu = (0, \vec{\sigma})$, where σ_i are the usual Pauli matrices. For the tensor $T_{\mu\nu}$, there are five possible independent Lorentz structures that one can construct with the two independent four-momenta:

$$T^{\mu\nu} \quad = \quad ag^{\mu\nu} + bP^{\mu}P^{\nu} + cP^{\mu}K^{\nu} + dK^{\mu}P^{\nu} + eK^{\mu}K^{\nu}\,.$$

This expression is simplified by noting that, due to the Lorentz condition $\epsilon_\nu K^\nu = 0$, the terms with the coefficients c and e in Eq. (5.3) will not contribute to the radiative decay amplitude of Eq. (5.2). Moreover, gauge invariance imposes $T_{\mu\nu}K^\nu = 0$ and we obtain:

$$\big(a + d(PK)\big)K^{\mu} + b(PK)P^{\mu} \quad = \quad 0\,, \tag{5.3}$$

	g_{RBM}	
MB	$2790 + i0.25$ [MeV]	$2970 + i2.5$ [MeV]
$\pi\Xi_c$	$0.01 + i0.06$	$0.008 - i0.37$
$\pi\Xi_c'$	$0 + i0.002$	$-0.25 - i0.08$
$\bar{K}\Lambda_c$	$-0.06 - i0.22$	$0.1 + i0.17$
$\bar{K}\Sigma_c$	$-0.003 - i1.5$	$-0.17 + i0.03$
$D\Lambda$	$0.08 - i2.1$	$-0.21 - i3.2$
$\eta\Xi_c$	$-0.07 - i0.33$	$0.08 - i0.02$
$D\Sigma$	$-0.03 + i12.$	$-0.07 - i1.76$
$\eta\Xi_c'$	$-0.001 - i0.73$	$-0.02 - i0.05$
$K\Omega_c$	$-0.003 + i0.08$	$-0.21 + i0.15$
$D_s\Xi$	$-0.08 + i6.54$	$0.18 + i2.8$
$\eta'\Xi_c$	$0.005 - i0.76$	$-0.007 - i0.08$
$\eta'\Xi_c'$	$0.004 + i0.16$	$-0.01 - i0.31$
$\bar{D}_s\Xi_{cc}$	$0.04 + i0.44$	$-0.02 - i0.006$
$\bar{D}\Omega_{cc}$	$-0.03 + i0.03$	$-0.03 + i0.04$
$\eta_c\Xi_c$	$-0.007 - i1$	$0.05 + i0.91$
$\eta_c\Xi_c'$	$-0.01 - i0.46$	$0.04 + i0.9$

Table 5.3: Coupling coefficients g_{RBM} of the $\Xi_c(2790)$ and $\Xi_c(2980)$ poles to the different channels

from where we conclude that $b = 0$, while a and d are related through $a = -d(PK)$. The expression for the amplitude can be further simplified if we work in the rest frame of the decaying baryon ($\vec{P} = \vec{0}$) and take the Coulomb gauge ($\epsilon^0 = 0$). In this way only the a term contributes to the amplitude. Moreover, the a coefficient is more easily calculated through the d coefficient, using the above mentioned relation, $a = -d(PK)$. This is so because, as we will show, the integral for evaluating the d coefficient converges and only the (b) and (c) diagrams of Fig. 5.1 contribute to it.

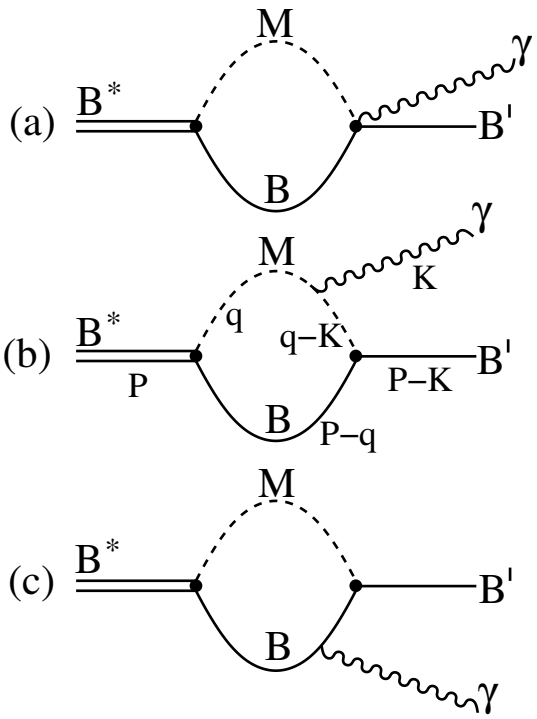

Figure 5.1: Diagrams needed for the evaluation of the radiative decay of dynamically generated baryons.

The amplitude for diagram 5.1(b) is given by:

$$-i\mathcal{M} = -ig_{RBM}g_{BBM}g_{\gamma MM}\int\frac{d^4q}{(2\pi)^4}\frac{1}{(q-K)^2-m^2}$$
$$\times\frac{1}{q^2-m^2}\frac{2M}{(P-q)^2-M^2}\bar{\chi}_f(q-K)\sigma\chi_i(2q-K)\epsilon\,, \tag{5.4}$$

where g_{RBM} is the coupling of the resonance to its meson and baryon constituents, g_{BBM} is the coupling of the baryonic current to a meson, $g_{\gamma MM}$ is the coupling of the meson to a photon, and m and M are masses of the meson and baryon in

the loop, respectively. Using the Feynman parameterization

$$\frac{1}{abc} = 2\int_0^1 dx \int_0^{1-x} dy \frac{1}{\big(x(a-b)+y(c-b)+b\big)^3} , \tag{5.5}$$

and the identity

$$\int d^4q' \frac{1}{(q'^2+s+i\epsilon)^3} = \frac{i\pi^2}{2}\frac{1}{s+i\epsilon} , \tag{5.6}$$

together with the relation between the a and d terms of the amplitude, one finds the following contribution of diagram 5.1(b) to the a term:

$$-i\mathcal{M}^a_{(\mathrm{b})} = g_{RBM}g_{BBM}g_{\gamma MM}\frac{2M}{(4\pi)^2}\int_0^1 dx\int_0^{1-x} dy \frac{x(y-1)}{s+i\epsilon}2PK , \tag{5.7}$$

$$s = x\big(P^2(1-x)-M^2+m^2-2yPK\big)-m^2 . \tag{5.8}$$

Analogously, one can calculate the contribution coming from the diagram in Fig. 5.1 (c) as:

$$-i\mathcal{M}^a_{(\mathrm{c})} = g_{RBM}g_{BBM}g_{\gamma BB}\frac{2M}{(4\pi)^2}\int_0^1 dx\int_0^{1-x} dy \frac{-yx}{s+i\epsilon}2PK , \tag{5.9}$$

$$s = x\big(P^2(1-x)-m^2+M^2-2yPK\big)-M^2 . \tag{5.10}$$

The value of the g_{RBM} couplings appearing in Eqs. (5.7) and (5.9), relating the resonance to its meson–baryon constituents in the isospin basis, are listed in Tables 5.1 to 5.3 of the previous Section. The couplings of the mesons to the photon, $g_{\gamma MM}$, and those of the baryons to the photon, $g_{\gamma BB}$, are eQ where Q is the electric charge ($-1, 0, 1$ or 2) of the meson or the baryon which emits the photon. Finally, the coupling of the mesons to the ground state baryons is given

by:

$$g_{BBM} = \alpha_i \frac{D+F}{2f} + \beta_i \frac{D-F}{2f} \tag{5.11}$$

where $D+F = 1.26$, $D-F = 0.33$ [OR98]. We have taken $f = 1.15 f_M$ with $f_M = f_\pi = 93$ MeV for light mesons and $f_M = f_D = 165$ MeV for heavy mesons. The coefficients α_i and β_i, which depend on the SU(4) flavor structure of the interaction, have been obtained from the Lagrangian for the interaction of the ground state spin $\frac{1}{2}^+$ baryons and the pseudo-scalar mesons, which is constructed in the following.

Our prescription of field definition for the baryons is that of [HL05] and was already presented in Chapter 2, in Eq. (2.6) and the pseudo-scalar meson field is represented by the following matrix:

$$\Phi = \begin{pmatrix} \frac{\pi^0}{\sqrt{2}} + \frac{\eta_8}{\sqrt{6}} + \frac{\eta_{15}}{\sqrt{12}} & \pi^+ & K^+ & \bar{D}^0 \\ \pi^- & \frac{\pi^0}{\sqrt{2}} + \frac{\eta_8}{\sqrt{6}} + \frac{\eta_{15}}{\sqrt{12}} & K^0 & -D^- \\ K^- & \bar{K}^0 & \frac{-2\eta_8}{\sqrt{6}} + \frac{\eta_{15}}{\sqrt{12}} & D_s^- \\ D^0 & -D^+ & D_s^+ & \frac{-3\eta_{15}}{\sqrt{12}} \end{pmatrix} \tag{5.12}$$

The Lagrangian for the BBM interaction reads:

$$\begin{aligned} \mathcal{L}_{BBM} &= \frac{\sqrt{2}}{4f} \sum_{i,j,k,l=1}^{4} \bar{\mathcal{B}}_{ijk} \gamma^\mu \Big((D+F) \partial_\mu \Phi_{kl} \mathcal{B}_{ijl} \\ &- 2(D-F) \partial_\mu \Phi_{jl} \mathcal{B}_{ilk} \Big) . \end{aligned} \tag{5.13}$$

Note that the physical η, η' and η_c fields are related to the mathematical η_8 and η_{15} fields, belonging to the pseudo-scalar meson fifteen-plet, and the singlet

η_1 field. The mixture is given by:

$$\begin{pmatrix} \eta_1 \\ \\ \eta_8 \\ \\ \eta_{15} \end{pmatrix} = \begin{pmatrix} \frac{1}{2\sqrt{3}} & \sqrt{\frac{2}{3}} & \frac{1}{2} \\ \\ \frac{2\sqrt{2}}{3} & -\frac{1}{3} & 0 \\ \\ \frac{1}{6} & \frac{\sqrt{2}}{3} & -\frac{\sqrt{3}}{2} \end{pmatrix} \cdot \begin{pmatrix} \eta \\ \\ \eta' \\ \\ \eta_c \end{pmatrix} . \tag{5.14}$$

Therefore, in order to obtain a Lagrangian for the physical fields, we need to add to Eq. (5.13) an interaction of the baryon current with the singlet field η_1:

$$\begin{aligned} \mathcal{L}'_{BBM} &= \mathcal{L}_{BBM} \\ &+ \frac{\sqrt{2}}{4f}(D\delta_D + F\delta_F)\frac{1}{2}\sum_{i,j,k=1}^{4} \bar{\mathcal{B}}_{ijk}\gamma^\mu \mathcal{B}_{ijk}\partial_\mu \eta_1 \ , \end{aligned} \tag{5.15}$$

where the coefficients $\delta_D = -\frac{1}{\sqrt{2}}$ and $\delta_F = \frac{3}{\sqrt{2}}$ are obtained by consistently imposing that processes where the η_c meson couples to light baryons (N, Λ, Σ or Ξ) should vanish.

The complete Lagrangian $\mathcal{L}'_{BBM}$ of Eq. (5.15) allows us to determine all coupling constants g_{BBM}, which we write in the form of Eq. (5.11). The specific values of the α_i and β_i coefficients for all the transitions needed in the different radiative decays are collected in Tables C.1 to C.4 of the appendix C.

With all the required ingredients having been established, one can finally obtain the radiative decay width from:

$$\Gamma = \frac{1}{\pi}\left|\sum_i \mathcal{M}_i^a\right|^2 E_\gamma \frac{M}{m_{B^*}} \tag{5.16}$$

where E_γ is the photon energy, $\mathcal{M}_i^a = \mathcal{M}_{(b)}^a + \mathcal{M}_{(c)}^a$, and the sum runs over all contributing intermediate MB channels.

5.3 Results

We evaluate the following radiative decays:

$$\Lambda_c(2595) \rightarrow \Lambda_c\gamma \tag{5.17}$$
$$\Lambda_c(2595) \rightarrow \Sigma_c^+\gamma \tag{5.18}$$
$$\Sigma_c^+(2800) \rightarrow \Lambda_c\gamma \tag{5.19}$$
$$\Sigma_c^{++}(2800) \rightarrow \Sigma_c^{++}\gamma \tag{5.20}$$
$$\Sigma_c^+(2800) \rightarrow \Sigma_c^+\gamma \tag{5.21}$$
$$\Sigma_c^0(2800) \rightarrow \Sigma_c^0\gamma \tag{5.22}$$
$$\Xi_c^+(2790) \rightarrow \Xi_c^+\gamma \tag{5.23}$$
$$\Xi_c^0(2790) \rightarrow \Xi_c^0\gamma \tag{5.24}$$
$$\Xi_c^+(2790) \rightarrow \Xi_c^{\prime+}\gamma \tag{5.25}$$
$$\Xi_c^0(2790) \rightarrow \Xi_c^{\prime0}\gamma \tag{5.26}$$
$$\Xi_c^+(2980) \rightarrow \Xi_c^+\gamma \tag{5.27}$$
$$\Xi_c^0(2980) \rightarrow \Xi_c^0\gamma \tag{5.28}$$
$$\Xi_c^+(2980) \rightarrow \Xi_c^{\prime+}\gamma \tag{5.29}$$
$$\Xi_c^0(2980) \rightarrow \Xi_c^{\prime0}\gamma\ , \tag{5.30}$$

The theoretical decay widths obtained from the imaginary part of the pole position for these dynamically generated states are usually smaller than the experimental observed decay widths. The model considers only meson baryon channels where the meson is a pseudo-scalar coupled in s-wave with a $J^P = \frac{1}{2}^+$ baryon. In the case of the heavier resonances the model is probably missing possible three body decays of the resonance, or channels where the meson and the baryon belong to different multiplets than those assumed here, and this should partially explain the small widths found for the theoretical resonances. In any case one must assume some uncertainties for the couplings listed in Tables 5.1 to 5.3.

We calculate the uncertainties in the radiative decay widths assuming a 20% uncertainty in the g_{RBM} couplings. In order to do that we follow the same method used in [GDO07]: we generate random sets for the couplings of each resonance

Channel	$\Gamma_{\Lambda_c\gamma}$ [KeV]	[IKLR99] [KeV]	[Zhu00] [KeV]	[Cho96] [KeV]
$\pi^+\Sigma_c^0$	1.2(+)	–	–	–
$\pi^0\Sigma_c^+$	<0.1(+)	–	–	–
$\pi^-\Sigma_c^{++}$	0.7(−)	–	–	–
D^0p	9.1(+)	–	–	–
D^+n	83.4(+)	–	–	–
$\eta\Lambda_c$	<0.1(+)	–	–	–
$K^+\Xi_c^0$	<0.1(+)	–	–	–
$K^0\Xi_c^+$	<0.1(+)	–	–	–
$K^+\Xi_c'^0$	<0.1(+)	–	–	–
$K^0\Xi_c'^+$	<0.1(+)	–	–	–
$D_s^+\Lambda$	13.5(+)	–	–	–
$\eta'\Lambda_c$	<0.1(+)	–	–	–
$\eta_c\Lambda_c$	<0.1(+)	–	–	–
$\bar{D}^0\Xi_{cc}^+$	<0.1(+)	–	–	–
$D^-\Xi_{cc}^{++}$	<0.1(−)	–	–	–
Total	274 ±0.4	115	36	16

Table 5.4: Results for the radiative decay of the $\Lambda_c(2595) \to \Lambda_c\gamma$ compared with other theoretical approaches. The sign in brackets indicates the sign of the amplitude, so one can know when the interference between the channels is constructive or destructive.

to the channels with a 20% uncertainty around the values listed in Tables 5.1 to 5.3. For each resonance we generate 30 sets of random couplings and calculate the radiative decay for each set. Our final result for the radiative decay width is the averaged value of the widths calculated with each random set, while the uncertainty in the radiative decay width is the standard deviation from the average.

We start showing the results for the $\Lambda_c(2595)$, which is the analog in the charm sector of the $\Lambda(1405)$ in the strange one and, therefore, is a good candidate for being a meson-baryon molecular state. The radiative decay widths are:

$$\begin{aligned} \Gamma_{\Lambda_c(2595)\to\Lambda_c\gamma} &= (274.3 \pm 52.0)\ \text{KeV}\,, \\ \Gamma_{\Lambda_c(2595)\to\Sigma_c^+\gamma} &= (2.1 \pm 0.4)\ \text{KeV}\ . \end{aligned}$$

These values are also collected in Table 5.4 and 5.5, where the contribution to the width coming from each intermediate channel is also shown, together with the sign, (+) or (−), of the corresponding amplitude. This allows one to analyze the constructive or destructive character of the interferences between the various channels. First of all, we note the tremendous difference in size, of two orders of magnitude, between the radiative decay rate of the $\Lambda_c(2595)$ into $\Lambda_c\gamma$ and $\Sigma_c^+\gamma$ states. To understand the origin of this difference we focus on the most important contribution, which corresponds to the D^+n intermediate state in both cases. First of all, the ratio between the couplings $D^+n \to \Lambda_c$ and $D^+n \to \Sigma_c^+$ is 3.8, as can be inferred from the α and β coefficients of Table C.1. Moreover, the different kinematical variables of the two processes produce a D^+n loop which is, for $\Lambda_c\gamma$ decay, a factor 2 larger than for $\Sigma_c^+\gamma$ decay. The square of these two factors, together with the ratio of photon energies, which are $E_\gamma = 290$ MeV for $\Lambda_c\gamma$ and $E_\gamma = 138$ MeV for $\Sigma_c^+\gamma$, explain the factor 100 difference between the D^+n contributions to both decays. We also note that there are constructive interferences between the most important contributions (D^0p, D^+n, $D_s^+\Lambda$) to $\Lambda_c\gamma$ decay, which enhance even further this rate compared to the $\Sigma_c^+\gamma$ one.

The experimental width for the decay of the $\Lambda_c(2595)$ is 3.6 MeV and around 80% of it comes from the channel $\pi\Sigma_c$ which corresponds to a width of around 2.9 MeV. Our coupling for this channel is $|g_{\pi\Sigma_c}| = 0.32$ resulting in a width of 0.5 MeV. Changing our coupling to $|g_{\pi\Sigma_c}| = 0.76$ would result in a width around 2.9 MeV. Calculating the radiative decay of the $\Lambda_c(2595)$ with this new absolute value for the coupling to $\pi\Sigma_c$ states we obtain:

$$\begin{aligned} \Gamma_{\Lambda_c(2595)\to\Lambda_c\gamma} &= (289.1 \pm 53.3)\ \text{KeV}\,, \\ \Gamma_{\Lambda_c(2595)\to\Sigma_c^+\gamma} &= (7.9 \pm 1.5)\ \text{KeV}\,. \end{aligned}$$

Therefore, we obtain qualitatively similar results when a realistic coupling of the $\Lambda_c(2595)$ resonance to Σ_c states is employed. Correcting manually the couplings of the other resonances for which there is some experimental data on their decays has an even smaller effect on the results than those observed in the case of the $\Lambda_c(2595) \to \Sigma_c^+\gamma$ decay.

In Tables 5.4 and 5.5 we also compare our results to those obtained by other

Channel	$\Gamma_{\Sigma_c^+\gamma}$ [KeV]	[IKLR99] [KeV]	[Zhu00] [KeV]
$\pi^+\Sigma_c^0$	0.3(−)	−	−
$\pi^0\Sigma_c^+$	0	−	−
$\pi^-\Sigma_c^{++}$	0.2(−)	−	−
$D^0 p$	0.1(+)	−	−
$D^+ n$	0.8(−)	−	−
$\eta\Lambda_c$	0	−	−
$K^+\Xi_c^0$	<0.1(+)	−	−
$K^0\Xi_c^+$	<0.1(−)	−	−
$K^+\Xi_c'^0$	<0.1(−)	−	−
$K^0\Xi_c'^+$	<0.1(+)	−	−
$D_s^+\Lambda$	0	−	−
$\eta'\Lambda_c$	0	−	−
$\eta_c\Lambda_c$	0	−	−
$\bar{D}^0\Xi_{cc}^+$	<0.1(−)	−	−
$D^-\Xi_{cc}^{++}$	<0.1(−)	−	−
Total	2.1 ±52.0	77	11

Table 5.5: Results for the radiative decay of the $\Lambda_c(2595) \to \Sigma_c^+\gamma$ compared with other theoretical approaches. The sign in brackets indicates the sign of the amplitude, so one can know when the interference between the channels is constructive or destructive.

calculations performed within the relativistic quark model [IKLR99], using light-cone QCD sum-rules [Zhu00], or adopting a bound D^*N picture for the $\Lambda_c(2595)$ [Cho96]. We observe a large diversity of results. Note also that the two orders of magnitude difference between the radiative decays into $\Lambda_c\gamma$ or $\Sigma_c\gamma$ states found in the present thesis is not obtained by any of the other models displayed in Tables 5.4 and 5.5, nor by the HHCPT results of [Cho94], which estimated partial widths of the same order of magnitude. Obviously, the tremendous differences between models calls for a measurement of these decay modes which could bring essential information about the nature of the $\Lambda_c(2595)$.

The radiative decays of the other resonances, for which there is no experimental observation nor other theoretical predictions, are:

$$\Gamma_{\Sigma_c^{++}(2800)\to\Sigma_c^{++}\gamma} \quad = \quad (51.0 \pm 9.1)\ \text{KeV}$$

$$
\begin{aligned}
\Gamma_{\Sigma_c^+(2800)\to\Sigma_c^+\gamma} &= (28.4 \pm 3.3)\ \text{KeV} \\
\Gamma_{\Sigma_c^0(2800)\to\Sigma_c^0\gamma} &= (9.1 \pm 1.5)\ \text{KeV} \\
\Gamma_{\Sigma_c^+(2800)\to\Lambda_c\gamma} &= (33.5 \pm 8.8)\ \text{KeV} \\
\Gamma_{\Xi_c^+(2790)\to\Xi_c^+\gamma} &= (249.6 \pm 41.9)\ \text{KeV} \\
\Gamma_{\Xi_c^0(2790)\to\Xi_c^0\gamma} &= (119.3 \pm 21.7)\ \text{KeV} \\
\Gamma_{\Xi_c^+(2790)\to\Xi_c^{\prime+}\gamma} &= (0.8 \pm 0.5)\ \text{KeV} \\
\Gamma_{\Xi_c^0(2790)\to\Xi_c^{\prime 0}\gamma} &= (1.3 \pm 0.4)\ \text{KeV} \\
\Gamma_{\Xi_c^+(2980)\to\Xi_c^+\gamma} &= (56.4 \pm 19.2)\ \text{KeV} \\
\Gamma_{\Xi_c^0(2980)\to\Xi_c^0\gamma} &= (2.5 \pm 1.7)\ \text{KeV} \\
\Gamma_{\Xi_c^+(2980)\to\Xi_c^{\prime+}\gamma} &= (40.1 \pm 6.9)\ \text{KeV} \\
\Gamma_{\Xi_c^0(2980)\to\Xi_c^{\prime 0}\gamma} &= (9.2 \pm 1.0)\ \text{KeV}
\end{aligned}
$$

It would also be interesting to see whether our predictions, based in a molecular picture for these resonances, are also very different from those obtained in quark-model theoretical approaches.

Part II

In-medium

6

Properties of charmed hadrons in hot and dense matter

In this Chapter we study the behavior of the dynamically-generated baryonic resonances in hot dense and matter, as well as the spectral features of the open charm mesons (D, $\bar{D}$, D_s and $\bar{D}_s$), within a self-consistent coupled-channel approach that considers the full t-dependent TVME interaction kernel. The in-medium scattering amplitudes are obtained by solving the L-S equation at finite temperature including Pauli blocking effects, baryon dressing, as well as D, $\bar{D}$, D_s and $\bar{D}_s$ self-energies taking their mutual influence into account. We pay a particular attention to the influence that the dressed mesons exert on each other.

6.1 Introduction

The study of charmed hadrons in the nuclear medium has received an increased attention in the past years. Nuclear medium modifications have been lately incorporated in the study of charmed resonant states, such as the $\Lambda_c(2595)$ to test their dynamics in the nuclear medium. The properties of open-charmed mesons in nuclear matter can influence the charmonium production in hot dense matter, which might indicate the formation of the quark-gluon plasma phase of QCD at high density and temperature [MS86]. Another exciting scenario is the possible formation of D-mesic nuclei [TLT$^+$99, GRNT10] and of exotic nuclear bound states like J/Ψ in nuclei [BST90, LMS92, KTT11]. From the experimental side, the physics program of the CBM experiment as well as part of the PANDA collaboration at FAIR [FAI] will be devoted to the properties of open and hidden charm in dense matter. In particular, the physical goal is to extend to the heavy-quark sector the GSI program for in-medium modifications of hadron properties in the light sector, and to provide insight into the charm-nucleus interaction.

Works based on mean-field approaches provided important shifts for the D and $\bar{D}$ open-charmed meson masses [TLT$^+$99, STT99, Hay00, MBSB$^+$04], which alters the formation of charmonium [ABMRS08]. Some of those models have been recently revised [HTK09, MM09, KM10]. A different perspective is offered by models that, working within coupled-channel unitarized schemes, go beyond mean field and provide the spectral features of the charm mesons in symmetric nuclear matter at zero [TSBM04, MR06, LK06] and finite temperature [TSBS06, TRM08]. Lately, this meson-baryon basis has been extended to incorporate Heavy Quark Symmetry (HQS). In this way, not only D-meson but also D^*-meson features have been studied [TGRN09].

A common feature of the previous models is the use of an interaction kernel in the zero-range approximation ($t \to 0$). However, as we have justified in the Chapter 4, the zero-range approximation is not valid for charm-exchange processes because the difference in masses between the external mesons is comparable with the mass of the charmed vector meson being exchanged. For this reason, to study the properties of the open-charmed mesons and the different resonant states, we will implement in this Chapter the in-medium and temperature

$(I,\ S,\ C)$	Channels
$(\frac{1}{2}, -1, -1)$	$\bar{D}_s N(2908)$ $\bar{D}\Lambda(2985)$ $\bar{D}\Sigma(3062)$
$(0, 0, -1)$	$\bar{D}N(2806)$
$(1, 0, -1)$	$\bar{D}N(2806)$
$(0, 0, 1)$	$\pi\Sigma_c(2591)$ $DN(2806)$ $\eta\Lambda_c(2832)$ $K\Xi_c(2963)$ $K\Xi'_c(3070)$ $D_s\Lambda(3085)$ $\eta'\Lambda_c(3243)$ $\eta_c\Lambda_c(5265)$ $\bar{D}\Xi_{cc}(5307)$
$(1, 0, 1)$	$\pi\Lambda_c(2424)$ $\pi\Sigma_c(2591)$ $DN(2806)$ $K\Xi_c(2963)$ $\eta\Sigma_c(2999)$ $K\Xi'_c(3070)$ $D_s\Sigma(3162)$ $\eta'\Sigma_c(3410)$ $\bar{D}\Xi_{cc}(5307)$ $\eta_c\Sigma_c(5432)$
$(\frac{1}{2}, 1, 1)$	$K\Lambda_c(2779)$ $D_s N(2908)$ $K\Sigma_c(2946)$

Table 6.1: Coupled-channel meson-baryon states involved in DN, $\bar{D}N$, D_sN, or $\bar{D}_sN$ interactions. The energy threshold of each state is given in brackets.

effects in our coupled-channel formalism for the non local TVME kernel.

6.2 Charmed sectors and free space ingredients

In this Section, we will firstly introduce the coupled channel sectors which will be employed to study the in-medium open-charmed mesons, and next we will review the results obtained from the coupled-channel approach employed in [JTRV09] and presented in Chapter 4. After that, we will implement in Sec. 6.3 the main sources of medium effects in our coupled-channel formalism and, finally, we will present the results in Section 6.4.

Since the properties of the D, $\bar{D}$, D_s and $\bar{D}_s$ mesons in a hot and dense environment will be determined, respectively, from the DN, $\bar{D}N$, D_sN and $\bar{D}_sN$ amplitudes, we list in Table 6.1 the corresponding set of coupled channels in each of the related isospin (I), strangeness (S) and charm (C) sectors.

Given the limited amount of data for charmed baryon resonances, and in order to simplify the analysis, the cut-off λ is adjusted to 903 MeV/c, a value that reproduces the position of the well-known $J^P = \frac{1}{2}^-$ $\Lambda_c(2595)$ having $(I,\ S,\ C) = (0,\ 0,\ 1)$, and the same value is used for the other sectors explored in this work. In Table 6.2, we summarize the position, width and most important couplings of the dynamically generated states appearing in the various $(I,\ S,\ C)$ sectors listed in Table 6.1. Note that there are no resonances in the singled-channel $(I,\ S,\ C) = (0,\ 0,\ -1)$ and $(1,\ 0,\ -1)$ sectors of the $\bar{D}N$ interaction. In the other $C = -1$ case, having $(I = \frac{1}{2},\ S = -1)$, we find a pole just below the $\overline{D}_s N$ threshold. The remaining cases have $C = 1$ and, although they were deeply analyzed in Chapter 4, we briefly comment here a few essential characteristics that will be useful for our discussion of the in-medium results in the next Section. In the $(I = 0,\ S = 0)$ sector, apart from the $\Lambda_c(2595)$ resonance to which we fit the model, there is another very narrow one at 2805 MeV, just below the threshold for DN states but coupling very little to them. We also predict two narrow resonances in the $(I = 1,\ S = 0)$ sector at 2551 and 2804 MeV, right below the thresholds of the channels to which they couple more strongly, namely $\pi\Sigma_c$ and DN, respectively. In the $(I = \frac{1}{2},\ S = 1)$ case, we predict a cusp-like structure placed at the threshold of $K\Sigma_c$, the channel that shows the largest coupling to this state.

6.3 Medium and finite temperature effects

The are two main sources of medium effects to consider. One is the Pauli blocking effect, which is a consequence of the exclusion principle according to which the nucleon in the intermediate loop function cannot be placed in those states already occupied by the nucleons of the Fermi sea. The allowed intermediate states of the perturbative expansion must have momenta larger than the Fermi momentum and, consequently, the position of the dynamically generated states shifts to higher energies. Another way of justifying this effect is by realizing that the in-medium meson-nucleon interaction is expected to be less attractive because the intermediate nucleons need more energy to access free or empty states. The other in-medium effect is related to the fact that the properties of all mesons and

$(I,\ S,\ C)$	M, Γ [MeV]	Main decay modes $\lvert g\rvert(channel)$
$(\frac{1}{2},\ -1,\ -1)$	$2906, 0$	$1.3(\overline{D}_s N)$, $1.1(\overline{D}\Lambda)$, $1.9(\overline{D}\Sigma)$
$(0,\ 0,\ 1)$	$2595, 0.5$	$0.31(\pi\Sigma_c)^*$, $11(DN)$, $6.0(D_s\Lambda)$,$2.0(\eta_c\Lambda_c)$
	$2805, 0.01$	$0.04(\pi\Sigma_c)^*$, $0.27(DN)$, $2.2(\eta\Lambda_c)$, $4.3(K\Xi_c)$
$(1,\ 0,\ 1)$	$2551, 0.16$	$0.05(\pi\Lambda_c)^*$, $3.7(\pi\Sigma_c)$, $1.1(DN)$, $2.1(K\Xi_c^{'})$
	$2804, 5$	$0.27(\pi\Lambda_c)^*$, $0.14(\pi\Sigma_c)^*$, $2.1(DN)$, $1.8(D_s\Sigma)$
$(\frac{1}{2},\ 1,\ 1)$	2946 (cusp)	$< 10^{-3}(K\Lambda_c)^*$, $< 10^{-3}(D_s N)^*$, $< 10^{-3}(K\Sigma_c)$

Table 6.2: Dynamically generated baryon resonances with open charm in various $(I,\ S,\ C)$ sectors for a cut-off momentum $\lambda = 903$ MeV/c. The Table shows the position (M) and width (Γ) of the resonance, together with the couplings to the most important meson-baryon channels, as well as the couplings to the channels in which it can decay (marked with an asterisk).

baryons are modified in the medium due to their interactions with the Fermi sea of nucleons, also called particle dressing. The effect of the finite temperature in nuclear matter will compensate the Pauli-blocking effect because baryons close to their respective Fermi seas will move upwards to higher momentum states, leaving the lowest momentum states partially occupied. Consequently, as the temperature increases the possibility of accessing states below the different Fermi seas becomes larger.

Pauli blocking, medium modification of the baryon energy spectra and finite temperature effects can be incorporated in the coupled-channel equations by simply replacing the free baryon propagator (Eq. (2.43) in Chapter 2) by the in-medium one,

$$G(p_0, \vec{p}, \rho, T) = \frac{M}{E(|\vec{p}|, T)} \left[\frac{1 - n(\vec{p}, \rho, T)}{p_0 - E(|\vec{p}|, T) + i\epsilon} + \frac{n(\vec{p}, \rho, T)}{p_0 - E(|\vec{p}|, T) - i\epsilon} \right] , \quad (6.1)$$

where $(p_0, \vec{p})$ is the total four-momentum of the baryon in the nuclear matter rest

ρ [fm^{-3}]	T [MeV]	Σ^s [MeV]	Σ^v [MeV]	$\Sigma^v - \Sigma^s$	$\Sigma^v_{Y_{(c)}} - \Sigma^s_{Y_{(c)}}$
0.16	0	360.1	281.7	−78.4	−52.3
0.16	100	304.7	281.7	−23	−15.3
0.32	0	496.5	421.5	−75	−50
0.32	100	428.8	421.5	−7.3	−4.9

Table 6.3: Nucleon scalar (Σ^s) and vector (Σ^v) self-energies for the densities and temperatures explored in this thesis. The last columns show the value of the baryon self-energy at zero momentum.

frame and $n(\vec{p}, \rho, T)$ is the usual Fermi–Dirac distribution function. Similarly to the in-medium D meson study of ref. [TRM08] the nucleon energy spectrum, $E_N(|\vec{p}|, T)$, is taken from a Walecka-type $\sigma - \omega$ model [Kap06]

$$E_N(|\vec{p}|, T) = \sqrt{\vec{p}^{\,2} + (M_N - \Sigma^s(T))^2} + \Sigma^v \ . \tag{6.2}$$

The values of the nucleon scalar (Σ^s) and vector (Σ^v) self-energies for the densities and temperatures explored in this thesis are given in Table 6.3. The hyperon (Y) and charmed baryon (Y_c) energy spectra are similarly given as

$$E_{Y_{(c)}}(|\vec{p}|, T) = \sqrt{\vec{p}^{\,2} + (M_{Y_{(c)}} - \Sigma^s_{Y_{(c)}}(T))^2} + \Sigma^v_{Y_{(c)}} \ . \tag{6.3}$$

Assuming that the σ and ω fields couple only to the u and d quarks, the scalar and vector self-energies of the hyperons and charmed baryons can be written in terms of Σ^s and Σ^v, as

$$\Sigma^s_{Y_{(c)}} = \frac{2}{3}\,\Sigma^s \ , \qquad \Sigma^v_{Y_{(c)}} = \frac{2}{3}\,\Sigma^v \ . \tag{6.4}$$

The resonances that play a relevant role in the properties of the open-charmed mesons do not couple significatively to baryons having only one light (u or d) quark. Therefore, we disregard the dressing of this type of baryons (Ξ_c, Ξ_c', Ξ_{cc}).

The nuclear medium effects on the mesons can be incorporated by including their corresponding self-energies, $\Pi_m(q_0, \vec{q}, \rho, T)$, in the meson propagator

$$D_m(q_0, \vec{q}, \rho, T) = \frac{1}{q_0^2 - \vec{q}^{\,2} - m_m^2 - \Pi_m(q_0, \vec{q}, \rho, T)} \ , \tag{6.5}$$

being $(q_0, \vec{q})$ the four-momentum of the meson. This is done in practice through the corresponding Lehmann representation of the meson propagator

$$D_m(q_0, \vec{q}, \rho, T) = \int_0^\infty \frac{S_m(\omega, \vec{q}, \rho, T)}{q_0 - \omega + i\epsilon} d\omega - \int_0^\infty \frac{S_{\bar{m}}(\omega, \vec{q}, \rho, T)}{q_0 + \omega - i\epsilon} d\omega \ , \tag{6.6}$$

where $S_{m(\bar{m})}(\omega, \vec{q}, \rho, T)$ is the spectral function of the meson $m(\bar{m})$:

$$\begin{aligned} S_m(q_0, \vec{q}, \rho, T) = & -\frac{1}{\pi} \mathrm{Im}\left(D_m(q_0, \vec{q}, \rho, T)\right) \\ = & -\frac{1}{\pi} \frac{\mathrm{Im}\left(\Pi_m(q_0, \vec{q}, \rho, T)\right)}{|q_0^2 - \vec{q}^{\,2} - m_m^2 - \Pi_m(q_0, \vec{q}, \rho, T)|^2} \ . \end{aligned} \tag{6.7}$$

We note here that in this thesis only the $D, \bar{D}, D_s$ and $\bar{D}_s$ mesons have been dressed by self-energy insertions. Mesons π, K, η, η' and η_c have not been dressed, as neglected also in [MR06, TRM08, TGRN09]. The reason is that the states containing these mesons couple weakly to the DN and D_sN ones and, therefore, it is expected that approximating the π, K, η, η' spectral functions by the free-space ones, *i.e.,* delta functions, will not influence much the in-medium properties of the D and D_s mesons. We emphasize, however, that the present work addresses for the first time the simultaneous dressing of the D and D_s mesons in the charm $C = 1$ sector, and that of the $\bar{D}$ and $\bar{D}_s$ mesons in the charm $C = -1$ one.

The loop function for the free case given by Eq. (2.43) must now be replaced by the one including the medium and temperature effects on the baryon and meson propagators, as given by Eqs. (6.1) and (6.6). Using the Imaginary Time (or

Matsubara) Formalism [Mat55] we obtain:

$$
\begin{aligned}
G_k^{(I,S,C)}(P_0,\vec{P},\vec{k},\rho,T) &= \frac{M_k}{E_k(|x\vec{P}+\vec{k}\,|,T)} \\
&\left(\int_0^\infty d\omega\ S_m(\omega,y\vec{P}-\vec{k},\rho,T)\frac{1-n(x\vec{P}+\vec{k},\rho,T)+f(\omega,T)}{P_0-\omega-E_k(|x\vec{P}+\vec{k}\,|,T)+i\epsilon}\right. \\
&\left.+\int_0^\infty d\omega\ S_{\bar{m}}(\omega,y\vec{P}-\vec{k},\rho,T)\frac{n(x\vec{P}+\vec{k},\rho,T)+f(\omega,T)}{P_0+\omega-E_k(|x\vec{P}+\vec{k}\,|,T)-i\epsilon}\right),
\end{aligned}
\tag{6.8}
$$

where $P_0 = q_0 + E_k(|\vec{p}|)$, $\vec{P} = \vec{q} + \vec{p}$ and $\vec{k} = y\vec{p} - x\vec{q}$, with $x = M_k/(m_k + M_k)$ and $y = m_k/(m_k + M_k)$, are the total energy, total momentum, and relative momentum of the meson-baryon pair in the nuclear matter rest frame, n is the Fermi distribution of the baryon and f is the Bose enhancement factor of the meson. In practice, given the nuclear densities and temperatures explored in this Chapter, we can set $f = 0$ for all mesons and $n = 0$ for all baryons except for nucleons. One might argue that the Bose enhancement factor for the pions should not be ignored. However, as tested in [TRM08], the DN amplitudes are insensitive to this factor due to the reduced coupling to $\pi\Sigma_c$ states resulting from the heavy mass of the meson exchanged in the transition potential.

The in-medium scattering amplitudes T are obtained by directly solving the coupled-channel L-S equation (Eq. (2.42)) with the medium modified loop function (see Eq. (6.8)). The in-medium self-energies for the $D, \bar{D}, D_s$ and $\bar{D}_s$ mesons are then obtained by integrating the in-medium diagonal scattering amplitudes over the nucleon Fermi sea as

$$
\begin{aligned}
\Pi_{D(\bar{D})}(q_0,\vec{q},\rho,T) = \int \frac{d^3p}{(2\pi)^3} n(\vec{p},\rho,T)\ &[T^{(I=0)}_{D(\bar{D})N}(P_0,\vec{P},\rho,T) \\
&+ 3T^{(I=1)}_{D(\bar{D})N}(P_0,\vec{P},\rho,T)]\ ,
\end{aligned}
\tag{6.9}
$$

for D and $\bar{D}$, and as

$$
\Pi_{D_s(\bar{D}_s)}(q_0,\vec{q},\rho,T) = 4\int \frac{d^3p}{(2\pi)^3} n(\vec{p},\rho,T)\ T^{(I=1/2)}_{D_s(\bar{D}_s)N}(P_0,\vec{P},\rho,T)\ , \tag{6.10}
$$

for D_s and $\bar{D}_s$.

Finally, we note that the self-energies Π_m ($m = D, \bar{D}, D_s, \bar{D}_s$) must be determined in a self-consistent way since they are obtained from the in-medium scattering amplitudes T_{DN}, $T_{\bar{D}N}$, T_{D_sN} and $T_{\bar{D}_sN}$, which contain the loop functions $G_{DN}^{(I,S,C)}$, $G_{D_sY}^{(I,S,C)}$ (DN case); $G_{\bar{D}N}^{(I,\ S,C)}$ ($\bar{D}N$ case); $G_{D_sN}^{(I,S,C)}$ (D_sN case); and $G_{\bar{D}_sN}^{(I,S,C)}$, $G_{\bar{D}Y}^{(I,S,C)}$ ($\bar{D}_sN$ case), that are themselves functions of the self-energies Π_m.

6.4 In-medium results

6.4.1 Cold matter

We will start discussing our results for the $C = 1$ mesons, D and D_s. First of all, we note that their in-medium properties will be influenced by the charm $C = 1$ baryonic resonances that couple significatively to DN and D_sN. From the results presented in Chapter 4, summarized in Table 6.2, we find the well known $\Lambda_c(2595)$, coupling very strongly to DN states in the $(I = 0,\ S = 0)$ sector, and two other resonances, $\Sigma_c(2551)$ and $\Sigma_c(2804)$, coupling also significatively to DN in the sector $(I = 1,\ S = 0)$. The cusp-like structure found in the $(I = 1/2,\ S = 1)$ sector shows also a sizable coupling to D_sN states.

In Fig. 6.1, we show the imaginary part of the DN amplitude at normal nuclear matter saturation density, $\rho_0 = 0.17$ fm^{-1}, and zero temperature, as a function of the center-of-mass energy P_0, covering an energy range that includes the most relevant resonance in each isospin sector, $I = 0$ (left panel) and $I = 1$ (right panel), for various approximations. The amplitude in free space ($\rho = 0$) is also shown (thin-solid lines), as a reference. When only Pauli blocking effects are included (dashed line) we observe that the $\Lambda_c(2595)$ and $\Sigma_c(2804)$ states appear displaced to higher energies, by about 60 and 50 MeV, respectively. This repulsive effect is well known, and has to do with the loss of phase space associated to the fact that the nucleons are forced to occupy empty states that are located at momentum states above the Fermi momentum. However, when the dressing of the D meson is incorporated self-consistently (dotted line) the $\Lambda_c(2595)$ resonance moves to substantially lower energies and the $\Sigma_c(2804)$ dilutes. This is naturally explained in terms of the D-meson strength distribution which, as we will see,

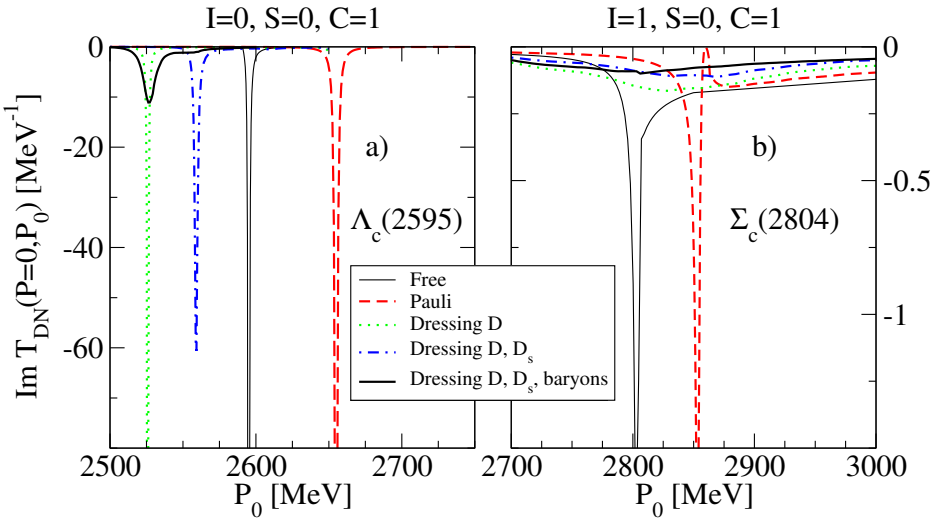

Figure 6.1: Imaginary part of the $I = 0$ (left panel) and $I = 1$ (right panel) $DN \to DN$ scattering amplitudes in nuclear matter at normal saturation density ρ_0 and zero temperature, as function of the total energy P_0, for a total momentum $\vec{P} = 0$ and various approximations.

shows a quasiparticle peak at a lower energy than in free space and a pronounced peak at even lower energies related to $\Lambda_c(2595)N^{-1}$ excitations. The reduced in-medium DN threshold opens decay channels for the $\Sigma_c(2804) \to \Lambda_c(2595)N^{-1}N$ which, therefore, broadens considerably. As for the $\Lambda_c(2595)$, its position is very sensitive to the low energy strength of the D spectral function and, together with the large coupling to DN states, explains why the resonance acquires such a large amount of attraction.

In [MR06], where the TVME in the $t \to 0$ limit is employed, a similar behavior is observed for the $\Lambda_c(2595)$. The repulsive shift with respect to the free space position due to Pauli blocking effects is compensated by the attractive self-consistent dressing of the D meson. However, the shift is smaller in [MR06], as it can be seen from Fig. 5 of this reference (model B). Moreover, this TVME ($t \to 0$) model also generates a Σ_c resonance, which lies around 2795 MeV for model B.

This structure melts down as the dressing of D mesons is incorporated, because of the opening of new absorption channels, and stays close to the position with only Pauli blocking effects, in agreement with our present results. In the TVME model of [LK06] both resonances are generated but the Σ_c one is localized at a much smaller energy, around 2620 MeV. In that work the self-consistent dressing of D mesons results in an attractive shift for both Λ_c and Σ_c dynamically generated resonances, in contrast to our results. Within the SU(8) Weinberg-Tomozawa model of [GR$^+$09], where heavy-quark spin symmetry is implemented, the Σ_c state lies around 2900 MeV and has a different spin, $J = 3/2$. In this scheme, the Σ_c resonance couples strongly to the D^*N channel instead of DN and behaves similarly in matter as the $\Lambda_c(2595)$ [TGRN09].

It is clear from Table 6.2 that the sizable coupling of the $\Lambda_c(2595)$ resonance to the $D_s\Lambda$ channel and that of the $\Sigma_c(2804)$ to $D_s\Sigma$ states, makes it advisable to consider also the medium modifications of the D_s meson in the intermediate D_sY loops of the DN amplitude. This is a quite arduous task that, up to our knowledge, has been attempted for the first time in this thesis. Our results, represented by the dash-dotted lines in Fig. 6.1, clearly show the importance of such dressing. The strength of the dressed D_sY loop gets diluted, making the $\Lambda_c(2595)$ to appear 35 MeV higher in energy with respect to the case of considering free D_sY loops. The changes on the $\Sigma_c(2804)$ resonance are more moderate. Finally, including the baryon self-energies (solid line), which produce attraction in the baryon spectrum at ρ_0 and T=0, moves the resonances to lower energies due to the fact that the threshold for intermediate DN states has also been lowered.

The real and imaginary parts of the D and D_s self-energies and spectral functions at normal nuclear matter saturation density and zero temperature are shown in Fig. 6.2, as functions of the meson energy, q_0, and for a meson momentum $q = 0$ MeV/c. The approximations displayed include: Pauli blocking effects; the additional self-consistent dressing of the given meson; and, in the case of the D meson, the additional dressing of the D_s meson in the D_sY intermediate states coupling to DN. Results obtained when baryon self-energies are taken into account are also shown.

The features discussed for the DN amplitude in Fig. 6.1 are also reflected

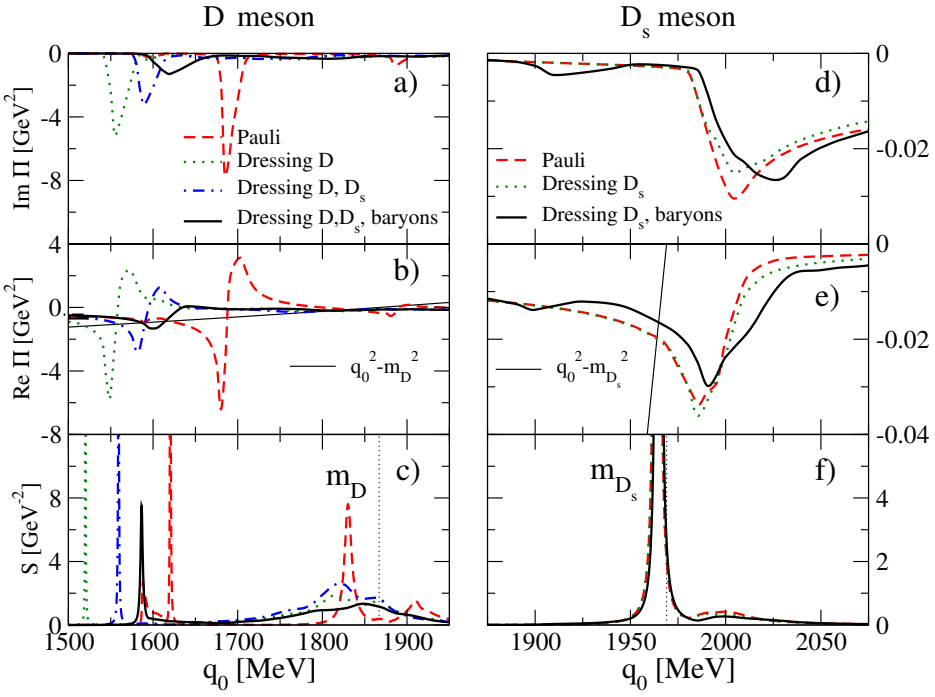

Figure 6.2: Imaginary (upper panels) and real (middle panels) parts of the D (left panel) and D_s (right panel) meson self-energies and spectral functions (lower panels), as functions of the meson energy q_0, at normal nuclear matter saturation density, for $q = 0$ MeV/c and different approximations. The mass of the D meson and the function $q_0^2 - m_D^2$ (left panel) and the mass of the D_s meson and the function $q_0^2 - m_{D_s}^2$ (right panel) are shown for comparison.

in the imaginary part of the D-meson self-energy displayed in the upper left panel of Fig. 6.2. The middle panel shows the corresponding real part of the self-energy, $\mathrm{Re}\,\Pi(q_0, \vec{q} = 0)$, together with the function $q_0^2 - m_D^2$ (thin solid line), such that the crossing points of these two functions signal the appearance of pronounced maxima in the spectral function, as long as the imaginary part does not show a pronounced minimum there. Actually, the distribution of the D-meson strength shown in the lower-left panel is very rich. All the approximations give a quasiparticle peak located around 35 MeV below the free D-meson mass, signalled by a thin vertical dotted line. In addition, each resonance leaving a signature in

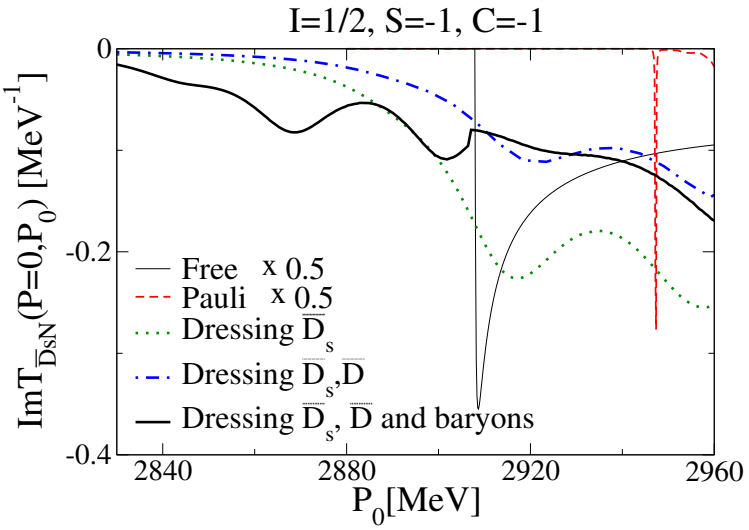

Figure 6.3: Imaginary part of the $I = 1/2$, $S = -1$ and $C = -1$ $\overline{D}_s N \to \overline{D}_s N$ scattering amplitude in nuclear matter at normal saturation density ρ_0 and zero temperature, as a function of the total energy P_0, for a total momentum $\vec{P} = 0$ and various approximations.

the self-energy produces a resonant-hole excitation peak in the spectral function, located at a somewhat different value of energy due to the complex structure of the self-energy. The common behavior is that the resonance-hole modes in the spectral function get displaced, with respect to the energy signalling the mode in Im(Π), in the direction of moving further away from the quasiparticle peak. In the case of Pauli blocking, we can clearly distinguish three of such modes at 1590 MeV, 1625 MeV and 1910 MeV associated to $\Sigma_c(2551)N^{-1}$, $\Lambda_c(2595)N^{-1}$ and $\Sigma_c(2804)N^{-1}$ excitations.

When meson dressing is incorporated, only the $\Lambda_c(2595)N^{-1}$ excitation mode is clearly visible. The $\Sigma_c(2804)N^{-1}$ mode merges with the quasiparticle peak, and the $\Sigma_c(2551)N^{-1}$ one is no longer visible in the spectral function as compared to the $\Lambda_c(2595)N^{-1}$ mode. A similar behavior has been observed in [MR06, TRM08]. In contrast, in [LK06], the $\Sigma_c(2804)N^{-1}$ mode appears at a much lower energy and mixes with the $\Lambda_c(2595)N^{-1}$ one, while the quasiparticle peak of the D meson

experiences a repulsive shift of 32 MeV. It is also worth mentioning that in the SU(8)-inspired model of [TGRN09] the quasiparticle peak appears at slightly lower energies than the free mass but the D-meson spectral function shows a completely different shape due to the different resonant-hole composition of the D-meson self-energy.

The imaginary part of the D_s self-energy, displayed in the upper right panel of Fig. 6.2, shows only a small enhancement at around 2 GeV. This is a reflection of the enhanced cusp found in the ($I = 1/2,\ S = 1,\ C = 1$) amplitude at the $K\Sigma_c$ threshold [JTRV09]. This structure generates a small but non-negligible amount of strength in the D_s spectral function to the right of the quasiparticle peak, which barely moves from its free location. This is in contrast to [LK06], where a resonance is generated dynamically 75 MeV below the D_sN threshold, and the corresponding resonance-hole state in the spectral function appears on the left-hand side of the quasiparticle peak.

In spite of the featureless aspect of the D_s spectral function in our model, this relocation of strength from the quasiparticle peak to higher energies diminishes the size of the D_sY loops involved in the coupled-channel problem. Therefore, the simultaneous dressing of the D and D_s mesons in our self-consistent coupled-channel model produces a less bound $\Lambda_c(2595)$ resonance in nuclear matter, as already shown in Fig. 6.1. From Fig. 6.2 we can see that the corresponding $\Lambda_c(2595)N^{-1}$ excitation mode of the D-meson spectral function appears approximately 40 MeV higher in energy than when only the D-meson dressing is considered. Finally, including the dressing of the baryons moves the $\Lambda_c(2595)N^{-1}$ structure to higher energies by 27 MeV because the attraction felt by the $\Lambda_c(2595)$ resonance in the medium is smaller than that felt by the dressed nucleon.

The in-medium properties of the $C = -1$ mesons, $\bar{D}$ and $\bar{D}_s$, will be determined by the behavior of the corresponding $\bar{D}N$ and $\bar{D}_sN$ amplitudes in the nuclear medium. In Fig. 6.3 we display the imaginary part of the $\bar{D}_sN$ amplitude at normal nuclear matter saturation density and zero temperature as a function of the center-of-mass energy P_0, for various approximations: free (thin-solid line), Pauli blocking (dashed line), the self-consistent calculation including only the dressing of D_s (dotted line) or including both D_s and D dressings (dash-dotted line), and, finally, the full calculation that also incorporates the dressing of the

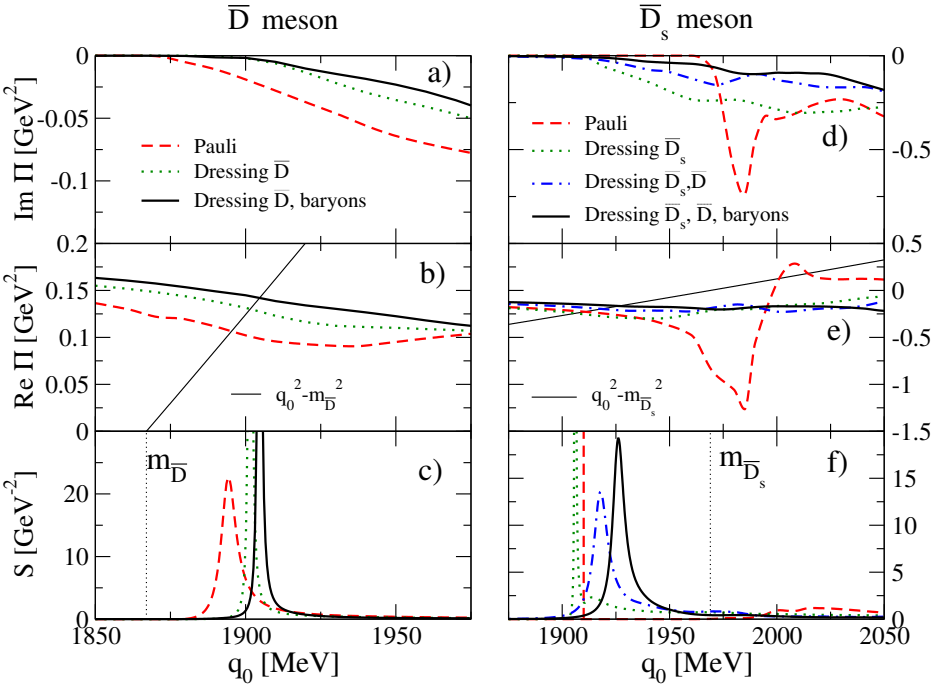

Figure 6.4: The same as Fig. 6.2 for the $\bar{D}$ (left panels) and $\bar{D}_s$ (right panels) mesons.

baryons (solid line). This is the most interesting of the $C = -1$ sectors considered since the $\bar{D}_s N$ system develops in free space a subthreshold bound state at 2906 MeV that couples significatively to $\bar{D}_s N$ states. Therefore, this pole will be very sensitive to the medium effects. Indeed, when only Pauli blocking effects are considered, the pole moves about 40 MeV towards higher energy as expected. We observe very drastic changes when the dressing of the $\bar{D}$ and $\bar{D}_s$ mesons is incorporated. The reason is that, as we will see, the in-medium quasiparticle peak of the $\bar{D}_s$ meson experiences a strong attraction. This moves the in-medium threshold for $\bar{D}_s N$ states below the position of the resonance, making its decay possible and quite probable due to the significant coupling to these states. When the baryon self-energies are included, the amplitude shifts towards lower energies by an amount consistent with the attraction felt by the dressed baryons.

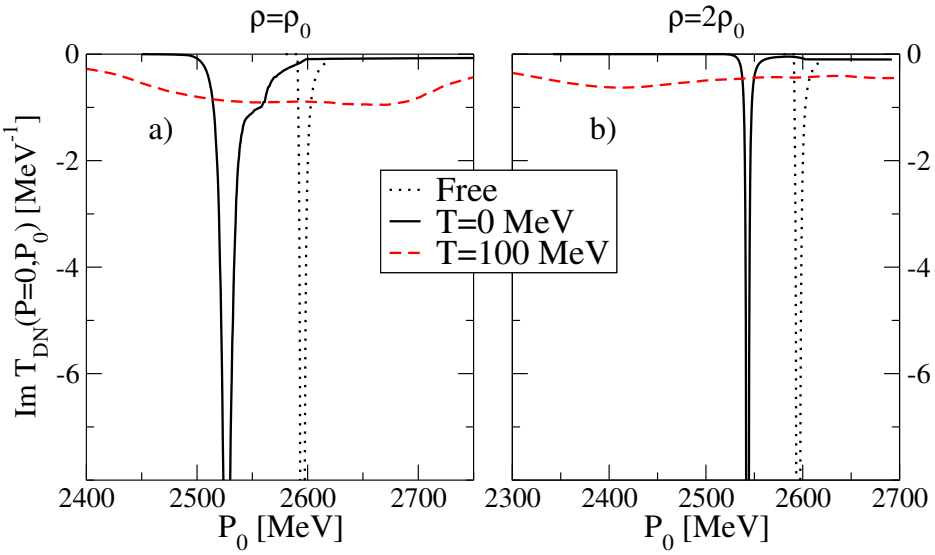

Figure 6.5: Imaginary part of the $I = 0$, $DN \to DN$ scattering amplitudes in nuclear matter at ρ_0 (left panel) and $2\rho_0$ (right panel), as functions of the total energy P_0, for a total momentum $\vec{P} = 0$ and two temperatures, $T = 0$ (solid lines) and $T = 100$ MeV (dashed lines). The calculation in free space is also given for reference.

The $\bar{D}$ and $\bar{D}_s$ self-energies and spectral functions are shown in Fig. 6.4 as functions of q_0, including Pauli blocking effects, the additional self-consistent dressing of the given meson, and, in the case of the $\bar{D}_s$, incorporating also the dressing of the $\bar{D}$ meson in the $\bar{D}Y$ intermediate states coupling to $\bar{D}_s N$. Results when baryon dressing is included are also shown. Again the thin solid lines indicate the $q_0^2 - m_{\bar{D}}^2$ (left panel) and the $q_0^2 - m_{\bar{D}_s}^2$ functions (right panel). The self-energy of the $\bar{D}$ mesons is quite smooth due to the absence of resonances in the $\bar{D}N$ sector. The repulsive character of the $\bar{D}N$ amplitude gives rise to a quasiparticle peak in the $\bar{D}$ spectral function appearing at higher energy than the $\bar{D}$ meson mass, by 30 MeV in the case of considering Pauli blocking effects only, or by 35 MeV when the additional self-consistent dressing of the $\bar{D}$ meson is also taken into account. The repulsive mass shift obtained in [TRM08, LK06] is somewhat smaller, of the order of 20 MeV for both cases. On the other hand, the

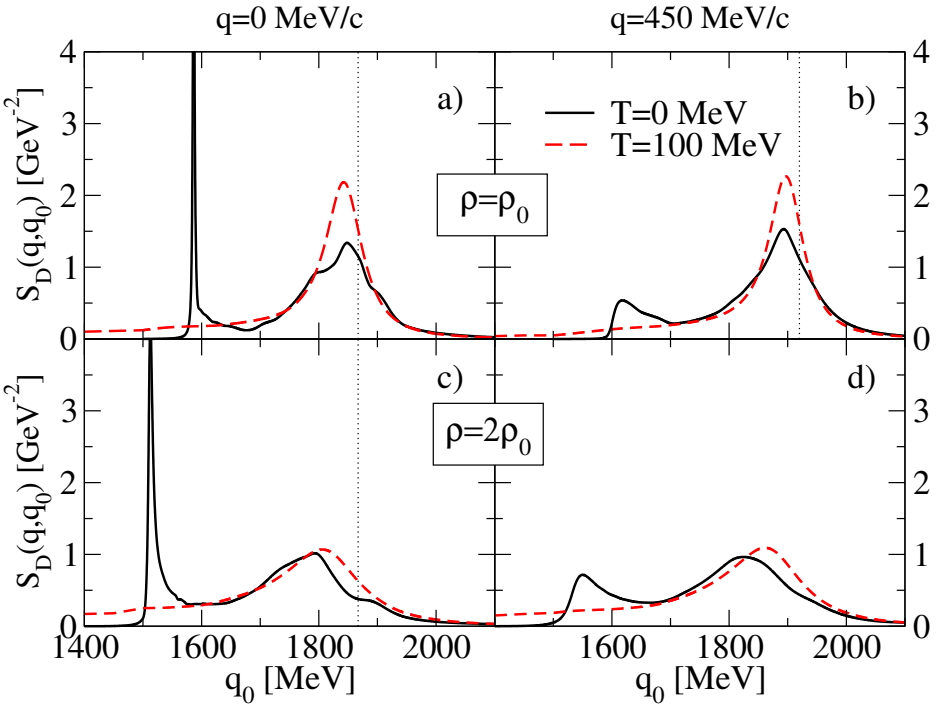

Figure 6.6: The spectral function of the D meson at $\rho = \rho_0$ (upper panels) and $\rho = 2\rho_0$ (lower panels), two temperatures, $T = 0$ (solid lines) and $T = 100$ (dashed lines) and two values of momentum, $q = 0$ MeV/c (left panels) and $q = 450$ MeV/c (right panels). Dotted lines indicates the free mass of the meson

self-energy of the $\bar{D}_s$ meson shows a richer structure, which, in the case of Pauli-blocking, it is seen as a bump in the spectral function around 2000 MeV. This is a reflection of the presence, in the $\bar{D}_s N$ amplitude, of a pole at 2906 MeV, which appears shifted about 40 MeV to higher energies when Pauli blocking effects are incorporated (Fig. 6.3). The dressing of the $\bar{D}_s$ meson smears this structure in such a way that one barely sees any trace of it in the corresponding spectral function. Moreover, the delta-like quasiparticle peak, appearing 60 MeV below the free $\bar{D}_s$ mass when only Pauli blocking effects are considered, moves to slightly lower energies when the $\bar{D}_s$ meson is dressed. Considering the additional dressing of the $\bar{D}$ meson in the related $\bar{D}Y$ loops produces a substantial change in the $\bar{D}_s$

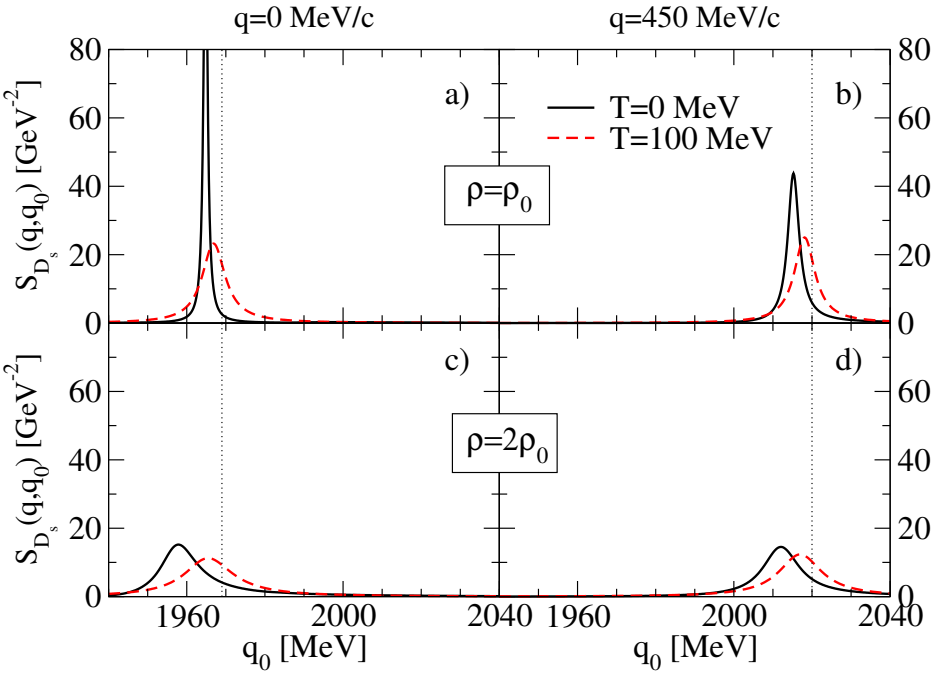

Figure 6.7: The same as Fig. 6.6 for the D_s meson.

self-energy. This is easy to understand from the results of Table 6.2, where we see that the pole at 2906 MeV couples also very strongly to $\bar{D}Y$ states. The loss of attraction in the region of the quasiparticle peak moves it towards a higher energy. Finally, the effect of including the dressing of the baryons moves the $\overline{D}_s$ quasiparticle peak further up which ends being around 40 MeV below the free mass. Our findings differ again quite strongly from those of [LK06], which are dominated by an exotic coupled-channel molecule at 2780 MeV [HL05], which is the equivalent to the pole at 2906 MeV found in the model of [JTRV09] and used in the present Chapter.

As a consequence, the spectral function for the $\bar{D}_s$ meson found in [LK06] shows two distinct peaks, the quasiparticle one located about 10 MeV above the free $\bar{D}_s$ mass, and a narrow resonance-hole mode located 150 MeV below.

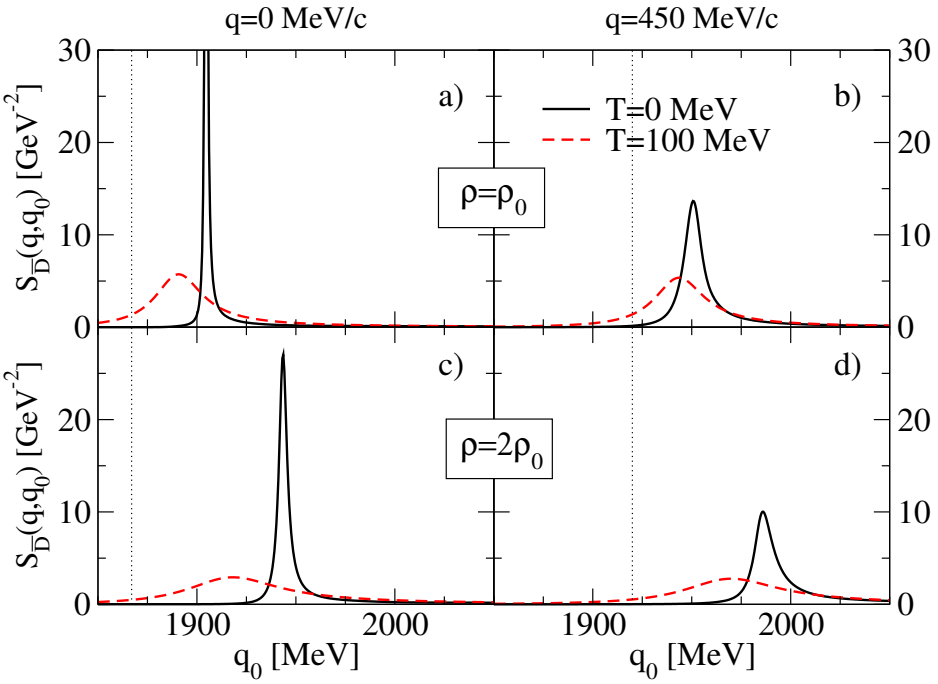

Figure 6.8: The same as Fig. 6.6 for the $\bar{D}$ meson.

6.4.2 Finite temperature

In Fig. 6.5 we display the behavior of the $\Lambda_c(2595)$ resonance at two densities, ρ_0 and $2\rho_0$, and two temperatures, $T = 0$ and $T = 100$ MeV. Results are presented for the complete model that includes the self-consistent meson self-energies and the dressing of the baryons. We observe that the in-medium resonance at $T = 0$ appears below the free space position, by 75 MeV for ρ_0 and 50 MeV for $2\rho_0$. This behavior can be essentially understood from the stronger Pauli blocking effect at $2\rho_0$. The changes associated with temperature are also very significant. As already seen in [TRM08], increasing the temperature broadens the $\Lambda_c(2595)$ considerably due to the spreading of the D-meson strength because of the effect of smearing of the Fermi motion effects.

The effect of density and temperature in the spectral functions of the D,

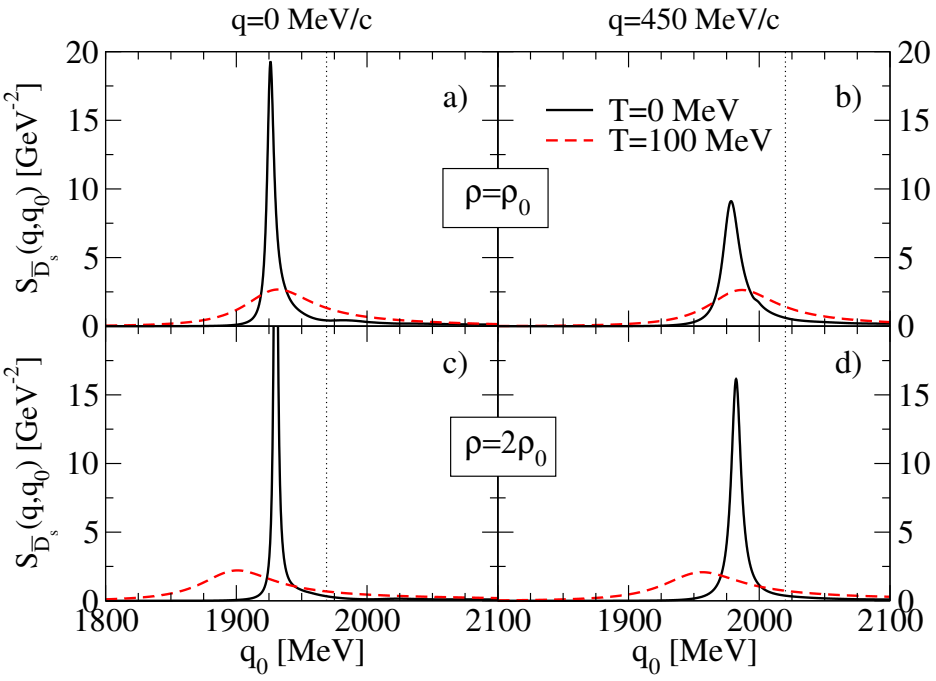

Figure 6.9: The same as Fig. 6.6 for the $\bar{D}_s$ meson.

D_s, $\bar{D}$ and $\bar{D}_s$ mesons are shown in Figs. 6.6 to 6.9, where we compare results for two temperatures, $T = 0$ (solid lines) and $T = 100$ (dashed lines), and two densities, $\rho = \rho_0$ (upper panels) and $\rho = 2\rho_0$ (lower panels), for two values of momentum, $q = 0$ MeV/c (left panels) and $q = 450$ MeV/c (right panels), in the case of the complete self-consistent calculation, which includes Pauli blocking and dressing of mesons and baryons. A common behavior in all spectral functions is that increasing the temperature moves the quasiparticle peak towards its free location. This is a reflection of the reduced size of the self-energy, because, being built up from an average over the smeared thermal Fermi distribution, involves higher momentum components for which the meson-nucleon interaction is weaker. Except for a few cases, increasing the temperature gives rise to wider quasiparticle peaks because of the increase of collisional width. However, the opposite effect is seen for the D meson in Fig. 6.6. As already discussed in [TRM08], this is

due to the fact that the strength under this peak also receives contributions from $\Sigma_c(2804)N^{-1}$ hole excitations, which are washed out by temperature as any other resonant-hole mode. Consequently, the peak of the D-meson spectral function becomes narrower and more symmetric as temperature increases, similarly to what is found in [TRM08].

The density effects observed in the spectral functions are also clearly understood. In general, we find that the self-energy roughly doubles its size when going from nuclear matter at normal nuclear matter saturation density to a system which is two times denser. This is consistent with the low density limit behavior and points at a weak density dependence of the in-medium meson-nucleon amplitude in this density region. This is the reason why, in general, the quasiparticle peak of the spectral functions at $2\rho_0$ are found approximately twice further away from the free space position and are twice wider than in the case of ρ_0.

7

Summary and Conclusions

The purpose of this thesis has been to study the properties of the dynamically generated baryon resonances and mesons in the charm sector. We have solved the Bethe-Salpeter (B-S) equation through a coupled channel procedure in order to obtain the scattering matrix. We have looked for poles in the second Riemann sheet and have characterized the different bound states with the position, width and couplings of the resonance to the different channels. This method has allowed us to understand the differences and similarities between the $\Lambda(1405)$ resonance from the strange sector and the $\Lambda_c(2595)$ resonance from the charm one. Moreover, we have identified some of the s-wave baryon resonances (with $C = 1$ and $J^P = \frac{1}{2}^-$) obtained in our model with observed experimental states, and have studied its radiative decay into the ground state baryons. By including in our model the temperature and the in-medium effects we have understood the properties of the charmed baryon resonances and mesons in hot and dense matter. The analysis and conclusions of the results are summarized in the following lines.

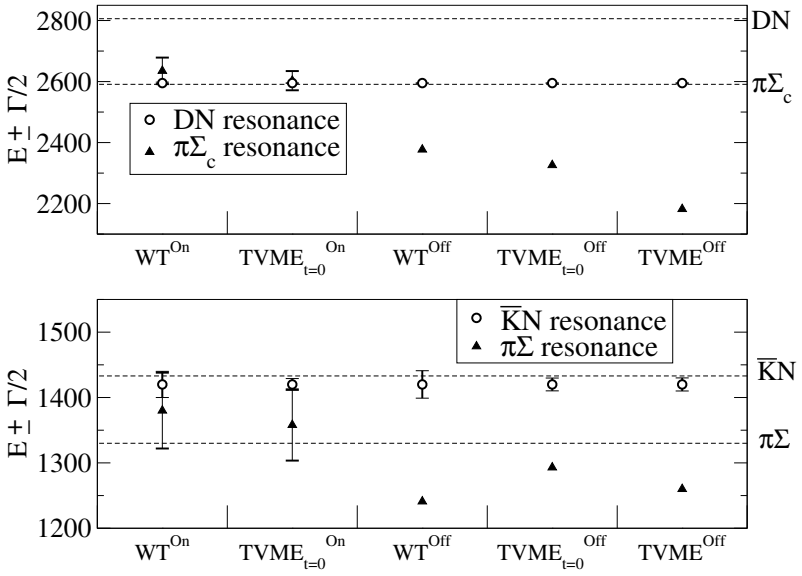

Figure 7.1: Summary of the results obtained in Chapter 3 for the different models applied to study the $\Lambda_c(2595)$ and the $\Lambda(1405)$ resonances. The upper panel shows the resonances that couple mostly to $\pi\Sigma_c$ (triangles) and DN (circles) channels while in the lower panel, the resonances that couple mostly to $\pi\Sigma$ (triangles) and $\overline{K}N$ (circles) states are plotted. The error bars represent the width of each resonance and the dashed lines indicate the meson-baryon decay channels in each sector. For more details, see Tables 3.6 and 3.7.

In Chapter 3 we have compared two different flavor sectors with $I = 0$, focussing on the characteristics of the $\Lambda_c(2595)$ resonance versus those of the $\Lambda(1405)$ resonance. We have chosen a set of five different coupled-channel models, according to the different kernels employed (WT, $\text{TVME}_{t\to 0}$ and TVME) as well as to their on- and off-shell character in the unitarization procedure. In Fig. 7.1 we present a summary of the results where the position of the resonances are shown for the different models, once the cut-off is conveniently adjusted to reproduce the $\Lambda_c(2595)$ resonance in the $C = 1$ sector and the $\Lambda(1420)$ resonance in the $S = -1$ sector.

- All models reproduce the experimental information on the $\Lambda_c(2595)$ and the $\Lambda(1420)$ resonances, as dynamically generated DN and $\overline{K}N$ states,

respectively.

- The predicted widths agree with the order of magnitude of the experimental ones. The $\Lambda_c(2595)$ resonance is much narrower than the $\Lambda(1420)$ one. This is in agreement with the experimental data because the $\Lambda_c(2595)$ couples relatively weakly to $\pi\Sigma_c$ states and it lies only few MeV above their threshold, in contrast with the $\Lambda(1420)$ resonance, located about 90 MeV above the $\pi\Sigma$ threshold.

- In general, the resonances are further apart in off-shell models than in on-shell ones for both sectors, as it can be appreciated in Fig. 7.1. For this reason, the resonances which couple mostly to the first threshold (the $\pi\Sigma$ and the $\pi\Sigma_c$ resonances) acquire a certain width for on-shell models, while in off-shell ones they lay below the lightest threshold.

In Chapter 4 we have studied charmed baryon resonances with $J = \frac{1}{2}^-$ obtained from a coupled channels unitary approach using the full $t-$dependence of the TVME driving force. For that purpose we have solved the L-S equation to obtain the scattering amplitude. To the best of our knowledge, all previous models of dynamically generated baryon resonances in the charm sector rely on a local zero-range interaction, which is obtained by neglecting the four-momentum transfer t in front of the mass of the exchanged vector meson squared, m_v^2. We have analyzed in detail the effects of going beyond the $t \to 0$ approximation and, taking as reference the $I = 0$, $C = 1$, $J = 1/2$ sector of the $\Lambda_c(2595)$ resonance, we fix the model with a cut-off regularization value of 903 MeV/c. We summarize the results obtained for the $C = 1$ sectors in Fig. 7.2.

- We have illustrated that the value t/m_v^2 is not at all negligible in the heavy sector, especially for charm-exchange amplitudes which produce a large value of the four-momentum transfer due to the large difference between the masses of the mesons involved in the transition.

- Compared to the local models, our approach obtains basically the same amount of resonances in all sectors but appearing, in general, at somewhat larger energies because the diagonal amplitudes, largely responsible for generating the bound states, are smaller in magnitude. The non-local approach

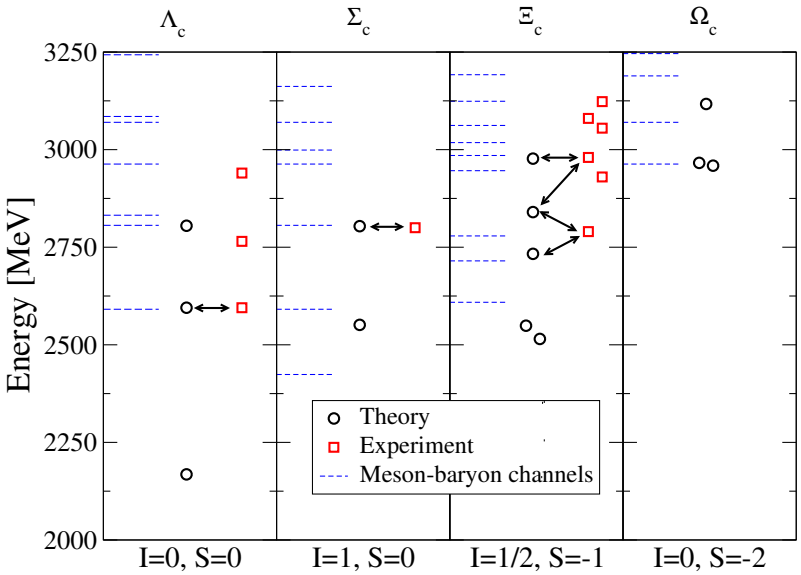

Figure 7.2: Summary of the $C = 1$ baryon resonances with $J^P = \frac{1}{2}^-$ obtained for the different (I, S) sectors in Chapter 4, for $\lambda = 903$ MeV/c. From left to right we show the results for the Λ_c, Σ_c, Ξ_c and Ω_c baryon families. The open circles are the predicted resonances in our model and the open squares are the experimental ones. The different meson-baryon decay channels for each sector are represented with dashed horizontal lines. For details on the width and couplings of the resonances to the different channels, see Tables 4.4, 4.6, 4.8 and 4.10 for the predicted resonances and Table 4.2 for the experimental ones. We have omitted, for the sake of clarity, the resonances placed at 5248 MeV and 5382 MeV in the Λ_c and Ξ_c spectrum, respectively. The arrows relate the resonances obtained in our model to the experimental states they could be identified with (see Tab. 4.13).

produces wider resonances because of the larger value of the non-diagonal amplitudes when $t \neq 0$.

- Varying the cut-off parameter within a reasonable range, we are able to locate some of our states, marked with circles in Fig 7.2, at the energy position of a measured resonance. In particular, we suggest the identification of the $\Lambda_c(2595)$, $\Sigma_c(2800)$, $\Xi_c(2790)$ and $\Xi_c(2980)$ as dynamically generated resonances.

- In general, the widths of the states produced by our model are smaller than the experimentally observed ones, since we do not account for three-particle decay channels.

- We find a possible resonance in the sector with quantum numbers $(I, S, C) = (\frac{1}{2}, 1, 1)$ that can only be realized by the consideration of a minimum of five quarks. The cusp-like structure observed at the threshold of the $K\Sigma_c$ channel for a cut-off value of 903 MeV/c, becomes a more bound and wider clear resonance as the cut-off value increases.

In Chapter 5 we have studied the radiative decay width of the dynamically generated charmed baryon resonances from Chapter 4, into ground state baryons with $J^P = \frac{1}{2}^+$.

- We have obtained a sizable value for the one-photon radiative width of the $\Lambda_c(2595)$ resonance. This resonance decays radiatively mostly into $\Lambda_c\gamma$ states, with a partial rate of $\Gamma_{\Lambda_c(2595)\to\Lambda_c\gamma} = (274.3 \pm 52.0)$ KeV, while only a tiny amount of the width, $\Gamma_{\Lambda_c(2595)\to\Sigma_c^+\gamma} = (2.1 \pm 0.4)$ KeV, is due to the decay into $\Sigma_c\gamma$ final states. Our results are very different, in size and distribution among decay channels, to what is found by other approaches in the literature.

- We have also presented predictions for the radiative decay of other excited charmed baryons. The radiative decay widths of the $\Sigma_c(2800)$ and $\Xi_c(2980)$ resonances are found to be relatively small, of the order of a few tenths of KeV. However, the transitions $\Xi_c(2790)^+ \to \Xi_c^+\gamma$ and $\Xi_c(2780)^0 \to \Xi_c^0\gamma$ are substantially larger, worth exploring experimentally.

- The sizable value of some widths, especially those of the $\Lambda_c(2595)$ and the $\Xi_c(2780)$ resonances, makes the study of these radiative reactions a very useful tool to obtain information about the characteristics of these charmed baryons.

In Chapter 6 we have studied the properties of open-charmed mesons, D, $\bar{D}$, D_s and $\bar{D}_s$, in nuclear matter at finite temperature within a self-consistent coupled-channel approach which uses, as meson-baryon interaction, a full

t-dependent vector meson exchange driving force. The in-medium scattering amplitudes are obtained by solving the L-S equation at finite temperature including Pauli blocking effects, the self-consistent D, $\bar{D}$, D_s and $\bar{D}_s$ self-energies, paying a particular attention to their mutual influence, and the dressing of the baryons.

- We have analyzed how our dynamically generated resonances are affected by density and temperature. As in other similar approaches, the resonances that couple strongly to intermediate states involving nucleons, move upwards in energy when Pauli blocking effects are considered, as a consequence of the loss of phase space. When the self-consistent dressing of the charmed mesons is incorporated, the resonances gain attraction again.

- We have seen that dressing the D_s meson has a non-negligible effect on the DN amplitude and on the properties of the D meson. Therefore, we conclude that is necessary a simultaneous in-medium treatment of the D and D_s mesons. Similarly, the in-medium properties of the $\bar{D}_s$ and $\bar{D}$ mesons are interrelated and must also be considered together.

- The spectral functions of the D and $\bar{D}_s$ mesons are quite rich. At $T = 0$ MeV and normal nuclear matter density one finds a quasiparticle peak located below the corresponding free meson mass, as well as strength associated to resonant-hole excitations. In the particular case of the D meson, a narrow $\Lambda_c(2595)N^{-1}$ excitation peak is clearly visible.

- In general, increasing the temperature has the effect of moving the quasiparticle peak towards its free location making it wider, as a consequence of a milder meson-baryon interaction and a larger amount of collisions. The exception found for the D-meson is naturally explained in terms of the mixing of the quasiparticle peak with a resonant-hole mode.

- For the densities explored, up to twice nuclear matter normal saturation density, we have found that the density effects follow the linear behavior expected for the low density regime: the self-energy roughly doubles its size when going from nuclear matter at normal saturation density to a system which is two times denser, indicating a mild density dependence of the in-medium meson-baryon interaction amplitudes.

We are aware that imposing the aproximate heavy quark symmetry observed in nature, according to which all types of spin interactions vanish for infinitely massive quarks, would imply treating heavy pseudoscalars and heavy vector mesons on an equal footing. Therefore, our approach should be extended to the vector mesons such that it also includes, for instance, the D^*N and D_s^*Y channels in the $C = 1$, $S = 0$ sector. This has been already considered by the SU(8) inspired approaches, which employ local meson-baryon interactions involving both $J^P = 0^-$ and 1^- mesons, as well as $J^P = 1/2^+$ and $3/2^+$ baryons. Vector meson-baryon interactions induced by vector meson exchange can also be built using, for instance, the VVV lagrangians of the local hidden gauge formalism. However, the coupling of VB states to PB states is not a trivial task in the framework of non-local models. Therefore, incorporating the coupling to states involving vector mesons in our approach, which uses a coupled-channel formalism, an interaction that goes beyond the $t \to 0$ limit, and, in the case of hot and dense matter, the simultaneous consideration of the in-medium D and D_s ($\bar{D}_s$ and $\bar{D}$) meson self-energies, requires an enormous computational effort that goes beyond our means. We hope that, by first identifying which channels play a relevant role and which ones might be omitted, we can make progress toward this goal in the nearby future.

Resumen

El objetivo principal de esta tesis es el estudio de las resonancias bariónicas generadas a partir de la interacción dinámica entre dos hadrones. Estamos interesados en este estudio como un enfoque alternativo para explicar el creciente número de estados con encanto observados experimentalmente, y que aparentemente no encajan con la imagen tradicional de un barión como partícula compuesta por tres quarks. En particular, se estudian las moléculas bariónicas con números cuánticos $J^P = \frac{1}{2}^-$ que se forman a partir de la interacción atractiva en onda-s ($l = 0$), de un mesón pseudoescalar (0^-) y un barión del estado fundamental ($\frac{1}{2}^+$). Por lo tanto, nuestro cometido es contribuir a la comprensión del espectro experimental de bariones con encanto, comprobando si un origen dinámico puede explicar aquellos estados que son candidatos potenciales a ser una resonancia bariónica con $J^P = \frac{1}{2}^-$.

7.1 Espacio libre

La primera parte de la tesis está orientada a estudiar este tipo de bariones moleculares en el espacio libre. Con el fin de aprender sobre la naturaleza de un barión es importante estudiar sus diferentes tipos de desintegración. Por esta razón, vamos a calcular el desintegración fuerte de cada resonancia generada dinámicamente en los canales mesón-barión disponibles y la transición electromagnética de estos bariones al estado fundamental o de más baja energía. El esquema de los diferentes Capítulos que conforman esta primera parte es el siguiente.

En el Capítulo 2 presentamos el formalismo para la dispersión de dos partículas y los diferentes potenciales que describen la interacción entre los mesones pseudoscalares y los bariones del estado fundamental. Además, introducimos la ecuación de Bethe-Salpeter (B-S) a partir de la cual obtenemos la amplitud para cada canal. Cada resonancia, extraída como un polo en la matriz de dispersión para energías complejas, se caracteriza por un conjunto de parámetros específicos, masa, anchura (inversamente proporcional a la vida media) y el acoplo que presenta la resonancia a cada uno de los canales meson-barión.

En el Capítulo 3 se han estudiado dos sectores de diferente sabor, ambos con $I = 0$, centrándonos en las características de la resonancia $\Lambda_c(2595)$ ($C = 1$) y comparándola con la resonancia $\Lambda(1405)$ ($S = -1$). Para llevarlo a cabo, hemos escogido un conjunto de cinco modelos diferentes basados en el acoplamiento de canales. Los modelos se diferencian los unos de los otros por el carácter "on-shell" y "off-shell" en el proceso de unitarización, así como por los potenciales empleados (WT, TVME $_{t\to 0}$ y TVME). Todos los modelos reproducen los datos experimentales disponibles sobre las resonancias $\Lambda_c(2595)$ y $\Lambda(1420)$, y las generan de forma dinámica como estados ligados meson–barión, DN y $\overline{K}N$, respectivamente. Las anchuras calculadas teóricamente están en concordancia con el orden de magnitud de las medidas experimentales. Tal y como se observa en el experimento, en nuestros cálculos la resonancia $\Lambda_c(2595)$ es mucho más estrecha que la $\Lambda(1420)$. Esto se debe a que la resonancia $\Lambda_c(2595)$ acopla débilmente al canal $\pi\Sigma_c$, encontrándose a tan sólo unos pocos MeV por encima de este umbral, en contraste con la resonancia $\Lambda(1420)$, la cual está situada a unos 90 MeV por encima del umbral $\pi\Sigma$. En general, las resonancias se encuentran más separadas en los mo-

delos "off-shell" que en los modelos "on-shell". Esta es la razón por la cual las resonancias que se acoplan en su mayoría al primer umbral ($\pi\Sigma$ y $\pi\Sigma_c$) se situan por encima de él y por lo tanto adquieren cierta anchura en los modelos "on-shell". Sin embargo, en los modelos "off-shell" se encuentran por debajo del umbral y en consecuencia carecen de anchura.

En el Capítulo 4 hemos estudiado las resonancias bariónicas con $C = 1$ y números cuánticos $J = \frac{1}{2}^-$, utilizando el potencial de intercambio de mesones vectoriales TVME, sin ninguna aproximación. Para llevarlo a cabo, hemos resuelto la ecuación de Lippmann-Schwinger (L-S) para obtener la amplitud de dispersión. En modelos anteriores a nuestro trabajo, donde también generan resonancias bariónicas con encanto de forma dinámica, la interacción entre mesón y barión quedaba descrita con un potencial local, que se obtiene despreciando el cuadrimomento transferido t con respecto al cuadrado de la masa del mesón intercambiado m_v. Hemos analizado en detalle los efectos de ir más allá de la aproximación $t \to 0$. Tomamos como referencia el sector de $I = 0$, $C = 1$, $J = \frac{1}{2}^-$ para ajustar la resonancia $\Lambda_c(2595)$ a su posición experimental. Para ello, ajustamos el parámetro con el que limitamos la integral divergente del propagador mesón-barión a un valor de 903 MeV/c. Destacamos que el valor de t/m_v^2 no es en absoluto despreciable en el sector del encanto, sobre todo para las amplitudes en las cuales ocurre el intercambio de encanto, debido a la gran diferencia de masas de los mesones que participan en dichas transiciones. En comparación con los modelos locales ($t \to 0$), con nuestro enfoque obtenemos la misma cantidad de resonancias en todos los sectores. La diferencia está en que aparecen, en general, a energías un poco más altas debido a que las amplitudes diagonales del potencial son de menor magnitud que para los modelos locales. La aproximación no-local produce resonancias más anchas debido al mayor valor de las amplitudes no diagonales cuando $t \neq 0$.

En el Capítulo 5 se han estudiado las anchuras de desintegración radiactiva de las resonancias bariónicas con encanto (generadas dinámicamente en el Capítulo 4) en los estado bariónicos de más baja energía ($J^P = \frac{1}{2}^+$). Hemos obtenido un valor considerable para la anchura electromagnética de la resonancia $\Lambda_c(2595)$. Esta resonancia se desintegra principalmente en estados $\Lambda_c\gamma$, con una tasa parcial de $\Gamma_{\Lambda_c(2595)\to\Lambda_c\gamma} = (274{,}3 \pm 52{,}0)$ KeV, mientras que tan sólo una parte

de las veces se desintegra en estados $\Sigma_c\gamma$, obteniendo una anchura radiactiva de $\Gamma_{\Lambda_c(2595)\to\Sigma_c^+\gamma} = (2{,}1 \pm 0{,}4)$ KeV. Nuestros resultados son muy diferentes a los obtenidos por otros métodos en la literatura, en cuanto al tamaño y distribución de los canales de desintegración. También hemos presentado predicciones acerca de la desintegración radiactiva de otros bariones con encanto. Las achuras de desintegración radiactivo de las resonancias $\Sigma_c(2800)$ y $\Xi_c(2970)$ son relativamente pequeñas, del orden de unas pocas décimas de KeV. Sin embargo, las transiciones $\Xi_c(2790)^+ \to \Xi_c^+\gamma$ y $\Xi_c(2790)^0 \to \Xi_c^0\gamma$ son considerablemente más grandes, y por lo tanto merece la pena validarlas experimentalmente. El valor considerable de determinadas anchuras, en especial para las resonancias $\Lambda_c(2595)$ y $\Xi_c(2790)$, hace que el estudio de estas reacciones sea una herramienta muy útil para obtener información sobre las características de estos bariones con encanto.

7.2 Medio nuclear

En la segunda parte de la tesis hemos incluido en el formalismo los efectos del medio y de la temperatura finita para estudiar las propiedades de las resonancias bariónicas con encanto en la materia densa y a altas temperaturas. Además, esto nos permitirá estudiar las propiedades de los mesones encantados (D, $\overline{D}$,D_s y $\overline{D_s}$) en el medio nuclear. El comportamiento de estos mesones influirá en la producción de "charmonium"(estados $c\bar{c}$) cuya supresión está relacionada con la posible formación de plasma de quark y gluones en materia densa y caliente. Para describir la interacción mesón-barión seguimos utilizando el potencial no-local de intercambio de mesones vectoriales, TVME. Las amplitudes de dispersión en el medio nuclear se obtienen resolviendo la ecuación de L-S a temperatura finita, incluyendo los efectos de bloqueo de Pauli para fermiones y la autoenergía que los mesones D, $\bar{D}$, D_s, y $\bar{D}_s$ desarrollan en el medio, prestando especial atención a su influencia mutua. Del mismo modo tenemos en cuenta la autoenergía que los bariones experimentan en el medio nuclear. Hemos analizado cómo las propiedades de las resonancias generadas dinámicamente se ven afectadas por la densidad y la temperatura. Las resonancias que se acoplan fuertemente a los estados intermedios de los nucleones se desplazan energéticamente hacia arriba cuando se consideran los efectos de bloqueo de Pauli, como consecuencia de

la disminución del espacio de fase. Cuando se incorpora la autoenergía de los mesones encantados de manera autoconsistente, las resonancias vuelven a ganar atracción de nuevo. Hemos comprobado que la incorporación de la autoenergía de los mesones D_s tiene un efecto no despreciable en la amplitud DN y también en las propiedades del mesón D. Por lo tanto, es necesario el tratamiento de los mesones D y D_s en el medio nuclear de manera simultánea. Del mismo modo, las propiedades de los mesones $\bar{D}_s$ y $\bar{D}$ en el medio también están interrelacionadas y deben ser consideradas en conjunto. Las funciones espectrales de los mesones D y $\bar{D}_s$ son muy ricas en estructura. Para $T = 0$ MeV y una densidad normal de materia nuclear se encuentra un pico de cuasipartícula por debajo de la masa libre del mesón. También se encuentran por debajo de esta energía los llamados picos de "resonancia-hueco", que en el caso del mesón D es un pico de excitación, $\Lambda_c(2595)N^{-1}$, claramente visible. En general, el aumento de la temperatura tiene el efecto de mover el pico de cuasipartícula hacia el lugar que ocupa en el espacio libre. Debido a que las interacciones entre mesón-barión son más débiles y hay muchas más colisiones por el efecto de la temperatura, el pico se hace más ancho. El pico de cuasipartícula para el mesón D no se comporta según este patrón. Esta excepción se debe al solapamiento del pico de cuasipartícula con un pico de excitación "resonancia-hueco". Hemos encontrado que los efectos de la densidad en las autoenergías de los mesones siguen el comportamiento esperado para las densidades exploradas, que van hasta el doble de la densidad normal de saturación de la materia nuclear. La autoenergía duplica su tamaño al pasar de la materia nuclear con densidad de saturación normal a un sistema dos veces más denso, lo que indica que las amplitudes mesón-barión en el medio tienen una dependencia leve con la densidad.

A

The SU(4) meson-baryon coefficients

We present the SU(4) coefficients, $C_{ij,v}$, which denote the strength of the interaction between a pseudoscalar meson and a ground-state baryon mediated by the vector meson interchange in the different isospin (I), strangeness (S) and charm (C) sectors and channels (i, j). The first and second column at the tables show the initial (i) and the final (j) meson-baryon states, the third column (v) denotes the possible vector mesons interchanged ($\rho, K^*, \overline{K}^*, \omega, \phi, D^*, D_s^*, \overline{D}^*, \overline{D}_s^*, J/\Psi$) and the fourth column is the value of the coefficient. We only show in the tables the coefficients which are different from 0.

$(I=0,\ S=0,\ C=1)$			
i	j	v	$C_{ij,v}$
$\pi\Sigma_c$	$\pi\Sigma_c$	ρ	8
	DN	D^*	$\sqrt{6}$
	$K\Xi_c'$	K^*	$2\sqrt{3}$
	$\overline{D}\Xi_{cc}$	D^*	$\sqrt{6}$
DN	DN	ρ	3
		ω	3
	$\eta\Lambda_c$	D^*	$-\sqrt{2}$
	$D_s\Lambda$	K^*	$-2\sqrt{3}$
	$\eta'\Lambda_c$	D^*	-2
	$\eta_c\Lambda_c$	D^*	$2\sqrt{3}$
$\eta\Lambda_c$	$K\Xi_c$	K^*	$-2\sqrt{3}$
	$D_s\Lambda$	D_s	$-2\sqrt{2/3}$
	$\overline{D}\Xi_{cc}$	D^*	$-\sqrt{2}$
$K\Xi_c$	$K\Xi_c$	ρ	3
		ω	-1
		ϕ	2
	$D_s\Lambda$	D^*	$-\sqrt{2}$
	$\overline{D}\Xi_{cc}$	D_s	$\sqrt{6}$
$K\Xi_c'$	$K\Xi_c'$	ρ	3
		ω	-1
		ϕ	2
	$D_s\Lambda$	D^*	$-\sqrt{6}$
	$\overline{D}\Xi_{cc}$	D_s	$\sqrt{2}$
$D_s\Lambda$	$K\Xi_c'$	ϕ	2
	$\eta'\Lambda_c$	D_s	$2/\sqrt{3}$
	$\eta_c\Lambda_c$	D_s	-2
$\eta'\Lambda_c$	$\overline{D}\Xi_{cc}$	D^*	-2
$\eta_c\Lambda_c$	$\overline{D}\Xi_{cc}$	D^*	$2\sqrt{3}$
$\overline{D}\Xi_{cc}$	$\overline{D}\Xi_{cc}$	ρ	3
		ω	-1
		J/Ψ	4

Table A.1: The SU(4) $C_{ij,v}$ coefficients for $(I=0,\ S=0,\ C=1)$.

$(I=1,\ S=0,\ C=1)$			
i	j	v	$C_{ij,v}$
$\pi\Lambda_c$	DN	D^*	$-\sqrt{6}$
	$K\Xi_c$	K^*	2
	$\overline{D}\Xi_{cc}$	D^*	$\sqrt{6}$
$\pi\Sigma_c$	$\pi\Sigma_c$	ρ	4
	DN	D^*	2
	$K\Xi_c'$	K^*	$2\sqrt{2}$
	$\overline{D}\Xi_{cc}$	D^*	2
DN	DN	ρ	-1
		ω	3
	$\eta\Sigma_c$	D^*	$\sqrt{2/3}$
	$D_s\Sigma$	K^*	-2
	$\eta'\Sigma_c$	D^*	$2/\sqrt{3}$
	$\eta_c\Sigma_c$	D^*	-2
$K\Xi_c$	$K\Xi_c$	ρ	-1
		ω	-1
		ϕ	2
	$D_s\Sigma$	D^*	$\sqrt{6}$
	$\overline{D}\Xi_{cc}$	D_s	$\sqrt{6}$
$\eta\Sigma_c$	$K\Xi_c'$	K^*	$-2\sqrt{3}$
	$D_s\Sigma$	D_s	$2\sqrt{2/3}$
	$\overline{D}\Xi_{cc}$	D^*	$-\sqrt{2/3}$
$K\Xi_c'$	$K\Xi_c'$	ρ	-1
		ω	-1
		ϕ	2
	$D_s\Sigma$	D^*	$-\sqrt{2}$
	$\overline{D}\Xi_{cc}$	D_s	$\sqrt{2}$
$D_s\Sigma$	$D_s\Sigma$	ϕ	2
	$\eta'\Sigma_c$	D_s	$-2/\sqrt{3}$
	$\eta_c\Sigma_c$	D_s	2
$\eta'\Sigma_c$	$\overline{D}\Xi_{cc}$	D^*	$-2/\sqrt{3}$
$\overline{D}\Xi_{cc}$	$\overline{D}\Xi_{cc}$	ρ	-1
Continued on next page			

Continued from previous page			
$(I=1,\ S=0,\ C=1)$			
i	j	v	$C_{ij,v}$
		ω	-1
		J/Ψ	4
	$\eta_c\Sigma_c$	D^*	2

Table A.2: The SU(4) $C_{ij,v}$ coefficients for $(I=1,\ S=0,\ C=1)$.

$(I=\frac{1}{2},\ S=-1,\ C=1)$			
i	j	v	$C_{ij,v}$
$\pi\Xi_c$	$\pi\Xi_c$	ρ	4
	$\overline{K}\Lambda_c$	K^*	$\sqrt{6}$
	$D\Lambda$	D^*	$-\sqrt{3/2}$
	$D\Sigma$	D^*	$-\sqrt{3/2}$
	$\overline{D}\Omega_{cc}$	D^*	-3
$\pi\Xi_c'$	$\pi\Xi_c'$	ρ	4
	$\overline{K}\Sigma_c$	K^*	$-\sqrt{2}$
	$D\Lambda$	D^*	$-3/\sqrt{2}$
	$D\Sigma$	D^*	$1/\sqrt{2}$
	$K\Omega_c$	K^*	$2\sqrt{3}$
	$\overline{D}\Omega_{cc}$	D^*	$\sqrt{3}$
$\overline{K}\Lambda_c$	$\overline{K}\Lambda_c$	ω	2
	$D\Lambda$	D_s	2
	$\eta\Xi_c$	K^*	$-\sqrt{6}$
	$\overline{D}_s\Xi_{cc}$	D^*	$\sqrt{6}$
$\overline{K}\Sigma_c$	$\overline{K}\Sigma_c$	ρ	4
		ω	2
	$D\Sigma$	D_s	-2
	$\eta\Xi_c$	K^*	$-3\sqrt{2}$
	$\overline{D}_s\Xi_{cc}$	D^*	$\sqrt{6}$
$D\Lambda$	$D\Lambda$	ω	2
	$\eta\Xi_c$	D^*	$1/\sqrt{6}$
Continued on next page			

Continued from previous page			
$(I = \frac{1}{2},\ S = -1,\ C = 1)$			
i	j	v	$C_{ij,v}$
	$\eta\Xi_c$	D^*	$1/\sqrt{2}$
	$D_s\Xi$	K^*	$\sqrt{6}$
	$\eta'\Xi_c$	D^*	$1/\sqrt{3}$
	$\eta'\Xi'_c$	D^*	1
	$\eta_c\Xi_c$	D^*	-1
	$\eta_c\Xi'_c$	D^*	$-\sqrt{3}$
$\eta\Xi_c$	$D\Sigma$	D^*	$-\sqrt{3/2}$
	$D_s\Xi$	D_s	-2
	$\overline{D}_s\Xi_{cc}$	D_s	-2
	$\overline{D}\Omega_{cc}$	D^*	-1
$D\Sigma$	$D\Sigma$	ρ	4
		ω	2
	$\eta\Xi_c$	D^*	$1/\sqrt{2}$
	$D_s\Xi$	K^*	$-\sqrt{6}$
	$\eta'\Xi_c$	D^*	$-\sqrt{3}$
	$\eta'\Xi'_c$	D^*	1
	$\eta_c\Xi_c$	D^*	$-2\sqrt{3}+3/2$
	$\eta_c\Xi'_c$	D^*	$-\sqrt{3}$
$\eta\Xi_c$	$K\Omega_c$	K^*	$2\sqrt{3}$
	$D_s\Xi$	D_s	$-2/\sqrt{3}$
	$\overline{D}_s\Xi_{cc}$	D_s	$-2/\sqrt{3}$
	$\overline{D}\Omega_{cc}$	D^*	$1/\sqrt{3}$
$K\Omega_c$	$K\Omega_c$	ϕ	4
	$D_s\Xi$	D^*	-2
	$\overline{D}\Omega_{cc}$	D_s	2
$D_s\Xi$	$D_s\Xi$	ϕ	4
	$\eta'\Xi_c$	D_s	$\sqrt{2}$
	$\eta'\Xi'_c$	D_s	$\sqrt{2/3}$
	$\eta_c\Xi_c$	D_s	$-\sqrt{6}$
	$\eta_c\Xi'_c$	D_s	$-\sqrt{2}$
$\eta'\Xi_c$	$\overline{D}_s\Xi_{cc}$	D_s	$\sqrt{2}$
Continued on next page			

Continued from previous page			
$(I = \frac{1}{2},\ S = -1,\ C = 1)$			
i	j	v	$C_{ij,v}$
	$\overline{D}\Omega_{cc}$	D^*	$-\sqrt{2}$
$\eta'\Xi'_c$	$\overline{D}_s\Xi_{cc}$	D_s	$\sqrt{2/3}$
	$\overline{D}\Omega_{cc}$	D^*	$\sqrt{2/3}$
$\eta_c\Xi_c$	$\overline{D}_s\Xi_{cc}$	D_s	$-\sqrt{6}$
	$\overline{D}\Omega_{cc}$	D^*	$\sqrt{6}$
$\overline{D}_s\Xi_{cc}$	$\overline{D}_s\Xi_{cc}$	J/Ψ	4
	$\overline{D}\Omega_{cc}$	K^*	-2
	$\eta_c\Xi'_c$	D_s	$-\sqrt{2}$
$\overline{D}\Omega_{cc}$	$\overline{D}\Omega_{cc}$	J/Ψ	4
	$\eta_c\Xi'_c$	D^*	$-\sqrt{2}$

Table A.3: The SU(4) $C_{ij,v}$ coefficients for $(I = \frac{1}{2},\ S = -1,\ C = 1)$.

$(I = 2,\ S = 0,\ C = 1)$			
i	j	v	$C_{ij,v}$
$\pi\Sigma_c$	$\pi\Sigma_c$	ρ	-4

Table A.4: The SU(4) $C_{ij,v}$ coefficients for $(I = 2,\ S = 0,\ C = 1)$.

$(I=\frac{3}{2},\ S=-1,\ C=1)$			
i	j	v	$C_{ij,v}$
$\pi\Xi_c$	$\pi\Xi_c$	ρ	-2
	$D\Sigma$	D^*	$\sqrt{6}$
$\pi\Xi_c'$	$\pi\Xi_c'$	ρ	-2
	$\overline{K}\Sigma_c$	K^*	$2\sqrt{2}$
	$D\Sigma$	D^*	$-\sqrt{2}$
$\overline{K}\Sigma_c$	$\overline{K}\Sigma_c$	ρ	-2
		ω	2
	$D\Sigma$	D_s	-2
$D\Sigma$	$D\Sigma$	ρ	-2
		ω	2

Table A.5: The SU(4) $C_{ij,v}$ coefficients for $(I=\frac{3}{2},\ S=-1,\ C=1)$.

$(I = 0,\ S = -2,\ C = 1)$			
i	j	v	$C_{ij,v}$
$\overline{K}\Xi_c$	$\overline{K}\Xi_c$	ρ	3
		ω	1
		ϕ	-2
	$D\Xi$	D_s	$\sqrt{6}$
	$\overline{D}_s\Omega_{cc}$	D^*	$-2\sqrt{3}$
$\overline{K}\Xi_c'$	$\overline{K}\Xi_c'$	ρ	3
		ω	1
		ϕ	-2
	$D\Xi$	D_s	$\sqrt{2}$
	$\eta\Omega_c$	K^*	$-2\sqrt{6}$
	$\overline{D}_s\Omega_{cc}$	D^*	2
$D\Xi$	$D\Xi$	ρ	3
		ω	1
	$\eta\Omega_c$	D^*	$-2/\sqrt{3}$
	$\eta'\Omega_c$	D^*	$-2\sqrt{2/3}$
	$\eta_c\Omega_c$	D^*	$2\sqrt{2}$
$\eta\Omega_c$	$\overline{D}_s\Omega_{cc}$	D_s	$-2\sqrt{2/3}$
$\eta'\Omega_c$	$\overline{D}_s\Omega_{cc}$	D_s	$2/\sqrt{3}$
$\overline{D}_s\Omega_{cc}$	$\overline{D}_s\Omega_{cc}$	ϕ	-2
		J/Ψ	4
	$\eta_c\Omega_c$	D_s	-2

Table A.6: The SU(4) $C_{ij,v}$ coefficients for $(I = 0,\ S = -2,\ C = 1)$.

$(I=1,\ S=-2,\ C=1)$			
i	j	v	$C_{ij,v}$
$\pi\Omega_c$	$\overline{K}\Xi_c'$	K^*	$-2\sqrt{2}$
	$D\Xi$	D^*	-2
$\overline{K}\Xi_c$	$\overline{K}\Xi_c$	ρ	-1
		ω	1
		ϕ	-2
	$D\Xi$	D_s	$\sqrt{6}$
$\overline{K}\Xi_c'$	$\overline{K}\Xi_c'$	ρ	-1
		ω	1
		ϕ	-2
	$D\Xi$	D_s	$\sqrt{2}$
$D\Xi$	$D\Xi$	ρ	-1
		ω	1

Table A.7: The SU(4) $C_{ij,v}$ coefficients for $(I=1,\ S=-2,\ C=1)$.

$(I=\frac{1}{2},\ S=1, C=1)$			
i	j	v	$C_{ij,v}$
$K\Lambda_c$	$K\Lambda_c$	ω	-2
	D_sN	D^*	$-\sqrt{6}$
D_sN	$K\Sigma_c$	D^*	$\sqrt{6}$
$K\Sigma_c$	$K\Sigma_c$	ρ	4
		ω	-2

Table A.8: The SU(4) $C_{ij,v}$ coefficients for $(I=\frac{1}{2},\ S=1,\ C=1)$.

$(I = \frac{3}{2},\ S = 1,\ C = 1)$			
i	j	v	$C_{ij,v}$
$K\Sigma_c$	$K\Sigma_c$	ρ	-2
		ω	-2

Table A.9: The SU(4) $C_{ij,v}$ coefficients for $(I = \frac{3}{2},\ S = 1,\ C = 1)$.

$(I = \frac{1}{2},\ S = -3,\ C = 1)$			
i	j	v	$C_{ij,v}$
$\overline{K}\Omega_c$	$\overline{K}\Omega_c$	ϕ	-4

Table A.10: The SU(4) $C_{ij,v}$ coefficients for $(I = \frac{1}{2},\ S = -3,\ C = 1)$.

$(I = \frac{1}{2},\ S = -1,\ C = -1)$			
i	j	v	$C_{ij,v}$
$\overline{D}_s N$	$\overline{D}\Lambda$	ρ	$\sqrt{6}$
	$\overline{D}\Sigma$	K^*	$\sqrt{6}$
$\overline{D}\Lambda$	$\overline{D}\Lambda$	ω	-2
$\overline{D}\Sigma$	$\overline{D}\Sigma$	ρ	4
		ω	-2

Table A.11: The SU(4) $C_{ij,v}$ coefficients for $(I = \frac{1}{2},\ S = -1,\ C = -1)$.

$(I=1,\ S=0,\ C=-1)$			
i	j	v	$C_{ij,v}$
$\overline{D}N$	$\overline{D}N$	ρ	-1
		ω	-3

Table A.12: The SU(4) $C_{ij,v}$ coefficients for $(I=1,\ S=0,\ C=-1)$.

$(I=0,\ S=0,\ C=-1)$			
i	j	v	$C_{ij,v}$
$\overline{D}N$	$\overline{D}N$	ρ	3
		ω	-3

Table A.13: The SU(4) $C_{ij,v}$ coefficients for $(I=0,\ S=0,\ C=-1)$.

B

Numerical solution of the L-S equation in free space

In this appendix we will show how to get the numerical solution of the L-S equation already presented in Chapter 2:

$$T_{ij}(\vec{k}_i,\vec{k}_j;\sqrt{s}) = V_{ij}(\vec{k}_i,\vec{k}_j) + \sum_l \int_0^\infty \frac{dk_n^3}{(2\pi)^3} \frac{F(\vec{k}_n)M_l}{E_l(\vec{k}_n)2\omega_l(\vec{k}_n)} \frac{V_{il}(\vec{k}_i,\vec{k}_n)T_{lj}(\vec{k}_n,\vec{k}_j;\sqrt{s})}{\sqrt{s}-E_l(\vec{k}_n)-\omega_l(\vec{k}_n)+i\eta}\,. \tag{B.1}$$

In free space and for a s-wave interaction, none of the members in the integrand depends on the solid angle, thus the problem is reduced to solve the integral of

the modulus of the relative momenta k_n:

$$T_{ij}(k_i,k_j) = V_{ij}(k_i,k_j) + \sum_{M_l B_l} \int_0^\infty \frac{dk_n}{(2\pi)^2} \frac{F(k_n) M_l k_n^2}{E_l(k_n)\omega_l(k_n)} \frac{V_{il}(k_i,k_n) T_{lj}(k_n,k_j)}{\sqrt{s} - E_l(k_n) - \omega_l(k_n) + i\eta} \ . \tag{B.2}$$

For that purpose we apply the Sokhotskyi-Plemelj formula:

$$\frac{1}{f(x)+i\eta} = P\frac{1}{f(x)} - i\pi\delta(f(x))\,, \tag{B.3}$$

and taking into account that the delta function of $f(x)$ is given by

$$\delta(f(x)) = \sum_i \frac{\delta(x-x_i^0)}{|f'(x_i^0)|}\,, \tag{B.4}$$

being x_i^0 the roots of the function f, the integral I gets

$$\begin{aligned} I &= \int_0^\infty \frac{dk_n}{(2\pi)^2} \frac{F(k_n) M_l k_n^2}{E_l(k_n)\omega_l(k_n)} \frac{V_{il}(k_i,k_n) T_{lj}(k_n,k_j)}{\sqrt{s} - E_l(k_n) - \omega_l(k_n) - i\pi\eta} \\ &= P\int_0^\infty \frac{dk_n}{(2\pi)^2} \frac{F(k_n) M_l k_n^2}{E_l(k_n)\omega_l(k_n)} \frac{V_{il}(k_i,k_n) T_{lj}(k_n,k_j)}{\sqrt{s} - E_l(k_n) - \omega_l(k_n)} \\ &\quad - i\pi \frac{F(k_0) M_l k_0}{(2\pi)^2\sqrt{s}} V_{il}(k_i,k_0) T_{lj}(k_0,k_j)\,. \end{aligned} \tag{B.5}$$

To solve the singularities of the former integral I, that appear when we get a zero in the denominator, we apply a method which consist on the substraction and the addition of another integral ($\tilde{I}$) which present the same behavior around the singularity or pole. This method was suggested by M. I. Haftel and F. Tabakin in 1970 [MIH70]. The trick lies on considering the numerical substraction of:

$$\tilde{I} = \frac{F(k_0) M k_0}{(2\pi)^2} P\int_0^\infty dk \frac{k}{E(k)\omega(k)} \frac{V_{il}(k_i,k_n) T_{lj}(k_n,k_j)}{\sqrt{s} - E(k) - \omega(k)}\,, \tag{B.6}$$

and the addition of its analytical solution:

$$\tilde{I} = \frac{F(k_0) M k_0}{(2\pi)^2} \frac{1}{\sqrt{s}} \ln\mid \frac{\sqrt{s}}{M+m} - 1 \mid V_{il}(k_i,k_0) T_{lj}(k_0,k_j)\,. \tag{B.7}$$

In the way we can suppress the numerical instabilities due to singularities without altering the value of the integral I. Making a discretization of the relative momenta, Eq. B.1 can be written as

$$T_{ij}(k_i,k_j) = V_{ij}(k_i,k_j) + \sum_{M_l m_l} \sum_{n} w_n V_{il}(k_i,k_n) \tilde{G}(k_n)_{M_l m_l} T_{lj}(k_n,k_j)\,, \tag{B.8}$$

where $\tilde{G}(k_n)_{M_l m_l}$ is a diagonal matrix of $(N+1)\times(N+1)$ dimensions defined as

$$\tilde{G}(k_n)_{M_l m_l} = \begin{cases} \frac{F(k_n) M_l k_n^2}{E_l(k_n)\omega_l(k_n)} \frac{1}{\sqrt{s}-E_l(k_n)-\omega_l(k_n)}, & n < N+1\,, \\ \\ \frac{F(k_0) M_l k_0}{(2\pi)^2} \left(-\Gamma_{M_l m_l} + \frac{1}{\sqrt{s}} \ln \left| \frac{\sqrt{s}}{M_l+m_l} - 1 \right| + i \frac{\pi}{\sqrt{s}} \right), & n = N+1\,, \end{cases} \tag{B.9}$$

and

$$\Gamma_{M_l m_l} = \sum_{n=1}^{N} w_n \frac{k_n}{E_l(k_n)\omega_l(k_n)} \frac{1}{\sqrt{s}-E_l(k_n)-\omega_l(k_n)}\,, \tag{B.10}$$

We incorporate one more dimension (one more column and row) in order to perform the substraction of the pole, making $\tilde{G}=0$ when $n=N+1$ when there are no singularities in order to facilitate the calculation.

The points of the mesh and their corresponding weights can be treated with different types of mappings, like the logarithmic mapping:

$$k_n = C \ln\left(\frac{1+x_n}{1-x_n}\right) \quad ; \quad w_n = C \frac{2}{1-x_n^2} v_n\,, \tag{B.11}$$

with

$$C = \frac{k_N}{\ln\left(\frac{1+x_N}{1-x_N}\right)}\,, \tag{B.12}$$

or the tangential one:

$$k_n = \widetilde{C} \tan\left(\frac{\pi x_n}{2}\right) \quad ; \quad w_n = \widetilde{C} \frac{\pi}{2} \cos^{-2}\left(\frac{\pi x_n}{2}\right) v_n\,, \tag{B.13}$$

with

$$\widetilde{C} = \frac{k_N}{\tan\left(\frac{\pi x_N}{2}\right)}\,, \tag{B.14}$$

where x_n are the Gaussian points taken from 0 to 1 and v_n are the corresponding Gaussian weights. The constants C and $\tilde{C}$ are chosen by fitting the maximum momentum $k_N = k_{max}$ to an appropriate value. The result of the integral must not depend on the kind of mapping we choose, as one can see in Fig. B.1 of this appendix, where it is shown how the use of the logarithmic or the tangential mapping do not alter the results for the position and width of the $\Lambda_c(2595)$ resonance, once we choose the proper number of points in the mesh which make the integral stable. After the discretization of the integral we can solve the Lippmann-Schwinger equation by using the inversion method:

$$T = V + VGT \quad \longrightarrow \quad T = (1 - VG)^{-1} V\,. \tag{B.15}$$

The dimension of the final matrix $T_{ij}(k_i, k_j; \sqrt{s})$ for each value of $\sqrt{s}$, depends on the number of meson-baryon channels of an specific $(I,\ S,\ C)$ sector and the number of points considered for the external mesh in the relative momenta, thus the dimension gets fixed to $N_{channels}(N+1) \times N_{channels}(N+1)$.

B.1 Check of numerical stability

We present in Figures B.1 and B.2 three different tests to check the stability of the position and width of the $\Lambda_c(2595)$ resonance. In panel a) of Fig. B.1 we build two different mappings, the logarithmic and the tangential one, from a Gaussian mesh with $n = 24$ points taken from 0 to 1, as we can observe from the subfigure located in the upper-right corner of the panel. In panel b) of the same figure we plot the imaginary part of the T matrix with respect to the type of mapping chosen in order to discretize the integral (with the number of integral points n and the form factor fixed). In panel a of Fig. B.2 the T matrix is plotted but with respect to the number of points considered in the numerical integration once we chose a specific mapping and a form factor type, and in panel b of the same

figure the same is plotted but with respect to the form factor employed, once the number of points of the mesh and type of mapping have been fixed. We can observe in these figures how the use of any of the form factors, and any of the mapping does not change the position and width of the $\Lambda_c(2595)$ resonance, thus considering it as a stable result. We can see that the results are stable for $n \geq 24$ points, which is the number of points we choose to present the different results in the chapters where the L-S equation is solved, in free space (Chapters 3, 4 and 5), and in hot and dense matter (Chapter 6).

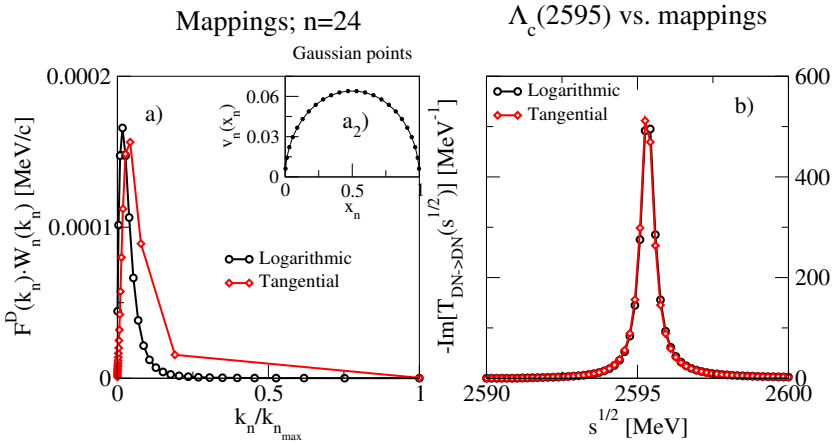

Figure B.1: The panel a) shows the logarithmic (circles) and tangential (diamonds) mappings (weighted by a dipolar form factor) we can build from the gaussian points on panel a_2) for n=24. On panel b) we show the imaginary part of the scattering amplitude of the $DN \to DN$ process in the $(I, S, C) = (0, 0, 1)$ sector as a function of $\sqrt{s}$ for the different mappings. The incoming and outgoing relative momenta $\vec{k}_i$ and $\vec{k}_j$ have been taken equal to 0.

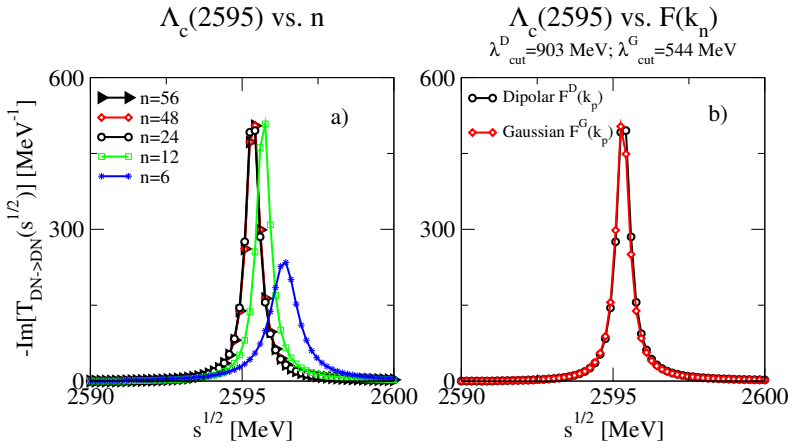

Figure B.2: The same as in panel b) on Fig.B.1, but the differences in the T matrix are shown in panel a) with respect the number of points chosen for the numerical integration, from $n = 6$ to $n = 56$, once the mapping and the form factor are fixed, and with respect to the dipolar (circle points) and gaussian (diamond points) form factors in panel b) once the number of integration points and the mapping are fixed.

C

Baryon-baryon-meson coupling constants

This Appendix gives the values of the coefficients α_i and β_i that define, according to Eq. (5.11), the BBM coupling constants g_{BBM}, needed in the diagrams that determine the various radiative decays.

	Λ_c		Σ_c^+	
MB	α	β	α	β
$\pi^+\Sigma_c^0$	$-\frac{1}{\sqrt{3}}$	$-\frac{1}{\sqrt{3}}$	1	-1
$\pi^0\Sigma_c^+$	$-\frac{1}{\sqrt{3}}$	$-\frac{1}{\sqrt{3}}$	0	0
$\pi^-\Sigma_c^{++}$	$-\frac{1}{\sqrt{3}}$	$-\frac{1}{\sqrt{3}}$	-1	1
D^0p	$\frac{2}{\sqrt{3}}$	$-\frac{1}{\sqrt{3}}$	0	1
D^+n	$-\frac{2}{\sqrt{3}}$	$\frac{1}{\sqrt{3}}$	0	1
$\eta\Lambda_c$	$\frac{\sqrt{2}}{3\sqrt{3}}$	$\frac{5\sqrt{2}}{3\sqrt{3}}$	0	0
$K^+\Xi_c^0$	$-\frac{1}{3\sqrt{2}}$	$\frac{5}{3\sqrt{2}}$	$\frac{1}{\sqrt{6}}$	$\frac{1}{\sqrt{6}}$
$K^0\Xi_c^+$	$-\frac{1}{3\sqrt{2}}$	$\frac{5}{3\sqrt{2}}$	$-\frac{1}{\sqrt{6}}$	$-\frac{1}{\sqrt{6}}$
$K^+\Xi_c^{\prime 0}$	$-\frac{1}{\sqrt{6}}$	$-\frac{1}{\sqrt{6}}$	$\frac{1}{\sqrt{2}}$	$-\frac{1}{\sqrt{2}}$
$K^0\Xi_c^{\prime +}$	$\frac{1}{\sqrt{6}}$	$\frac{1}{\sqrt{6}}$	$\frac{1}{\sqrt{2}}$	$-\frac{1}{\sqrt{2}}$
$D_s^+\Lambda$	$-\frac{2\sqrt{2}}{3}$	$\frac{\sqrt{2}}{3}$	0	0
$\eta'\Lambda_c$	$\frac{1}{3\sqrt{3}}$	$-\frac{5}{3\sqrt{3}}$	0	0
$\eta_c\Lambda_c$	$\frac{2\sqrt{2}}{3}$	$-\frac{\sqrt{2}}{3}$	0	0
$\bar{D}^0\Xi_{cc}^+$	$\frac{1}{\sqrt{3}}$	$-\frac{2}{\sqrt{3}}$	-1	0
$D^-\Xi_{cc}^{++}$	$-\frac{1}{\sqrt{3}}$	$\frac{2}{\sqrt{3}}$	-1	0
$\pi^0\Lambda_c$	0	0	$-\frac{1}{\sqrt{3}}$	$-\frac{1}{\sqrt{3}}$

Continued on next page

Continued from previous page				
	Λ_c		Σ_c^+	
MB	α	β	α	β
$\eta\Sigma_c^+$	0	0	$\sqrt{\frac{2}{3}}$	$-\sqrt{\frac{2}{3}}$
$D_s^+\Sigma^0$	0	0	0	$-\sqrt{2}$
$\eta'\Sigma_c^+$	0	0	$\frac{1}{\sqrt{3}}$	$-\frac{1}{\sqrt{3}}$
$\eta_c\Sigma_c^+$	0	0	0	$-\sqrt{2}$

Table C.1: The α and β coefficients for the channels involved in the radiative decay of resonances into Λ_c and Σ_c^+

	Ξ_c^+		$\Xi_c'^+$	
MB	α	β	α	β
$\pi^+\Xi_c^0$	$-\frac{1}{3\sqrt{2}}$	$\frac{5}{3\sqrt{2}}$	$-\frac{1}{\sqrt{6}}$	$-\frac{1}{\sqrt{6}}$
$\pi^0\Xi_c^+$	$\frac{1}{6}$	$-\frac{5}{6}$	$\frac{1}{2\sqrt{3}}$	$\frac{1}{2\sqrt{3}}$
$\pi^+\Xi_c'^0$	$\frac{1}{\sqrt{6}}$	$\frac{1}{\sqrt{6}}$	$\frac{1}{\sqrt{2}}$	$-\frac{1}{\sqrt{2}}$
$\pi^0\Xi_c'^+$	$\frac{1}{2\sqrt{3}}$	$\frac{1}{2\sqrt{3}}$	$\frac{1}{2}$	$-\frac{1}{2}$
$\bar{K}^0\Lambda_c$	$\frac{1}{3\sqrt{2}}$	$-\frac{5}{3\sqrt{2}}$	$\frac{1}{\sqrt{6}}$	$\frac{1}{\sqrt{6}}$
$\bar{K}^0\Sigma_c^+$	$-\frac{1}{\sqrt{6}}$	$-\frac{1}{\sqrt{6}}$	$\frac{1}{\sqrt{2}}$	$-\frac{1}{\sqrt{2}}$
$K^-\Sigma_c^{++}$	$\frac{1}{\sqrt{3}}$	$\frac{1}{\sqrt{3}}$	-1	1
$D^+\Lambda$	$-\frac{\sqrt{2}}{3}$	$\frac{1}{3\sqrt{2}}$	0	$\sqrt{\frac{3}{2}}$
Continued on next page				

Continued from previous page				
	Ξ_c^+		$\Xi_c'^+$	
MB	α	β	α	β
$\eta\Xi_c^+$	0	0	$\frac{\sqrt{2}}{3}$	$\frac{\sqrt{2}}{3}$
$D^+\Sigma^0$	$\sqrt{\frac{2}{3}}$	$-\frac{1}{\sqrt{6}}$	0	$-\frac{1}{\sqrt{2}}$
$D^0\Sigma^+$	$\frac{2}{\sqrt{3}}$	$-\frac{1}{\sqrt{3}}$	0	-1
$\eta\Xi_c'^+$	$\frac{\sqrt{2}}{3}$	$\frac{\sqrt{2}}{3}$	0	0
$K^+\Omega_c$	$\frac{1}{\sqrt{3}}$	$\frac{1}{\sqrt{3}}$	1	-1
$D_s^+\Xi^0$	$\frac{2}{\sqrt{3}}$	$-\frac{1}{\sqrt{3}}$	0	1
$\eta'\Xi_c^+$	$\frac{1}{2\sqrt{3}}$	$\frac{5}{2\sqrt{3}}$	$-\frac{1}{6}$	$-\frac{1}{6}$
$\eta'\Xi_c'^+$	$-\frac{1}{6}$	$-\frac{1}{6}$	$\frac{\sqrt{3}}{2}$	$-\frac{\sqrt{3}}{2}$
$D_s^-\Xi_{cc}^{++}$	$-\frac{1}{\sqrt{3}}$	$\frac{2}{\sqrt{3}}$	1	0
$\bar{D}^0\Omega_{cc}$	$\frac{1}{\sqrt{3}}$	$-\frac{2}{\sqrt{3}}$	1	0
$\eta_c\Xi_c^+$	$\frac{2\sqrt{2}}{3}$	$-\frac{\sqrt{2}}{3}$	0	0
$\eta_c\Xi_c'^+$	0	0	0	$-\sqrt{2}$

Table C.2: The α and β coefficients for the channels involved in the radiative decay of resonances into Ξ_c^+ and $\Xi_c'^+$

	Ξ_c^0		$\Xi_c'^0$	
MB	α	β	α	β
$\pi^-\Xi_c^+$	$-\frac{1}{3\sqrt{2}}$	$\frac{5}{3\sqrt{2}}$	$\frac{1}{\sqrt{6}}$	$\frac{1}{\sqrt{6}}$
$\pi^-\Xi_c'^+$	$-\frac{1}{\sqrt{6}}$	$-\frac{1}{\sqrt{6}}$	$\frac{1}{\sqrt{2}}$	$-\frac{1}{\sqrt{2}}$
$K^-\Lambda_c$	$-\frac{1}{3\sqrt{2}}$	$\frac{5}{3\sqrt{2}}$	$-\frac{1}{\sqrt{6}}$	$-\frac{1}{\sqrt{6}}$
$K^-\Sigma_c^+$	$\frac{1}{\sqrt{6}}$	$\frac{1}{\sqrt{6}}$	$\frac{1}{\sqrt{2}}$	$-\frac{1}{\sqrt{2}}$
$D^+\Sigma^-$	$-\frac{2}{\sqrt{3}}$	$\frac{1}{\sqrt{3}}$	0	-1
$D_s^+\Xi^-$	$\frac{2}{\sqrt{3}}$	$-\frac{1}{\sqrt{3}}$	0	-1
$D_s^-\Xi_{cc}^+$	$-\frac{1}{\sqrt{3}}$	$\frac{2}{\sqrt{3}}$	-1	0
$D^-\Omega_{cc}$	$\frac{1}{\sqrt{3}}$	$-\frac{2}{\sqrt{3}}$	-1	0

Table C.3: The α and β coefficients for the channels involved in the radiative decay of resonances into Ξ_c^0 and $\Xi_c'^0$. We only show the coefficients for channels with charged particles.

	Σ_c^{++}	
MB	α	β
$\pi^+\Lambda_c$	$-\frac{1}{\sqrt{3}}$	$-\frac{1}{\sqrt{3}}$
$\pi^+\Sigma_c^+$	-1	1
$\pi^0\Sigma_c^{++}$	1	-1
D^+p	0	$-\sqrt{2}$
$K^+\Xi_c^+$	$\frac{1}{\sqrt{3}}$	$\frac{1}{\sqrt{3}}$
$\eta\Sigma_c^{++}$	$\sqrt{\frac{2}{3}}$	$-\sqrt{\frac{2}{3}}$
$K^+\Xi_c'^+$	-1	1
$D_s^+\Sigma^+$	0	$-\sqrt{2}$
$\eta'\Sigma_c^{++}$	$\frac{1}{\sqrt{3}}$	$-\frac{1}{\sqrt{3}}$
$\bar{D}^0\Xi_{cc}^{++}$	$-\sqrt{2}$	0
$\eta_c\Sigma_c^{++}$	0	$-\sqrt{2}$

Table C.4: The α and β coefficients for the channels involved in the radiative decay of resonances into Σ_c^{++}. We only show the coefficients for channels with charged particles.

	Σ_c^0	
MB	α	β
$\pi^-\Lambda_c$	$-\frac{1}{\sqrt{3}}$	$-\frac{1}{\sqrt{3}}$
$\pi^-\Sigma_c^+$	1	-1
$D_s^+\Sigma^-$	0	$-\sqrt{2}$
$D^-\Xi_{cc}^+$	$\sqrt{2}$	0

Table C.5: The α and β coefficients for the channels involved in the radiative decay of resonances into Σ_c^0. We only show the coefficients for channels with charged particles.

Bibliography

[A$^+$74a] J. J. Aubert *et al.* (E598), *Experimental Observation of a Heavy Particle J*, Phys. Rev. Lett. **33** (1974) 1404–1406.

[A$^+$74b] J. E. Augustin *et al.* (SLAC-SP-017), *Discovery of a Narrow Resonance in e+ e- Annihilation*, Phys. Rev. Lett. **33** (1974) 1406–1408.

[A$^+$93a] H. Albrecht *et al.* (ARGUS), *Observation of a new charmed baryon*, Phys. Lett. **B317** (1993) 227–232.

[A$^+$93b] V. V. Ammosov *et al.*, *Observation of the production of charmed Sigma(c)*++ baryons in neutrino interactions at the SKAT bubble chamber*, JETP Lett. **58** (1993) 247–251.

[A$^+$95] P. Avery *et al.* (CLEO), *Observation of a narrow state decaying into Xi(c)+ pi-*, Phys. Rev. Lett. **75** (1995) 4364–4368, [hep-ex/9508010].

[A$^+$97] H. Albrecht *et al.* (ARGUS), *Evidence for* $\Lambda_c(2593)^+$ *production*, Phys. Lett. **B402** (1997) 207–212.

[A$^+$99] J. P. Alexander *et al.* (CLEO), *Evidence of new states decaying into Xi/c* pi*, Phys. Rev. Lett. **83** (1999) 3390–3393, [hep-ex/9906013].

[A+01] M. Artuso *et al.* (CLEO), *Observation of new states decaying into Lambda/c+ pi- pi+*, Phys. Rev. Lett. **86** (2001) 4479–4482, [hep-ex/0010080].

[A+05] B. Aubert *et al.* (BABAR), *A Precision measurement of the Lambda+(c) baryon mass*, Phys. Rev. **D72** (2005) 052006, [hep-ex/0507009].

[A+06] B. Aubert *et al.* (BABAR), *Observation of an excited charm baryon Ω_c^* decaying to $\Omega_c^0\gamma$*, Phys. Rev. Lett. **97** (2006) 232001, [hep-ex/0608055].

[A+07a] K. Abe *et al.* (Belle), *Experimental constraints on the possible J(P) quantum numbers of the $\Lambda_c(2880)^+$*, Phys. Rev. Lett. **98** (2007) 262001, [hep-ex/0608043].

[A+07b] B. Aubert *et al.* (BABAR), *Observation of a charmed baryon decaying to D^0 p at a mass near 2.94-GeV/c^2*, Phys. Rev. Lett. **98** (2007) 012001, [hep-ex/0603052].

[A+08a] B. Aubert *et al.* (BaBar), *A study of $\bar{B} \to Xi_c\Lambda_c^-$ and $\bar{B} \to \Lambda_c^+\Lambda_c^-\bar{K}$ decays at BABAR*, Phys. Rev. **D77** (2008) 031101, [arXiv:0710.5775].

[A+08b] B. Aubert *et al.* (BABAR), *A Study of Excited Charm-Strange Baryons with Evidence for new Baryons $\Xi_c(3055)^+$ and $\Xi_c(3123)^+$*, Phys. Rev. **D77** (2008) 012002, [arXiv:0710.5763].

[ABMRS08] A. Andronic, P. Braun-Munzinger, K. Redlich and J. Stachel, *Charmonium and open charm production in nuclear collisions at SPS/FAIR energies and the possible influence of a hot hadronic medium*, Phys. Lett. **B659** (2008) 149–155, [arXiv:0708.1488].

[ASZ65] G. S. Abrams and B. Sechi-Zorn, *Charge-Exchange Scattering of Low-Energy K- Mesons in Hydrogen*, Phys. Rev. **139** (1965) B454–B457.

[B-S] http://www.bethe-salpeter.org/.

[B$^+$69a] E. D. Bloom *et al.*, *High-Energy Inelastic e p Scattering at 6-Degrees and 10- Degrees*, Phys. Rev. Lett. **23** (1969) 930–934.

[B$^+$69b] M. Breidenbach *et al.*, *Observed Behavior of Highly Inelastic electron-Proton Scattering*, Phys. Rev. Lett. **23** (1969) 935–939.

[B$^+$77] O. Braun *et al.*, *New Information About the Kaon-Nucleon-Hyperon Coupling Constants: G/anti-K n* $\Sigma(1197)$*, G / anti-K n* $\Sigma(1385)$ *and G anti-K n* $\Lambda(1405)$, Nucl. Phys. **B129** (1977) 1.

[B$^+$83] S. F. Biagi *et al.*, *Observation of a Narrow State at 2.46-GeV/c**2: A Candidate for the Charmed Strange Baryon a+*, Phys. Lett. **B122** (1983) 455.

[B$^+$85] S. F. Biagi *et al.*, *Properties of the Charmed Strange Baryon A+ and Evidence for the Charmed Doubly Strange Baryon T0 at 2.74- GeV/c**2*, Z. Phys. **C28** (1985) 175.

[BBMN05] B. Borasoy, P. C. Bruns, U. G. Meissner and R. Nissler, *Gauge invariance in two-particle scattering*, Phys. Rev. **C72** (2005) 065201, [hep-ph/0508307].

[Bet09] S. Bethke, *The 2009 Wolrd Average of* $\alpha_s(M_Z)$, Eur. Phys. J. **C64** (2009) 689–703, [arXiv:0908.1135].

[BF61] J. S. Ball and W. R. Frazer, *Possible Explanation of the Higher Pion-Nucleon and* $K^- - p$ *Resonances in Terms of Inelastic Thresholds*, Phys. Rev. Lett. **7** (1961) 204–207.

[BFPY03] A. E. Blechman, A. F. Falk, D. Pirjol and J. M. Yelton, *Threshold effects in excited charmed baryon decays*, Phys. Rev. **D67** (2003) 074033, [hep-ph/0302040].

[BG64] J. D. Bjorken and S. L. Glashow, *Elementary Particles and SU(4)*, Phys. Lett. **11** (1964) 255–257.

[BHMG$^+$90] R. Buettgen, K. Holinde, A. Mueller-Groeling, J. Speth and P. Wyborny, *A meson exchange model for the* K^+N *interaction*, Nucl. Phys. **A506** (1990) 586–614.

[BMN06] B. Borasoy, U. G. Meissner and R. Nissler, *K^-p scattering length from scattering experiments*, Phys. Rev. **C74** (2006) 055201, [hep-ph/0606108].

[BMO11] T. Branz, R. Molina and E. Oset, *Radiative decays of the Y(3940), Z(3930) and the X(4160) as dynamically generated resonances*, Phys. Rev. **D83** (2011) 114015, [arXiv:1010.0587].

[BNW05] B. Borasoy, R. Nissler and W. Weise, *Chiral dynamics of kaon nucleon interactions, revisited*, Eur. Phys. J. **A25** (2005) 79–96, [hep-ph/0505239].

[BPS00] M. C. Banuls, A. Pich and I. Scimemi, *Electromagnetic decays of heavy baryons*, Phys. Rev. **D61** (2000) 094009, [hep-ph/9911502].

[BST90] S. J. Brodsky, I. A. Schmidt and G. F. de Teramond, *Nuclear bound quarkonium*, Phys. Rev. Lett. **64** (1990) 1011.

[C$^+$75] E. G. Cazzoli *et al.*, *Evidence for $\Delta S = -\Delta Q$ Currents or Charmed Baryon Production by Neutrinos*, Phys. Rev. Lett. **34** (1975) 1125–1128.

[C$^+$80] M. Calicchio *et al.* (BEBC TST Neutrino), *First obervation of the production and decay of the Σ_c^+*, Phys. Lett. **B93** (1980) 521.

[C$^+$93] H.-Y. Cheng *et al.*, *Chiral Lagrangians for radiative decays of heavy hadrons*, Phys. Rev. **D47** (1993) 1030–1042, [hep-ph/9209262].

[C$^+$01a] S. E. Csorna *et al.* (CLEO), *Evidence of new states decaying into Xi/c' pi*, Phys. Rev. Lett. **86** (2001) 4243–4246, [hep-ex/0012020].

[C$^+$01b] S. E. Csorna *et al.* (CLEO), *Evidence of new states decaying into $Xi_c'\pi$*, Phys. Rev. Lett. **86** (2001) 4243–4246, [hep-ex/0012020].

[C$^+$06a] R. Chistov *et al.* (BELLE), *Observation of new states decaying into Lambda/c+ K- pi+ and Lambda/c+ K0(S) pi-*, Phys. Rev. Lett. **97** (2006) 162001, [hep-ex/0606051].

[C$^+$06b] R. Chistov *et al.* (BELLE), *Observation of new states decaying into $\Lambda_c^+ K^- \pi^+$ and $\Lambda_c^+ K^0(S) \pi^-$*, Phys. Rev. Lett. **97** (2006) 162001, [hep-ex/0606051].

[CC07] H.-Y. Cheng and C.-K. Chua, *Strong decays of charmed baryons in heavy hadron chiral perturbation theory*, Phys. Rev. **D75** (2007) 014006, [hep-ph/0610283].

[Che97] H.-Y. Cheng, *Remarks on the strong coupling constants in heavy hadron chiral Lagrangians*, Phys. Lett. **B399** (1997) 281–286, [hep-ph/9701234].

[Cho94] P. L. Cho, *Strong and electromagnetic decays of two new Λ_c^* baryons*, Phys. Rev. **D50** (1994) 3295–3302, [hep-ph/9401276].

[Cho96] C.-K. Chow, *Radiative Decays of Excited Λ_Q Baryons in the Bound State Picture*, Phys. Rev. **D54** (1996) 3374–3376, [hep-ph/9510421].

[CI86] S. Capstick and N. Isgur, *Baryons in a Relativized Quark Model with Chromodynamics*, Phys. Rev. **D34** (1986) 2809.

[D$^+$11] M. Doring *et al.*, *The reaction pi+ p –¿ K+ Sigma+ in a unitary coupled- channels model*, Nucl. Phys. **A851** (2011) 58–98, [arXiv:1009.3781].

[DFG$^+$10] Y. Dong, A. Faessler, T. Gutsche, S. Kumano and V. E. Lyubovitskij, *Radiative decay of $\Lambda_c(2940)^+$ in a hadronic molecule picture*, Phys. Rev. **D82** (2010) 034035, [arXiv:1006.4018].

[Dor07] M. Doring, *Radiative decay of the Delta(1700)*, Nucl. Phys. **A786** (2007) 164–182, [nucl-th/0701070].

[DOS06a] M. Doring, E. Oset and S. Sarkar, *Radiative decay of the* $\Lambda(1520)$, Phys. Rev. **C74** (2006) 065204, [nucl-th/0601027].

[DOS06b] M. Doring, E. Oset and D. Strottman, *The* $\pi^- p \to K^0 \pi^0 \Lambda$ *reaction and clues to the nature of the Delta*(1700) resonance*, Phys. Lett. **B639** (2006) 59–67, [nucl-th/0602055].

[DSVD94] J. Dey, V. Shevchenko, P. Volkovitsky and M. Dey, *Radiative decays of S wave charmed baryons*, Phys. Lett. **B337** (1994) 185–188.

[DT59a] R. H. Dalitz and S. F. Tuan, *A possible resonant state in pion-hyperon scattering*, Phys. Rev. Lett. **2** (1959) 425–428.

[DT59b] R. H. Dalitz and S. F. Tuan, *The energy dependence of low energy* K^-*-proton processes*, Annals Phys. **8** (1959) 100.

[DT60] R. H. Dalitz and S. F. Tuan, *The phenomenological description of -K -nucleon reaction processes*, Annals Phys. **10** (1960) 307.

[DWR67] R. H. Dalitz, T. C. Wong and G. Rajasekaran, *Model calculation for Y*(0) (1405) resonance state*, Phys. Rev. **153** (1967) 1617–1623.

[E$^+$95] K. W. Edwards *et al.* (CLEO), *Observation of excited baryon states decaying to* $\Lambda_c^+ \pi^+ \pi^-$, Phys. Rev. Lett. **74** (1995) 3331–3335.

[EAY10] J. Esmaili, Y. Akaishi and T. Yamazaki, *Experimental confirmation of the* $\Lambda(1405)$ *Ansatz from resonant formation of a K-p quasi-bound state in K- absorption by 3He and 4He*, Phys. Lett. **B686** (2010) 23–28, [arXiv:0906.0505].

[EFG08] D. Ebert, R. N. Faustov and V. O. Galkin, *Masses of excited heavy baryons in the relativistic quark model*, Phys. Lett. **B659** (2008) 612–620, [arXiv:0705.2957].

[F$^+$96] P. L. Frabetti *et al.* (E687), *Study of higher mass charm baryons decaying to* Λ_c^+, Phys. Lett. **B365** (1996) 461–469.

[FAI] `http://www.gsi.de/portrait/fair.html`.

[FGLM07] A. Faessler, T. Gutsche, V. E. Lyubovitskij and Y.-L. Ma, *Strong and radiative decays of the $D_s^{0*}(2317)$ meson in the DK-molecule picture*, Phys. Rev. **D76** (2007) 014005, [`arXiv:0705.0254`].

[FH64] W. R. Frazer and A. W. Hendry, *S-Matrix Poles Close to Threshold*, Phys. Rev. **134** (1964) B1307–B1314.

[Fla76] S. M. Flatte, *Coupled - Channel Analysis of the pi eta and K anti-K Systems Near K anti-K Threshold*, Phys. Lett. **B63** (1976) 224.

[FR97] Fayyazuddin and Riazuddin, *Masses and decays of charmed and bottom baryons*, Mod. Phys. Lett. **A12** (1997) 1791–1802.

[GDO07] D. Gamermann, L. R. Dai and E. Oset, *Radiative decay of the dynamically generated open and hidden charm scalar meson resonances D(s0)*(2317) and X(3700)*, Phys. Rev. **C76** (2007) 055205, [`arXiv:0709.2339`].

[GIM70] S. L. Glashow, J. Iliopoulos and L. Maiani, *Weak Interactions with Lepton-Hadron Symmetry*, Phys. Rev. **D2** (1970) 1285–1292.

[GM64] M. Gell-Mann, *A Schematic Model of Baryons and Mesons*, Phys. Lett. **8** (1964) 214–215.

[GO07] D. Gamermann and E. Oset, *Axial Resonances in the Open and Hidden Charm Sectors*, Eur. Phys. J. **A33** (2007) 119–131, [`arXiv:0704.2314`].

[GOD07] L. S. Geng, E. Oset and M. Doring, *The radiative decay of the $\Lambda(1405)$ and its two- pole structure*, Eur. Phys. J. **A32** (2007) 201–211, [`hep-ph/0702093`].

[GOSVV07] D. Gamermann, E. Oset, D. Strottman and M. J. Vicente Vacas, *Dynamically Generated Open and Hidden Charm Meson Systems*, Phys. Rev. **D76** (2007) 074016, [`hep-ph/0612179`].

[GOV09] P. Gonzalez, E. Oset and J. Vijande, *An explanation of the $\Delta_{5/2^-}(1930)$ as a $\rho\Delta$ bound state*, Phys. Rev. **C79** (2009) 025209, [arXiv:0812.3368].

[GR+09] C. Garcia-Recio *et al.*, *The s-wave charmed baryon resonances from a coupled- channel approach with heavy quark symmetry*, Phys. Rev. **D79** (2009) 054004, [arXiv:0807.2969].

[GRNRAVV03] C. Garcia-Recio, J. Nieves, E. Ruiz Arriola and M. J. Vicente Vacas, *$S = -1$ Meson-Baryon Unitarized Coupled Channel Chiral Perturbation Theory and the $S_{01}-$ $\Lambda(1405)$ and $-\Lambda(1670)$ Resonances*, Phys. Rev. **D67** (2003) 076009, [hep-ph/0210311].

[GRNS06] C. Garcia-Recio, J. Nieves and L. L. Salcedo, *SU(6) extension of the Weinberg-Tomozawa meson-baryon Lagrangian*, Phys. Rev. **D74** (2006) 034025, [hep-ph/0505233].

[GRNT10] C. Garcia-Recio, J. Nieves and L. Tolos, *D mesic nuclei*, Phys. Lett. **B690** (2010) 369–375, [arXiv:1004.2634].

[GVV08] P. Gonzalez, J. Vijande and A. Valcarce, *Meson-baryon threshold effects in the light-quark baryon spectrum*, Phys. Rev. **C77** (2008) 065213, [arXiv:0805.4677].

[Hay00] A. Hayashigaki, *Mass modification of D meson at finite density in QCD sum rule*, Phys. Lett. **B487** (2000) 96–103, [nucl-th/0001051].

[HDH+95] M. Hoffmann, J. W. Durso, K. Holinde, B. C. Pearce and J. Speth, *Role of correlated two pion exchange in K^+N scattering*, Nucl. Phys. **A593** (1995) 341–361, [nucl-th/9504029].

[HJH08] T. Hyodo, D. Jido and A. Hosaka, *Origin of the resonances in the chiral unitary approach*, Phys. Rev. **C78** (2008) 025203, [arXiv:0803.2550].

[HJR08] T. Hyodo, D. Jido and L. Roca, *Structure of the (1405) baryon resonance from its large N(c) behavior*, Phys. Rev. **D77** (2008) 056010, [arXiv:0712.3347].

[HKMS07] J. Haidenbauer, G. Krein, U.-G. Meissner and A. Sibirtsev, *Dbar-N interaction from meson-exchange and quark-gluon dynamics*, Eur. Phys. J. **A33** (2007) 107–117, [arXiv:0704.3668].

[HKMT10] J. Haidenbauer, G. Krein, U.-G. Meissner and L. Tolos, *DN interaction from meson exchange*, Eur. Phys. J. **A 37** (2010) 18, [arXiv:1008.3794].

[HL04] J. Hofmann and M. F. M. Lutz, *Open-charm meson resonances with negative strangeness*, Nucl. Phys. **A733** (2004) 142–152, [hep-ph/0308263].

[HL05] J. Hofmann and M. F. M. Lutz, *Coupled-channel study of crypto-exotic baryons with charm*, Nucl. Phys. **A763** (2005) 90–139, [hep-ph/0507071].

[HL06] J. Hofmann and M. F. M. Lutz, *D-wave baryon resonances with charm from coupled-channel dynamics*, Nucl. Phys. **A776** (2006) 17–51, [hep-ph/0601249].

[HLLZ07] X.-G. He, X.-Q. Li, X. Liu and X.-Q. Zeng, *Lambda/c(2940)+: A possible molecular state?*, Eur. Phys. J. **C51** (2007) 883–889, [hep-ph/0606015].

[HTK09] T. Hilger, R. Thomas and B. Kampfer, *QCD sum rules for D and B mesons in nuclear matter*, Phys. Rev. **C79** (2009) 025202, [arXiv:0809.4996].

[IKL99] M. A. Ivanov, J. G. Korner and V. E. Lyubovitskij, *One-photon transitions between heavy baryons in a relativistic three-quark model*, Phys. Lett. **B448** (1999) 143–151, [hep-ph/9811370].

[IKLR99] M. A. Ivanov, J. G. Korner, V. E. Lyubovitskij and A. G. Rusetsky, *Strong and radiative decays of heavy flavored baryons*, Phys. Rev. **D60** (1999) 094002, [hep-ph/9904421].

[IOVV02] T. Inoue, E. Oset and M. J. Vicente Vacas, *Chiral unitary approach to S-wave meson baryon scattering in the strangeness $S = 0$ sector*, Phys. Rev. **C65** (2002) 035204, [hep-ph/0110333].

[IW89] N. Isgur and M. B. Wise, *Weak Decays of Heavy Mesons in the Static Quark Approximation*, Phys. Lett. **B232** (1989) 113.

[J$^+$99a] C. P. Jessop *et al.* (CLEO), *Observation of two narrow states decaying into Xi/c+ gamma and Xi/c0 gamma*, Phys. Rev. Lett. **82** (1999) 492–496, [hep-ex/9810036].

[J$^+$99b] C. P. Jessop *et al.* (CLEO), *Observation of two narrow states decaying into $\Xi_c^+\gamma$ and $\Xi_c^0\gamma$*, Phys. Rev. Lett. **82** (1999) 492–496, [hep-ex/9810036].

[JKE08] D. Jido and Y. Kanada-En'yo, *K anti-K N molecule state with I=1/2 and J^P=1/2$^+$ studied with three-body calculation*, Phys. Rev. **C78** (2008) 035203, [arXiv:0806.3601].

[JOO$^+$03] D. Jido, J. A. Oller, E. Oset, A. Ramos and U. G. Meissner, *Chiral dynamics of the two $\Lambda(1405)$ states*, Nucl. Phys. **A725** (2003) 181–200, [nucl-th/0303062].

[JOS09] D. Jido, E. Oset and T. Sekihara, *Kaonic production of $\Lambda(1405)$ off deuteron target in chiral dynamics*, Eur. Phys. J. **A42** (2009) 257–268, [arXiv:0904.3410].

[JTRV09] C. E. Jimenez-Tejero, A. Ramos and I. Vidana, *Dynamically generated open charmed baryons beyond the zero range approximation*, Phys. Rev. **C80** (2009) 055206, [arXiv:0907.5316].

[Kap06] Kapusta, *Finite Temperature Field Theory and Applications*, New York, Cambridge University Press (2006).

[KEJ08] Y. Kanada-En'yo and D. Jido, *anti-K anti-K N molecule state in three-body calculation*, Phys. Rev. **C78** (2008) 025212, [arXiv:0804.3124].

[KL04a] E. E. Kolomeitsev and M. F. M. Lutz, *On baryon resonances and chiral symmetry*, Phys. Lett. **B585** (2004) 243–252, [nucl-th/0305101].

[KL04b] E. E. Kolomeitsev and M. F. M. Lutz, *On heavy-light meson resonances and chiral symmetry*, Phys. Lett. **B582** (2004) 39–48, [hep-ph/0307133].

[KM10] A. Kumar and A. Mishra, *D mesons and charmonium states in asymmetric nuclear matter at finite temperatures*, Phys. Rev. **C81** (2010) 065204, [arXiv:1005.5018].

[KMTO08] K. P. Khemchandani, A. Martinez Torres and E. Oset, *The $N^*(1710)$ as a resonance in the $\pi\pi N$ system*, Eur. Phys. J. **A37** (2008) 233–243, [arXiv:0804.4670].

[KS66] Kawarabayashi and Suzuki, *Partially conserved axial-vector and the decays of the vector mesons*, Phys. Rev. Lett. **16** (1966) 255.

[KSW95] N. Kaiser, P. B. Siegel and W. Weise, *Chiral dynamics and the low-energy kaon - nucleon interaction*, Nucl. Phys. **A594** (1995) 325–345, [nucl-th/9505043].

[KTT11] G. Krein, A. W. Thomas and K. Tsushima, *J/Ψ mass shift in nuclear matter*, Phys. Lett. **B697** (2011) 136–141, [arXiv:1007.2220].

[Lei75] G. Leibbrandt, *Introduction to the Technique of Dimensional Regularization*, Rev. Mod. Phys. **47** (1975) 849.

[LK01] M. F. M. Lutz and E. E. Kolomeitsev, *Covariant meson baryon scattering with chiral and large N(c) constraints*, Found. Phys. **31** (2001) 1671–1702, [nucl-th/0105068].

[LK02] M. F. M. Lutz and E. E. Kolomeitsev, *Relativistic chiral SU(3) symmetry, large N(c) sum rules and meson baryon scattering*, Nucl. Phys. **A700** (2002) 193–308, [nucl-th/0105042].

[LK04a] M. F. M. Lutz and E. E. Kolomeitsev, *On charm baryon resonances and chiral symmetry*, Nucl. Phys. **A730** (2004) 110–120, [hep-ph/0307233].

[LK04b] M. F. M. Lutz and E. E. Kolomeitsev, *On meson resonances and chiral symmetry*, Nucl. Phys. **A730** (2004) 392–416, [nucl-th/0307039].

[LK05] M. F. M. Lutz and E. E. Kolomeitsev, *Baryon resonances from chiral coupled-channel dynamics*, Nucl. Phys. **A755** (2005) 29–39, [hep-ph/0501224].

[LK06] M. F. M. Lutz and C. L. Korpa, *Open-charm systems in cold nuclear matter*, Phys. Lett. **B633** (2006) 43–48, [nucl-th/0510006].

[LMO10] W. H. Liang, R. Molina and E. Oset, *Radiative open charm decay of the Y(3940), Z(3930), X(4160) resonances*, Eur. Phys. J. **A44** (2010) 479–486, [arXiv:0912.4359].

[LMS92] M. E. Luke, A. V. Manohar and M. J. Savage, *A QCD Calculation of the interaction of quarkonium with nuclei*, Phys. Lett. **B288** (1992) 355–359, [hep-ph/9204219].

[LS50] B. A. Lippmann and J. Schwinger, *Variational Principles for Scattering Processes. I*, Phys. Rev. **79** (1950) 469–480.

[LS08] M. F. M. Lutz and M. Soyeur, *Radiative and isospin-violating decays of D_s mesons in the hadrogenesis conjecture*, Nucl. Phys. **A813** (2008) 14–95, [arXiv:0710.1545].

[Lut02] M. F. M. Lutz, *The relativistic nuclear dynamics for the SU(3) Goldstone bosons of chiral QCD*, GSI-habil (2002), [nucl-th/0212021].

[LW67] R. K. Logan and H. W. Wyld, *Resonance Poles in a Simple Model of S-Wave Pseudoscalar- Meson-Baryon Scattering*, Phys. Rev. **158** (1967) 1467–1470.

[LWF02] M. F. M. Lutz, G. Wolf and B. Friman, *Scattering of vector mesons off nucleons*, Nucl. Phys. **A706** (2002) 431–496, [nucl-th/0112052].

[M$^+$02] M. Mattson *et al.* (SELEX), *First observation of the doubly charmed baryon Xi/cc+*, Phys. Rev. Lett. **89** (2002) 112001, [hep-ex/0208014].

[M$^+$05a] R. Mizuk *et al.* (Belle), *Observation of an isotriplet of excited charmed baryons decaying to Lambda/c+ pi*, Phys. Rev. Lett. **94** (2005) 122002, [hep-ex/0412069].

[M$^+$05b] R. Mizuk *et al.* (Belle), *Observation of an isotriplet of excited charmed baryons decaying to* $\Lambda_c^+\pi$, Phys. Rev. Lett. **94** (2005) 122002, [hep-ex/0412069].

[Mat55] Matsubara, *A New Approach to Quantum-Statistical Mechanics*, Prog. Theor. Phys **14** (1955) 351.

[MBSB$^+$04] A. Mishra, E. L. Bratkovskaya, J. Schaffner-Bielich, S. Schramm and H. Stoecker, *Kaons and antikaons in hot and dense hadronic matter*, Phys. Rev. **C70** (2004) 044904, [nucl-th/0402062].

[MGHS90] A. Mueller-Groeling, K. Holinde and J. Speth, *K- N interaction in the meson exchange framework*, Nucl. Phys. **A513** (1990) 557–583.

[MHE87] R. Machleidt, K. Holinde and C. Elster, *The Bonn Meson Exchange Model for the Nucleon Nucleon Interaction*, Phys. Rept. **149** (1987) 1–89.

[MIH70] F. T. M. I. Haftel, *Nuclear saturation and the smoothness of nucleon-nucleon potentials*, Nucl. Phys. A **158** (1970) 1.

[MM09] A. Mishra and A. Mazumdar, *D-mesons in asymmetric nuclear matter*, Phys. Rev. **C79** (2009) 024908, [arXiv:0810.3067].

[MNHO11] R. Molina, H. Nagahiro, A. Hosaka and E. Oset, *Decay of vector-vector resonances into γ and a pseudoscalar meson*, Phys. Rev. **D83** (2011) 094030, [arXiv:1009.4881].

[MO00] U.-G. Meissner and J. A. Oller, *Chiral unitary meson baryon dynamics in the presence of resonances: Elastic pion nucleon scattering*, Nucl. Phys. **A673** (2000) 311–334, [nucl-th/9912026].

[MOR05] V. K. Magas, E. Oset and A. Ramos, *Evidence for the two pole structure of the $\Lambda(1405)$ resonance*, Phys. Rev. Lett. **95** (2005) 052301, [hep-ph/0503043].

[MPV09] A. Majethiya, B. Patel and P. C. Vinodkumar, *Raditive decay of single charmed baryons*, Eur. Phys. J. **A42** (2009) 213–218, [arXiv:0902.2536].

[MR06] T. Mizutani and A. Ramos, *D mesons in nuclear matter: A DN coupled-channel equations approach*, Phys. Rev. **C74** (2006) 065201, [hep-ph/0607257].

[MS86] T. Matsui and H. Satz, *J/Ψ Suppression by Quark-Gluon Plasma Formation*, Phys. Lett. **B178** (1986) 416.

[MTKO08a] A. Martinez Torres, K. P. Khemchandani and E. Oset, *Three-body hadronic structure of low-lying $1/2^+$ Σ and Λ resonances*, Eur. Phys. J. **A35** (2008) 295–297, [arXiv:0805.3641].

[MTKO08b] A. Martinez Torres, K. P. Khemchandani and E. Oset, *Three body resonances in two meson-one baryon systems*, Phys. Rev. **C77** (2008) 042203, [arXiv:0706.2330].

[MW00] A. V. Manohar and M. B. Wise, *Heavy quark physics*, Camb. Monogr. Part. Phys. Nucl. Phys. Cosmol. **10** (2000) 1–191.

[N$^+$10] K. Nakamura *et al.* (Particle Data Group), *Review of particle physics*, J. Phys. **G37** (2010) 075021.

[Neu94] M. Neubert, *Heavy quark symmetry*, Phys. Rept. **245** (1994) 259–396, [hep-ph/9306320].

[NRA01a] J. Nieves and E. Ruiz Arriola, *Bethe-Salpeter approach for the P(33) elastic pion nucleon scattering in heavy baryon chiral perturbation theory*, Phys. Rev. **D63** (2001) 076001, [hep-ph/0008034].

[NRA01b] J. Nieves and E. Ruiz Arriola, *The S(11) N(1535) and N(1650) resonances in meson baryon unitarized coupled channel chiral perturbation theory*, Phys. Rev. **D64** (2001) 116008, [hep-ph/0104307].

[OM01] J. A. Oller and U. G. Meissner, *Chiral dynamics in the presence of bound states: Kaon nucleon interactions revisited*, Phys. Lett. **B500** (2001) 263–272, [hep-ph/0011146].

[OOP99] J. A. Oller, E. Oset and J. R. Pelaez, *Meson-Meson interaction in a non-perturbative chiral approach*, Phys. Rev. **D59** (1999) 074001, [Erratum-ibid.D60:099906,1999], [hep-ph/9804209].

[OOR00] J. A. Oller, E. Oset and A. Ramos, *Chiral unitary approach to meson meson and meson baryon interactions and nuclear applications*, Prog. Part. Nucl. Phys. **45** (2000) 157–242, [hep-ph/0002193].

[OPV05] J. A. Oller, J. Prades and M. Verbeni, *Surprises in threshold antikaon nucleon physics*, Phys. Rev. Lett. **95** (2005) 172502, [hep-ph/0508081].

[OR98] E. Oset and A. Ramos, *Non perturbative chiral approach to s-wave anti-K N interactions*, Nucl. Phys. **A635** (1998) 99–120, [nucl-th/9711022].

[OR10] E. Oset and A. Ramos, *Dynamically generated resonances from the vector octet- baryon octet interaction*, Eur. Phys. J. **A44** (2010) 445–454, [arXiv:0905.0973].

[ORB02] E. Oset, A. Ramos and C. Bennhold, *Low lying $S = -1$ excited baryons and chiral symmetry*, Phys. Lett. **B527** (2002) 99–105, [nucl-th/0109006].

[P+04] S. Prakhov *et al.* (Crystall Ball), *$K^- p \to \pi^0\pi^0\Sigma^0$ at $p(K)^- =$ 514-MeV/c to 750-MeV/c and comparison with other $\pi^0\pi^0$ production*, Phys. Rev. **C70** (2004) 034605.

[Raj72] G. Rajasekaran, *Empirical test for composite hadrons*, Phys. Rev. **D5** (1972) 610–623.

[RF66] Riazuddin and Fayyazuddin, *Algebra of current components and decay widths of ρ and K^* decays*, Phys. Rev. **147** (1966) 1071.

[ROB02] A. Ramos, E. Oset and C. Bennhold, *On the spin, parity and nature of the $\Xi(1620)$ resonance*, Phys. Rev. Lett. **89** (2002) 252001, [nucl-th/0204044].

[RSMO06] L. Roca, S. Sarkar, V. K. Magas and E. Oset, *Unitary coupled channel analysis of the $\Lambda(1520)$ resonance*, Phys. Rev. **C73** (2006) 045208, [hep-ph/0603222].

[Sav95] M. J. Savage, *E2 strength in the radiative charmed baryon decay $\Sigma_c^* \to \Lambda_c\gamma$*, Phys. Lett. **B345** (1995) 61–66, [hep-ph/9408294].

[SB51] E. E. Salpeter and H. A. Bethe, *A Relativistic equation for bound state problems*, Phys. Rev. **84** (1951) 1232–1242.

[SOVV05] S. Sarkar, E. Oset and M. J. Vicente Vacas, *Baryonic resonances from baryon decuplet-meson octet interaction*, Nucl. Phys. **A750** (2005) 294–323, [nucl-th/0407025].

[SSL09] N. Suzuki, T. Sato and T. S. H. Lee, *Extraction of Resonances from Meson-Nucleon Reactions*, Phys. Rev. **C79** (2009) 025205, [arXiv:0806.2043].

[SSOV10] S. Sarkar, B.-X. Sun, E. Oset and M. J. V. Vacas, *Dynamically generated resonances from the vector octet- baryon*

decuplet interaction, Eur. Phys. J. **A44** (2010) 431–443, [arXiv:0902.3150].

[STT99] A. Sibirtsev, K. Tsushima and A. W. Thomas, *On studying charm in nuclei through antiproton annihilation*, Eur. Phys. J. **A6** (1999) 351–359, [nucl-th/9904016].

[SW88] P. B. Siegel and W. Weise, *Low-energy K- Nucleon potentials and the nature of the* $\Lambda(1405)$, Phys. Rev. **C38** (1988) 2221–2229.

[TEFK73] D. W. Thomas, A. Engler, H. E. Fisk and R. W. Kraemer, *Strange particle production from* $\pi - p$ *interactions at 1.69 gev/c*, Nucl. Phys. **B56** (1973) 15–45.

[TGRN08] H. Toki, C. Garcia-Recio and J. Nieves, *Photon induced* $\Lambda(1520)$ *production and the role of the* K^* *exchange*, Phys. Rev. **D77** (2008) 034001, [arXiv:0711.3536].

[TGRN09] L. Tolos, C. Garcia-Recio and J. Nieves, *The properties of D and* D^* *mesons in the nuclear medium*, Phys. Rev. **C80** (2009) 065202, [arXiv:0905.4859].

[TKO01] S. Tawfiq, J. G. Korner and P. J. O'Donnell, *Electromagnetic transitions of heavy baryons in the SU(2N(f)) x O(3) symmetry*, Phys. Rev. **D63** (2001) 034005, [hep-ph/9909444].

[TLT+99] K. Tsushima, D.-H. Lu, A. W. Thomas, K. Saito and R. H. Landau, *Charmed mesic nuclei*, Phys. Rev. **C59** (1999) 2824–2828, [nucl-th/9810016].

[TRM08] L. Tolos, A. Ramos and T. Mizutani, *Open charm in nuclear matter at finite temperature*, Phys. Rev. **C77** (2008) 015207, [arXiv:0710.2684].

[TSBM04] L. Tolos, J. Schaffner-Bielich and A. Mishra, *Properties of D-mesons in nuclear matter within a self- consistent coupled-channel approach*, Phys. Rev. **C70** (2004) 025203, [nucl-th/0404064].

[TSBS06] L. Tolos, J. Schaffner-Bielich and H. Stoecker, *D-mesons: In-medium effects at FAIR*, Phys. Lett. **B635** (2006) 85–92, [nucl-th/0509054].

[Wyl67] H. W. Wyld, *S-Wave Pseudoscalar-Meson-Baryon Scattering in a Simple Model with Broken SU (3) Symmetry*, Phys. Rev. **155** (1967) 1649–1662.

[ZD99] S.-L. Zhu and Y.-B. Dai, *Radiative decays of heavy hadrons from light-cone QCD sum rules in the leading order of HQET*, Phys. Rev. **D59** (1999) 114015, [hep-ph/9810243].

[Zhu00] S.-L. Zhu, *Strong and electromagnetic decays of p-wave heavy baryons Lambda/c1, Lambda/c1**, Phys. Rev. **D61** (2000) 114019, [hep-ph/0002023].

[Zwe64] G. Zweig, *An SU(3) Model for Strong Interaction Symmetry and its Breaking*, Technical report, CERN (1964).